BEHAVIOUR OF CROSS-LAMINATED TIMBER SUBJECTED TO BLAST LOADING

by

Mathieu Michael Poulin

A thesis submitted in partial fulfillment of the requirements for the degree of
Master of Applied Science

in Civil Engineering

Under the auspices of the Ottawa-Carleton Institute for Civil Engineering

uOttawa

University of Ottawa

January 2019

Abstract

Heavy timber construction is emerging as a viable alternative to conventional building materials, such as steel and concrete, for mid- and high rise structures. With the increasing presence of timber structures at or near potential targets comes an increased risk for damage to the structure and more importantly human casualties. The current provisions related to wood in the blast code (CSA, 2012) are limited and based on general understanding of the material behaviour rather than thorough research studies. Also, the standard does not clearly distinguish between the various types of engineered wood products.

A study was undertaken to assess the behaviour of cross-laminated timber panels subjected to simulated blast loading using a shock tube apparatus. More specifically, the aim of this study was to investigate the behaviour of CLT panels subjected to static and dynamic loads to determine a dynamic increase factor in order to quantify high strain rate effects on this material. Testing was completed on a total of 18 CLT panels, with panel thicknesses of 105 and 175 mm corresponding to a 3-ply and 5-ply panel, respectively. An average dynamic increase factor of 1.28 on the resistance and no apparent increase in stiffness from static to dynamic loading were observed. Two resistance material predictive models that account for high strain-rate effects and the experimentally observed post-peak residual behavior were developed. A single degree-of-freedom model was validated using full-scale simulated blast load tests, and the predictions were found to match well with the experimental displacement-time histories.

Acknowledgements

At the end of this thesis, I would like to take some time to thank all the people without whom this project would never have been possible.

First and foremost, an enormous thank you to my supervisor Dr. Ghasan Doudak for all the help, time, and guidance you've provided over the last few years. The journey that has been my thesis has been a winding one, full of ups and downs, but he was always there, ready to lend a hand, when I needed it.

I am also indebted to Ms. Stephanie Piccoli, for all her love, support, and encouragement during the course of this journey. Thank you for putting up with my craziness, for always being there through the good and the bad, and for always brightening up my day with that wonderful smile of yours.

My sincerest thanks go out to family for all their support and patience, and to my friends for their persistent questioning as to how my thesis was going and when I would be done. But seriously, thank you for keeping me sane throughout this process.

Lastly, a big thank you to the many colleagues that have help me along the way, namely Daniel Lacroix, Christian Viau, Dominic Cote, and America Lopez-Molina. I am ever grateful for the assistance you've provided both in the lab and out. Thank you all!

Table of Contents

List of Tables

List of Figures

Glossary

Acronym		Definition
CLT	=	Cross-laminated timber
COV	=	Coefficient of variation
DIF	=	Dynamic increase factor
FJ	=	Finger Joint
LSL	=	Laminated strand lumber
LVDT	=	Linear variable displacement transducer
MDOF	=	Multi-degree-of-freedom
MOE	=	Modulus of elasticity
MOR	=	Modulus of rupture
MSR	=	Machine stress rated
OSB	=	Oriented-strand board
P-I	=	Pressure-impulse
PSL	=	Parallel strand lumber
SDOF	=	Single-degree-of-freedom
SIF	=	Strength increase factor
TNT	=	Trinitrotoluene
VCE	=	Vapour cloud explosion

Symbol		Definition
ϕ (x)	=	Shape function
$(P_{max})_{Avg}$	=	Average applied load at failure
$(P_{Xe})_{Avg}$	=	Average elastic deflection limit
$(X_{max})_{Avg}$	=	Average elastic deflection at failure
$\dot{\varepsilon}$	=	Strain rate
$\bar{m}(x)$	=	Distributed mass per length
$\ddot{y}$	=	Acceleration
M	=	Ductility ratio
A	=	Loaded area
C	=	Damping constant
$d_{max-avg}$	=	Average maximum experimental mid-span displacement
F	=	Total load
F(t)	=	Total external force as a function of time
f_b	=	Bending strength
I^-	=	Negative impulse
I^+	=	Positive impulse
I_R	=	Experimental reflected impulse
k	=	Spring constant or stiffness
K_L	=	Load transformation factor
K_{LM}	=	Load-mass transformation factor
K_M	=	Mass transformation factor
K_R	=	Resistance transformation factor
L	=	Clear span length
L_D	=	Driver length
m	=	Mass
P(t)	=	Pressure-time history
P_o	=	Ambient pressure

P_R	=	Experimental reflected pressure
P_S	=	Incident peak pressure
$R(t)$	=	Total internal force as a function of time
$R(y)$	=	Non-linear resistance term
t	=	time
t_a	=	Time of arrival of shock wave
t_d	=	Positive phase duration of explosion
t_d^-	=	Negative phase duration of explosion
X_e	=	Deflection at elastic limit
x_{max}	=	Maximum deflection
X_{max}	=	Deflection at failure
y	=	Displacement
$\dot{y}$	=	Velocity
y_o	=	Initial displacement
$\dot{y}_o$	=	Initial velocity
Z	=	Scaled distance
ω	=	Circular frequency

Chapter 1 - Introduction

1.1 Background and Research Needs

Heavy timber construction is emerging as a viable alternative to conventional building materials, such as steel and concrete, for mid- and high rise structures. The relative light weight, ease and speed of construction, and competitive cost of engineered wood products has given rise to their popularity in construction worldwide. Such engineered wood products include glue-laminated timber (Glulam), cross-laminated timber (CLT), laminated veneer lumber (LVL), and parallel strand lumber (PSL).

Several studies have demonstrated the suitability of utilising CLT as the primary structural material, or in hybrid systems (Van de Kuilen, et al., 2010; Van de Kuilen, et al., 2011; Green, 2012; Skidmore, et al., 2013). A key concern raised in relationship with using wood in taller buildings is related to the material being combustible. In response to this, there has been an increase in research concerning CLT's performance in fire under various loading conditions (Frangi, et al., 2004; Frangi, et al., 2009; Fragiacomo, et al., 2013; Schmid, et al., 2015). Additionally, extensive research has also been done in the area of CLT's performance under seismic loading at the connection, subsystem as well as system levels (Pei, et al., 2013; Matsumoto, et al., 2014; Miyake, et al., 2014, Schneider, et al., 2014; Tsuchimoto, et al., 2014). The research demonstrated the ability of CLT to be successfully used, when the shear walls are loaded in-plane, to lateral loads and be used in earthquake prone countries such as Canada, the United States, and Japan.

The advancements in design and construction techniques and government initiatives have greatly contributed to the revitalization of the wood culture in Canada. This has led to the design and construction of high-profile commercial and residential projects, such as the roof of the Olympic

Oval skating arena in Richmond, B.C., the University of British Columbia's Brock Commons student residence (18-storey wood-hybrid), and the Origine Condo Tower (13-storey building, 12 of which are built from CLT). With the increasing presence of timber structures at or near potential targets comes an increased risk for damage to the structure and more importantly human casualties. Accidental explosions (e.g., BP Texas City, 2005; Lac-Mégantic rail disaster, 2013) have also been responsible for claiming the lives of many that occupied or happened to be in the vicinity of a timber building. The notion that because a material has less resisting capability against blast would be a deterrent against a targeted attack, or would make it unlikely for an accidental explosion to cause damage and human casualties is simply not viable. This same thinking has also meant that unlike conventional construction materials (i.e. steel and concrete), there has been little blast research done on heavy timber in general. The Canadian Standards Association (CSA) has published a standard titled *Design and assessment of buildings subjected to blast loads* (CSA, 2012), which addresses blast loading on structures for the purpose of analysis and design. Although wood is included in the standard as a material option, the provisions related to wood has been limited and based on general understanding of the material behaviour rather than thorough research studies. Also, the standard does not clearly distinguish between wood species, engineered wood products, and the variety of structural sub-systems available. Although it is not expected that wood and heavy timber be a designer's primary choice when intentionally designing for blast loads (e.g. bomb shelter), it is still important to recognize that government, military and industrial buildings are increasingly being constructed out of wood or wood components. Understanding the behaviour of wood under high strain rate effects and focussing on heavy timber materials in constructing buildings requiring some level of blast resisting capabilities is becoming increasingly important.

The current research study presents an important first step towards characterizing the behaviour of CLT slab elements subjected to blast loading. The outcome from this study would contribute to towards the analysis and design capabilities of this structural system and allow its use in a safe manner. The results could also directly contribute to both the wood and blast design standards (CSA, 2014; CSA. 2012).

1.2 Cross-Laminated Timber

CLT is a plate-type element, consisting of multiple layers of lumber boards that are glued together in layers that are perpendicular to each other. Typical panel lay-ups consist of 3, 5, 7, and 9 layers, however more layers are also possible. The bonded laminates can vary in size but are typically 80 to 240 mm wide and 10 to 40 mm thick. Panel sizes can vary depending on the manufacturer or a designer’s needs, although transportation is often a limiting factor for larger slabs. CLT can either be used as a structural floor slabs or wall panels in timber only or timber-hybrid structures. Figure 1.1 shows a typical CLT 3-ply panel.

Figure 1.1: Typical 3-ply CLT Panel

Wood is a natural anisotropic material, which means that the material’s strength and stiffness vary according to the orientation of the wood fibres. In fact, wood can be considered as an orthotropic material, where the wood properties are defined in three orthogonal directions, namely longitudinal, tangential, and radial. Wood is strongest when loaded longitudinally (i.e. parallel to the grain), and is weakest when loaded in the transverse direction (i.e. perpendicular to the grain) (Riyanto and Gupta, 1996). Because it is a natural material, the strength and specific characteristics of wood are highly dependent on a number of variables: tree species, growing conditions, growth rate, imperfections within the tree such as knots, shakes, and checks, slope of the grain, decay and contamination from foreign species, moisture content, etc. (Keenan, 1986; Dickson and Parker, 2015).

Another important characteristic that is unique to CLT is its susceptibility to rolling shear, which causes strain perpendicular to the grain direction. The composition of wood can be thought of as a bundle of fibers held together with relatively weak bonds. The stress overcomes the bonding strength and causes the fibers to start rolling next to one another, leading to splitting of the wood grain. Several studies have investigated CLT's material properties including rolling shear (Zhou, et al., 2014; Flores, et al., 2016; Li and Lam, 2016), as well as the behaviour of CLT subjected to out-of-plane loading (Steiger and Gülzow, 2009; Jacquier, 2015; Sikora, et al., 2016), and in-plane loading (Ceccotti, et al., 2006; Ashtari, et al., 2014; Popovski and Gavric, 2016; Yasumura, et al., 2016). Figure 1.2 (Schafer, 2014) illustrates how shear stresses interact with the grain of the wood; LR and LT are two kinds of longitudinal shear, RL and TL are transverse shear, and RT and TR are rolling shear.

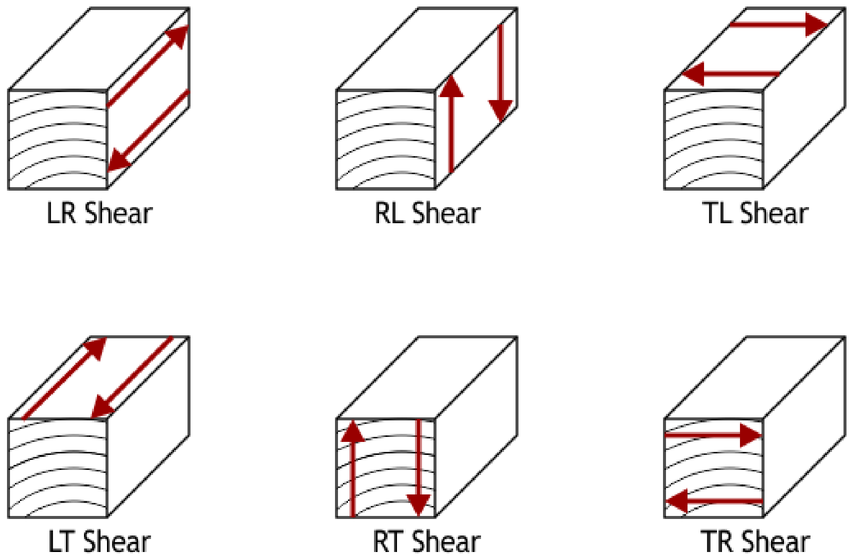

Figure 1.2: Shear Stress Interaction with Wood Grain (Schafer, 2014)

1.3 Explosions and Blast Waves

1.3.1 Blast Wave Characteristics

Explosives can generally be categorized as high explosives or low explosives. When high explosives are detonated, they tend to produce supersonic over-pressurising shock waves. High explosives include trinitrotoluene (TNT), C4, nitroglycerin, and ammonium nitrate fuel oil (ANFO), to name a few. Low explosives are much less energetic than high explosives. They deflagrate rather than detonate and thus lead to subsonic explosions and no shock wave. Low explosives include gunpowder, pipe bombs, and petroleum-based incendiary bombs such as gasoline bombs and Molotov cocktails. In most cases, only the resulting loading from high explosives is considered when examining the effects of blast loading on structures.

An explosion can be defined as a sudden and rapid release of energy, generally resulting from a chemical reaction involving a solid, liquid or gas. The energy is released in milliseconds and generates very hot gases under high pressures. These gases expand into their surrounding environment in a spherical form, forcing out the air that occupies the space. The air being forced out compresses into a layer that continues to propagate outwards from the source of the explosion, propelled by the expanding gases. The pressure of expanding gases is known as a blast wave, and the compressed layer of air is known as the shock front or as a shock wave. The pressure created by an explosion quickly surpasses the ambient pressure and is referred to as the side-on overpressure. As the blast wave continues to expand outwards, the overpressure gradually decays until it drops below the ambient pressure creating a partial vacuum, known as the negative phase. The negative phase of the explosive wave is generally not taken into account in design as the produced pressures are relatively small. The main structural damage occurs in the positive phase (Karlos, & Solomos, 2013). The simplest form of a blast wave is termed the Friedlander waveform and can be seen in Figure 1.3 (Dusenberry, 2010). Friedlander's equation, as expressed in Equation 1.1, describes the rate of decrease in pressure over time:

$$P(t) = P_s\left(1 - \frac{t}{t_0}\right)e^{-b\frac{t}{t_0}} \tag{1.1}$$

where P_s is the peak overpressure, t is the time elapsed, t_0 is the positive phase duration, b is a decay coefficient of the waveform. It is common practice to idealize actual pressure-time histories base on this model. The pressure-time history for each test in this study was idealized as an instantaneous rise in pressure, which decreases linearly to ambient pressure

Another important blast wave parameter is the impulse, which is described as the total force per unit area that is applied to a structure. It corresponds the area under the pressure-time history curve (Fig. 1.3). The positive, I^+, and negative, I^-, impulses correspond to the relevant phases of the blast wave, and can be expressed as shown in Equations 1.2 and 1.3, respectively:

$$I^{+} = \int_{t_a}^{t_a+t_0} P(t)dt \tag{1.2}$$

$$I^{-} = \int_{t_{a+t_0}}^{t_a+t_0+t_0^{-}} P(t)dt \tag{1.3}$$

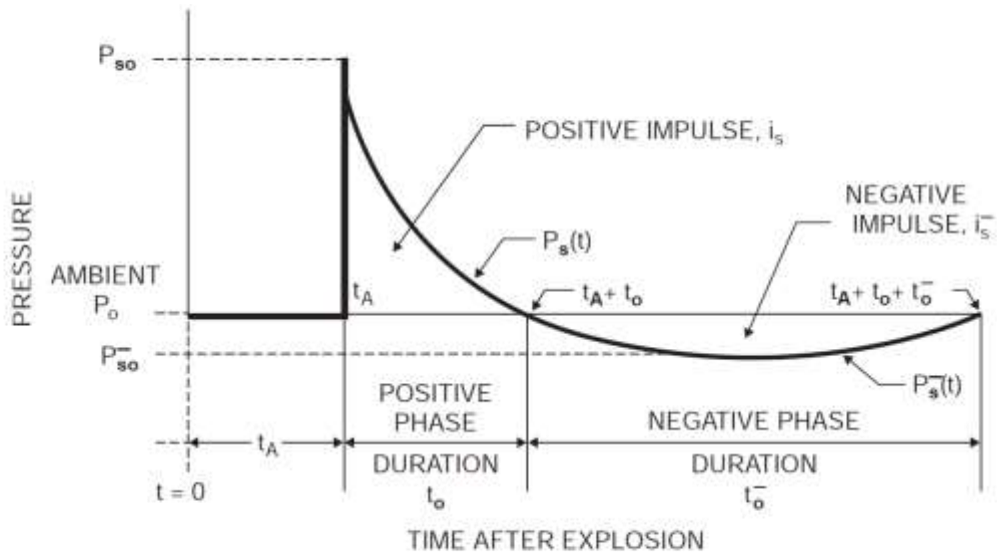

Figure 1.3: Typical pressure-time history of a blast wave (Dusenberry, 2010)

1.3.2 Scaling Laws

Field testing with live explosives is quite costly and depending on the type of explosives used, the outcome may be difficult to predict. For this reason, it is common to use scaling law to compare the effects of different explosions in similar atmospheric conditions. Two of the most critical parameters for blast loading are the distance at which the explosive is placed from its intended target, called the standoff distance, and the size (weight) of the explosive. For simplicity, the size and quantity of explosive materials are generally related to an equivalent TNT quantity, because the parameters of a blast wave generated from a detonation of TNT are well established. This normalizes the size parameter thus only requiring the distance to be scaled. Distance is a critical parameter for blast loading because the peak pressure value and velocity decreases rapidly over a given distance, as can be seen from Figure 1.4 (Ngo, et al., 2007).

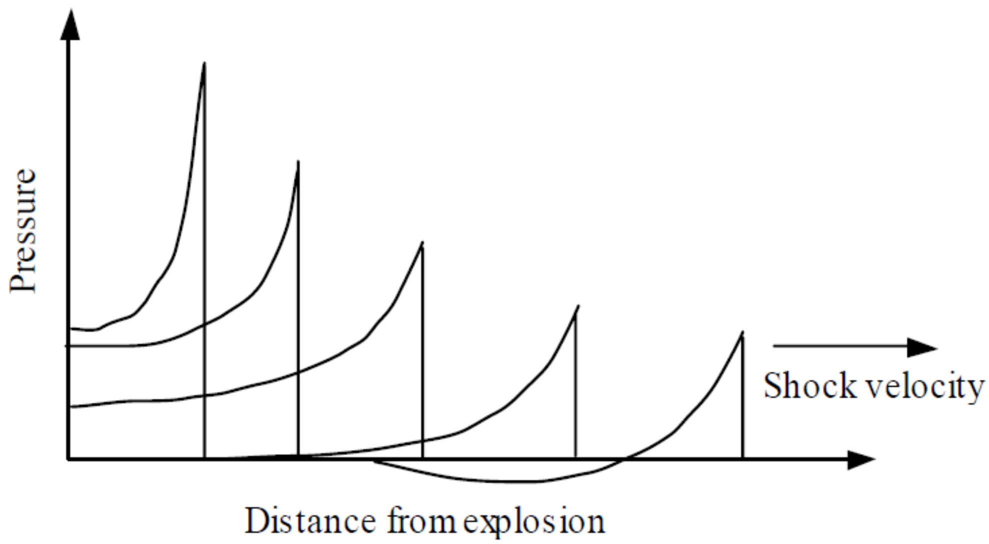

Figure 1.4: Blast wave propagation (Ngo, et al., 2007)

The Hopkinson-Cranz law is the most commonly used scaling law. This law is used to compare the effects of detonated charges of the same explosive that have similar geometry and are detonated in similar atmospheric conditions but are at different distances from a target surface. The idea behind the formulation is that similar blast waves are produced at a point of interest for two explosive charges of different weight as long as they consist of the same explosive substance, have similar geometry, are under the same atmospheric conditions, and are at the same scaled distance from a target surface (Karlos, & Solomos, 2013). According the Hopkinson-Cranz law, the scaled distance, Z, is calculated as indicated in Equation 1.4.

$$Z = \frac{R}{\sqrt[3]{W}} \tag{1.4}$$

where R is the standoff distance in m and W is the mass of the explosive in kg.

Therefore, for a target set at the same scaled distance, two different charges with different standoff distances would yield the same reflected pressure and initiate the same response in a structural member. This is illustrated in Figure 1.5 (Baker, 1973). The cube root scaling concept can be extended to other blast parameters such as the impulse (Krauthammer, 2008).

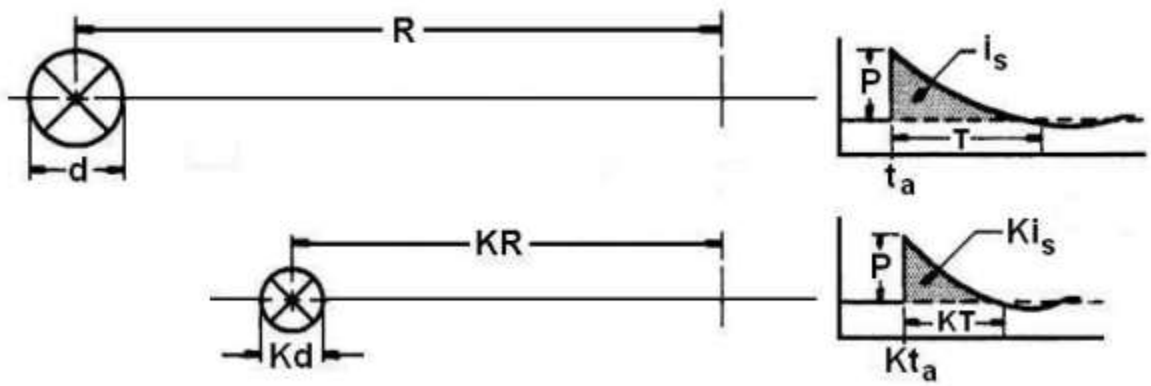

Figure 1.5: Geometric representation of Hopkinson-Cranz blast wave scaling (Baker, 1973)

1.3.3 Explosives, Explosions and Blast Loading

1.3.3.1 Types of Explosion

Four different types of explosions can be identified, namely chemical, electrical, mechanical, and nuclear. Chemical explosions are the most common type of artificial explosions (Ngo, et al., 2007). They usually involve a rapid and violent release of hot gases through an oxidation reaction. An external catalyst, such as an electric spark, is often required to initiate the chemical reaction. Explosions from commonly used explosives such as gunpowder, TNT, and C-4 are categorized at chemical explosions. Electrical explosions are the result of high electrical currents forming electrical arcs, which rapidly heats the surrounding gases and materials (metals, insulation, etc.) and results in an explosion. Examples of this type of explosion can be found at power stations, where electrical arcs occurring from energized switchgears pose a hazard to workers, as well as power surges in structures that are not properly protected against lightning strikes (i.e. residential buildings).

Mechanical explosions, or physical explosions, are the result of a physical process. An example includes the bursting of a sealed container due to internal pressure such as the failure of cylinder tank that contains compressed air or the rupture of an overheated boiler. Also included in this type of explosion is a vapour cloud explosion. A vapour cloud explosion (VCE), although technically a deflagration and not an explosion, can be as destructive as an explosion depending on the circumstances. If a container with flammable material ruptures (e.g. propane tank), the material inside will quickly evaporate and create a vapour cloud. When the material mixes with oxygen and is exposed to an ignition source, the vapour cloud will ignite and quickly burn. The resulting heat can have destructive consequences, especially if in a confined area. VCEs mostly occur in petrochemical facilities where flammable material is present.

Nuclear explosions derive their incredibly destructive forces from nuclear fission, which is a nuclear reaction in which the nucleus of an atom splits into smaller and lighter nuclei. This process produces free neutrons and releases a very large amount of energy. As a result, a nuclear weapon with a small yield will be significantly more powerful than even the largest conventional explosives. The Little Boy and Fat Man bombs that were used against Japan during WWII are examples of nuclear weapons, although modern day nuclear warheads are significantly more powerful.

As previously mentioned, TNT was selected as benchmark material to use in the computation of blast parameters. As such, other explosives are converted into an equivalent TNT charge weight based on the heat of detonation according to Equation 1.5.

$$W_e = W_{exp} \frac{H^d_{exp}}{H^d_{TNT}} \tag{1.5}$$

Where, W_e is the TNT equivalent weight *kg*,

W_{exp} is the weight of the explosive considered in *kg*,

H^d_{exp} is the heat of detonation of the explosive considered in *MJ/kg*,

H^d_{TNT} is the heat of detonation of TNT in *MJ/kg*.

TNT equivalency provides a mass factor and is useful in determining the resulting peak pressure and impulse generated from a variety of high explosives. Mass factors for many high explosives have been tabulated and are readily found in literature. These factors vary slightly from one source to another, and for this reason it is generally recommended to apply a factor of safety of approximately 20% to the charge weight (Karlos & Solomos, 2013). Table 1.1 lists mass factors for some common high explosives.

Table 1.1: TNT Equivalent Mass Factors

Explosive	Specific Energy (MJ/kg)	TNT Equivalent Mass Factor	
		Peak Pressure	Impulse
C3	4.88	1.08	1.01
C4	6.06	1.34	1.19
Compound B	5.02	1.11	0.98
HMX	5.65	1.25	1.25[1]
Nitroglycerin	6.69	1.48	1.48[1]
Octol (75/25)	4.79	1.06	1.06
Pentolite (Cast)	6.42	1.42	1.00
PETN	5.74	1.27	1.11
RDX	5.15	1.14	1.09
Semtex	5.65	1.25	1.25[1]
Tetryl	4.84	1.07	1.05
TNT	4.52	1.00	1.00

[1]Value is estimated.

1.3.3.2 Explosions and Blast Loading

In practice, unconfined external blast loading on structures can be divided into three basic types: free-air bursts, air bursts, and surface bursts. The types are dependent on the position of the explosive source relative to the structure, namely the elevation of the explosive above ground surface and its horizontal distance from the structure (Draganić & Vladimir, 2012).

A free-air burst occurs when an explosive charge is detonated in the air at a higher elevation. The blast waves propagate outwards spherically and strikes the target structure without prior interaction with the ground or other obstacles. Air bursts are similar in nature to free-air bursts with the exception that the blast waves initially interact with the ground prior to striking the target structure. A surface burst occurs when an explosive charge is detonated at or near the ground surface. The blast waves propagate hemi-spherically and immediately interact with the ground and surrounding obstacles prior to striking the target structure.

The important distinction between the loading types is regarding the propagation path of the blast waves. Interaction with surfaces, such as the ground and obstacles, leads to reflections and interference phenomena which can greatly modify the blast wave, and consequently modifying the loading pressure on a structure. A depiction of the three external loading types can be seen in Figure 1.6 (Karlos & Solomos, 2013).

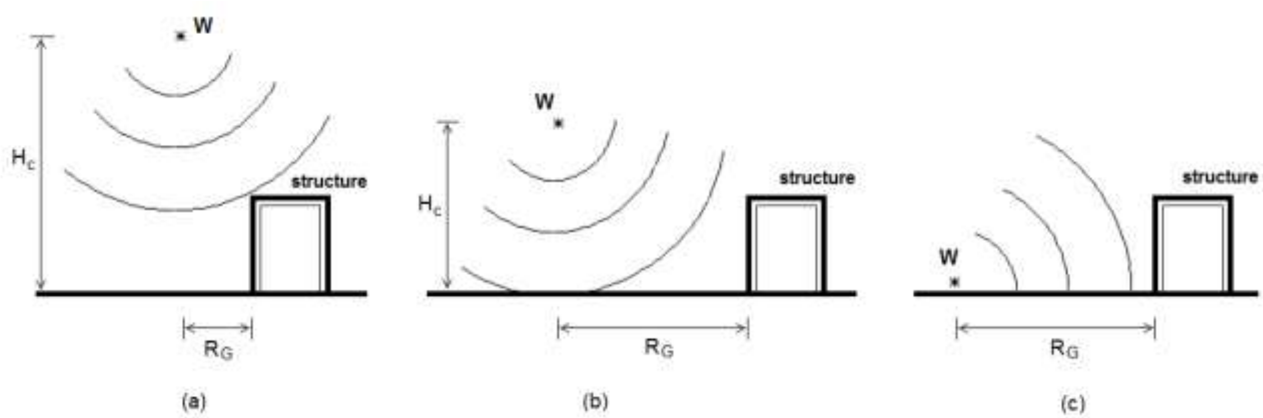

Figure 1.6: Types of external blast loading; (a) Free-air bursts, (b) Air bursts, and (c) Surface bursts

1.4 Dynamic Analysis

1.4.1 General

Blast loading on structures occurs over a very short period of time relative to static loads (i.e. dead and live loads) and other slower dynamic loads (i.e. wind and earthquake). This type of loading can incite much difference responses and behaviours in structures. The short loading duration requires that inertial forces and kinetic energy be accounted for to properly analyse and design structural elements. In such cases, it is generally acceptable to utilize a simplified dynamic analysis approach, such as single-degree-of-freedom (SDOF) models, which incorporate the kinetic energy and inertial forces. An SDOF analysis method can be employed when the motion of a structural element can be described using a single ordinate along its length (e.g. the mid-span deflection of a beam in flexure). Other, more complex, analysis methods (e.g. finite element analysis and multi-degree-of-freedom) could be used, however the computational effort required is significantly larger and it worth it (Biggs, 1964). Several recent studies have demonstrate that SDOF analysis can accurately describe the response of structural elements subjected to blast loads (Lloyd, 2010; Jacques, 2011; Burell, 2012; Ciornei, 2012).

1.4.2 Single-Degree-of-Freedom Analysis

The closed form solution of an SDOF model is obtained by solving the equation of motion shown in Equation 1.6.

$$m\ddot{y} + c\dot{y} + ky = F(t) \tag{1.6}$$

where *m* is the mass, *c* is the damping constant, *k* is the spring constant, *F(t)* is a time varying forcing function, and $\ddot{y}$, $\dot{y}$, and y are the acceleration, velocity and displacement of the system, respectively.

Damping effects can typically be neglected in blast due to the short loading period and because the maximum dynamic response is the point of interest (Biggs, 1964). The equation of motion presented in Equation 1.6 can be modified for an un-damped free vibration response, where the damping coefficient and external forcing function are equal to zero, as shown in equation 1.7.

$$m\ddot{y} + ky = 0 \tag{1.7}$$

The displacement solution resulting from a constant external loading function, F_0, and with damping omitted, is shown in Equation 1.8.

$$y = \frac{F_0}{k}(1 - \cos(\omega t)) \tag{1.8}$$

where F_0 is obtained from the peak reflected pressure and ω is the natural frequency of the system in rad/sec.

More closed-form solutions for differing loading scenarios are readily available in the literature (Biggs, 1964).

As previously mentioned, this close-form method assumes that the motion of a system is defined by a single point and that the mass and stiffness of this system are also lumped at that point. In reality, structural elements have distributed mass and stiffness, and therefore appreciable error is introduced. An equivalent SDOF system must be created by transforming the mass, stiffness, and loads of the real system to an equivalent system with the use of transformation factors that are based on an assumed static deflected shape (Biggs, 1964). Using the correct deflect shape is critical to the analysis. Transformation factors for the mass, K_M, load, K_L, and resistance, K_R, must be included in the equation of motion. For a simply supported beam deflecting according to the first mode shape (i.e. maximum deflection at mid-span), the transformation factor for mass and load can be calculated with Equations 1.9 and 1.10, respectively:

$$K_M = \frac{\int_0^L \bar{m}(x)\emptyset^2(x)dx}{\int_0^L \bar{m}(x)dx} \tag{1.9}$$

$$K_L = \frac{\int_0^L f(x,t)\emptyset(x)dx}{\int_0^L f(x,t)dx} \tag{1.10}$$

where $\bar{m}(x)$ is the distributed mass per length, $\emptyset(x)$ is the shape function based on the deflected shape of the element based on loading conditions, and $f(x,t)$ is the distributed load per unit length at a given time.

The modified equation of motion incorporating the transformation factors and neglecting the damping term is as follows:

$$K_M m\ddot{y}(t) + K_R R(y) = K_L A P_R \left(1 - \frac{t}{t_d}\right) \tag{1.11}$$

where $R(y)$ is the non-linear resistance and P_R is the maximum reflected pressure. It can also be seen that the forcing function introduce in Equation 1.6 has been replaced by the idealized pressure-time history function multiplied by the loaded area, A.

In general, the resistance factor, K_R, is always equal to the load factor, K_L (UFC, 2008). The reason is that the resistance of the system is equal to the internal forces counteracting applied loads. Therefore, an increase in the applied load will equate to an increase in resistance by the same amount. The load and mass factors can also be combined into a single variable call the load-mass factor, K_{LM}. The load-mass factor is defined as the ratio between the mass and load factors, as shown in Equation 1.12. Considering this, Equation 1.11 can be further simplified to have only one transformation factor, as shown in Equation 1.13. Transformation factors for common loading and support conditions are available in the literature (Biggs, 1964).

$$K_{LM} = \frac{K_M}{K_L} \tag{1.12}$$

$$K_{LM} m\ddot{y}(t) + R(y) = AP_R \left(1 - \frac{t}{t_d}\right) \tag{1.13}$$

1.5 Research Objective

The main goal in this research study is to establish the dynamic behaviour of CLT panels under the effects of simulated blast loading. More specifically, the objectives are:

- Investigate the failure modes of CLT panels under static and simulated blast loading,
- Establish a dynamic increase factor (DIF) by comparing experimental results based on static and dynamic testing,
- Develop a material predictive model and analysis procedure for CLT structures
- Validate the accuracy of the current design provisions outlined in the CSA S850 for engineered wood products.

1.6 Scope

The above mentioned research objectives will be achieved through the following:

- Carry out a detailed literature review on the behaviour of wood material, particularly heavy timber, when subjected to blast loads.
- Conduct static testing on six CLT specimens with two different layups to obtain their mechanical properties, and document their static failure modes.
- Conduct dynamic (shock tube) testing on five CLT specimens with three different layups to obtain their dynamic properties and document their dynamic failure modes. The

reactions measured from this set of specimens could be compared directly with the results obtained from the static testing in order to compare the performance and establish a value for the dynamic increase factor.

- Subject eight additional CLT specimens to dynamic loading in order to validate the analysis procedure developed in the current study.
- Discuss the results by comparing the experimental and analytical results and propose improvements to the existing analysis and design approaches.
- Investigate the validity of current design provisions and propose improvements where appropriate.

1.7 Structure of Thesis

Chapter 1 provides an introduction to CLT and the basis of blast design, and presents the objectives and scope of this research.

Chapter 2 presents a literature review of the available research in the area of wood under the effects of blast loading, development of dynamic increase factors for structural elements of other materials as well as the behaviour of CLT under static and dynamic loading in general.

Chapter 3 outlines the experimental methodology utilized during this research, as well as a detailed description of the specimens tested and the test setup.

Chapter 4 presents the results for the static and dynamic testing, including material evaluation tests and destructive tests.

Chapter 5 presents the analytical approach and methodology used to determine the dynamic increase factor. The proposed analysis method is also presented in this chapter.

Chapter 6 presents a discussion on the results of the experimental program, the implications of the modelling approach, and examines the validity of the provisions presented in the blast code and its implications on design.

Chapter 7 presents a summary of the findings from this study and identifies potential future work.

Appendix A and B contain the test results for all specimens tested under static and dynamic loading.

Chapter 2 – Literature Review

2.1 Introduction

CLT is an emerging structural material and, as such, available research is predominantly limited to establishing models of basic mechanical properties for varying layer configurations and wood types. Establishing these mechanical properties is paramount for designers but means that research into this material is still in its infancy. Lately, more in-depth research has been conducted with regards to CLT's behaviour under lateral loading. Very little research has been conducted for the behaviour of CLT, and other timber structures, under blast loading relative to other common building materials such as concrete and steel.

2.2 Mechanical Properties of CLT Panels

The use of cross-laminated timber is an establish construction alternative in Europe and is growing in popularity in North America and Australia. However, the understanding of this unique building material's behaviour is constantly growing. The spread in manufacturing utilizing local wood species also increases the complexities of this material. Several research projects have been completed and are ongoing in Europe, Canada, China, and several other nations to deepen the practical knowledge regarding this product and to further aid designers in using this project for future construction.

2.2.1 Comparison of Bending Stiffness of Cross-Laminated Solid Timber Derived by Modal Analysis of Full Panels and by Bending Tests of Strip-Shaped Specimens (Steiger et al., 2012)

This study aimed to evaluate if flexural stiffness properties of CLT panels could be reliably derived by testing 100mm and 300mm strips cut from larger panels and to what extent specimen widths influences the test results. The researchers tested 42 CLT specimens having various dimensions and lay-ups supplied by two producers. All specimens were fabricated using Norway spruce (Picea abies Karst.). Lay-up configurations for product A included 10/50/10 (70mm thick), 25/20/25 (70mm thick), 35/40/35 (110mm thick), 25/30/25 (80mm thick), 15/15/20/15/15 (110mm thick). Lamellas used in the outer layers were of strength class C24 and were 70mm wide. Lamellas in the cross layer were of strength class C20 and varied between 100 to 150mm in width. Layers were face-bonded using a polyurethane (PUR) adhesive. For Product B, lay-up configurations included 10/50/10 (70mm thick), 25/20/25 (70mm thick), 20/70/20 (110mm thick), 15/50/15 (80mm thick), 35/40/35 (110mm thick). Lamellas used in the outer and cross layers were of strength class C24 and were 25mm in width. Laminates in each layer were both edge-bonded and face-bonded using a melamine-urea-formaldehyde (MUF) adhesive.

Strip shaped specimens were initially cut from the full size panels, in both outer layer grain directions, in order to produce square panels (2.5m x 2.5m). The elastic parameters of these panels were then obtained through static bending tests under different loading configurations and through modal analysis. The researchers immediately noted that different panel production methods (e.g. layers without edge-bonding, end jointing of lamellas without overlap of fingers, etc.) significantly influenced the stiffness properties of the panels. Subsequently, four-point bending tests were carried out on the 100mm strip specimens having a span of 1,100mm. Three-point bending tests were then carried out on the 300mm strip specimens. Specimen spans varied to accommodate varying depth to span ratios ranging from 0.0037 to 0.035. The moduli of elasticity and shear moduli were evaluated and compared.

The authors noted the strong variability in bending stiffness between specimens originating from the same panel. Homogenization of the specimens through proper bonding of the lamellas seemed to be a leading factor in the variation in mechanical properties. They indicate that Product B showed overall less variation due to the incorporation of edge-bonding relative to Product A, which was only face-bonded. In addition, Product B used small sized lamellas which further improved the product due to more adequate strength grading of the raw material. As such, the 300mm strip specimens originating from Product B showed a higher degree in accuracy in ascertaining the stiffness properties of the panel. However, the authors also note that the presence of material defects (knots, cracks, bonding defects, etc.) in the strip specimen have a much larger influence in the bending stiffness relative to larger panels. The authors also concluded that the distance between center layer lamellas when the lumber was not edge-bonded, and the grooves purposely introduced to control deformation in the case of changing moisture, have a significant influence on the shear moduli. They indicate that strip specimens may not properly capture these effects and that an empirical relationship would be required to properly account for this influence.

2.2.2 Measurement of Rolling Shear Modulus and Strength of Cross Laminated Timber Fabricated with Black Spruce (Zhou et al., 2014)

This study aimed to assess the applicability of the two-plate shear test for measuring the rolling shear properties of edge-glued wooden cross layer (WCL). This test allowed for the measurement of the rolling shear modulus, which in turn was used to predict the deflection of a 3-layer CLT panel subjected to three-point bending through the use of the shear analogy method. These predictions were then compared to results obtained from three-point bending tests on specimens.

Specimens consist of black spruce (Picea mariana) lumber. Outer layers consisted of 38mm x 140mm visually graded No.2 lumber whereas the center cross layer consisted of 38mm x 89mm visually graded No.3 lumber. Laminates for the cross layer were edge-glued to one another and outer layers were face-glued perpendicularly to the cross layer with a two-component polyurethane adhesive to form the panel. The full size panel specimens were 96mm x 222mm x 2500mm. A total of twelve 32mm x 150mm x 450mm WCL specimens were cut from full size panels. Tested panel widths included 222mm (9 specimens), 144mm (9 specimens), 96mm (9 specimens), and 48mm (18 specimens) leading to four different span-to-depth ratios (6, 9, 14, and 17, respectively). Specimens with different widths were tested in order to assess the width effect on material properties (e.g. modulus of elasticity and shear modulus).

Through the two-plate shear test, the research found that the average rolling shear modulus and strength of the WCLs was 136 MPa and 1.09 MPa, respectively. The researchers observed several load peaks prior to a significant drop in resistance. Following this initial large drop in resistance, a stepwise decline in the resistance was observed until the complete failure of the specimen. This was attributed to the nature of the specimen; edge-glued laminates with similar properties would fail simultaneously or sequentially in short order as a redistribution of the load to the other laminates would occur following the first failure.

The results of the three-point bending tests revealed that specimen width did not have a statistically significant effect on the MOE or the shear modulus for 3-layer panels. The authors proposed an adjustment factor, α, which was derived in order to predict the deflection of CLT panels given a span-to-depth ratio (L/h). The adjustment factor was derived by comparing the measured deflection to the calculated deflection obtained through the shear analogy method.

2.2.3 Evaluation of Mechanical Properties with Elementary Beam Theories (Christovasilis et al., 2016)

This study aimed to investigate the accuracy of conventional beam theories in predicting the associated deformation and failure mechanisms and to assess the reliability of the estimated properties with respect to the expected values. In addition, the researchers investigated the consistency among specimens with different layer configurations. Panels were tested using the four-point bending test and results were compared to estimated mechanical properties based on the Modified Gamma method, the Timoshenko beam theory, and the Shear Analogy method for loading out-of-plane. The results indicated that the bending response and elastic and strength properties are well represented in the established theories. The authors noted that the Shear Analogy method is the most reliable with respect to the expected values for elastic and strength properties. The values for the modulus of elastic and the bending strength of 11,000 MPa and 24 MPa, respectively, were found to be reliable estimates for structural design for CLT panels made of boards graded as C24 in Europe (equivalent to CLT grade E1 and V1 in Canada). Rolling shear strength was noted to have significant variability among the different layer configurations for all applied methods.

2.2.4 Torque Loading Tests on the Rolling Shear Strength of CLT (Lam et al., 2016)

The rolling shear strength of CLT was evaluated in this study by submitting three-layer and five-layer CLT block samples with tubular cross layers to torque loading until brittle shear failure occurred in the middle cross layers. The block samples were cut from full-size slabs composed of Mountain Pine Beetle afflicted lumber boards. The rolling shear strength values were evaluate using finite-element modeling. The authors notes that due to the complicated orthotropic properties of wood, using simple analytical equations to calculate the rolling shear strength was not applicable. In addition, an investigation was also carried out on the occurrence probability of different shear failure modes (rolling shear and longitudinal shear) as a confirmation that the specimens failed predominantly in rolling shear. The researchers concluded that the probability of rolling shear failure was very high and that the torque loading test was a viable method to investigate rolling shear behaviour.

The researchers found that the rolling shear strength values obtained through finite element modelling differed greatly from other test results from bending tests or planer shear tests available in literature. The rolling shear strength obtained was 3.86 MPa and 4.83 MPa for three-layer and five-layer CLT specimens, respectively. However, the authors noted that these values cannot be used for design purposes as size effect played a significant role in the obtained results. They indicate that further study is required to determine the dependence of the size effect on rolling shear strength, which could help explain the strength differences between beam bending tests and torque loading tests.

2.2.5 Effects of the Thickness of CLT Panels Made from Irish Sitka Spruce on Mechanical Performance in Bending and Shear (Sikora et al., 2016)

This study investigated the effect of the thickness of CLT panels on the bending stiffness and strength and the rolling shear. Bending and shear tests were conducted on three-layer and five-layer panels made of Irish-grown Sitka spruce. The general tendency of the results showed that bending strength and rolling shear decreased as the thickness of the panels increased. The highest maximum bending stress values for three-ply panels originated from the thinnest specimen, while this thickest three-ply panel had the lowest bending stress values. Similar to the bending stress, values for rolling shear were also adversely influenced by an increase in panel thickness. The resulting mean values for rolling shear ranged from 1.0 MPa to 2.0 MPa for different thicknesses.

2.3 Mechanical Properties of Finger Joints and Bonding

Finger-joints are a very important element when considering engineered wood products such as CLT as they allow for economical manufacturing practices. Finger-joints allow for the joining of board segments longitudinally. In general, finger-joining allows for the removal of material defects in individual members and also allows for the production of larger sized wood products. The production of a finger-joint consists of cutting “finger” profiles at each end of boards, adding structural adhesive, and connecting the boards together end-to-end essentially forming one member. This type of joint has proven to be must stronger than a simple butt joint or scarf joint.

2.3.1 Influence of Bondline Brittleness and Defects on the Strength of Timber Finger-Joints (Serrano and Gustafsson, 1999)

A study was undertaken at Lund University to examine the mechanical behaviour of wooden finger joints commonly found in wood products such as glued-laminated or cross-laminated timber. The researchers aimed at examining the sensitivity of the material in strength due to material properties of the wood and the bondline, as well as the effect of defects within the glue line. The study involved fracture mechanics tests of bondlines taken from finger joints which provided quantification of parameters for a material model. This model was then implemented in a finite element analysis. Samples were fabricated using Norway spruce wood. The finger profile was identical for each sample.

Specimens were tested using a bi-axial testing machine consisting of two crossheads and load cells to measure the horizontal and vertical forces applied. The testing was carried out by applying relative vertical and horizontal displacements. The normal and shear stresses and the relative corresponding displacement across the bondline were recorded. Three loading paths were tested based on the grain direction rather than the bondline direction. The three testing modes corresponded to parallel to grain, perpendicular to grain, and at 2:1 (parallel: perpendicular) to grain. These three modes were respectively denoted by the authors as the shear-deformation test, the normal-deformation test, and the mixed-mode test.

The researchers also measure the strain softening behaviour of an RP adhesive bondline. A nonlinear fracture softening model was implemented into the finite element modeling in order to predict the behaviour of the finger joint. Through their model, the researchers were able to show that the strength of the finger joint was strongly influenced by the behaviour of the bondline post peak stress. They describe the potential for increasing the strength of finger joint made with brittle adhesives by increasing the bondline fracture energy, which would also aid in reducing the brittleness number. In addition, the researchers indicate importance of the presence of small defects, such as voids, in the bondline which can account for a reduction in strength of approximately 12%. The outermost fingers would seemingly be the most sensitive to defects. This study also showed that the joint is strongly influence by the stiffness of the lamination and by stiffness variability between the two finger joint halves.

2.3.2 Wood Finger-Joint Strength as Function of Finger Length and Slope Positioning of Tips (Habipi and Ajdinaj, 2015)

This study was carried out to analyse the relation of slope positions of finger tips and finger lengths in finger joints with regards to bending strength. Finger joints specimens were prepared using poplar (*Populus alba* L.) and silver fir (*Abies alba* Mill.), bonded with polyvinyl adhesive. Specimens having three different finger profile were produced with lengths of 6mm, 10mm and 14mm. Four variation of fingertip alignment was produced for each length. The fingertip slope angle was measured relative to the vertical and included a straight vertical alignment (0°), 10°, 20°, and 30°. Other parameters such as pitch were similar for all configurations. The specimens were subsequently subjected to static loading to initiate a bending response in accordance with the testing standards outlined in ISO 13061-3 and ISO 13061-4. The modulus of rupture and the modulus of elasticity were determined based on these tests.

The results showed that the bending resistance was strongly influenced by the length of the fingers. Joints with longer fingers yielded higher resistance. The authors noted that an overall higher finger length to pitch ratio provides an overall strong joint. The authors also note that joints with a sloped fingertip alignment provided an overall increase in the modulus of rupture relative to a straight fingertip alignment. The results showed that the modulus of elasticity was relatively unaffected by the varying finger lengths or alignments.

2.3.3 Shear Strength and Durability Testing of Adhesive Bonds in Cross-Laminated Timber (Sikora et al., 2016)

This study examined the interface- and edge-bonded joints in layers of CLT panels. The shear performance was investigated to assess the suitability of two different adhesives, polyurethane (PUR) and phenol–resorcinol–formaldehyde (PRF), and to determine the optimum clamping pressure in fabrication. A series of block shear tests were carried out on face-bonded specimens, consisting of crosslam with vertically and horizontally bonded elements, edge-bonded specimens, consisting of specimens bonded along the end grain and perpendicular to grain, and solid wood blocks. Loading during shear testing was applied in the vertical and horizontal directions for each specimen group. In addition, delamination tests were performed on samples which had been subjected to accelerated aging in order to assess the durability of the bonds.

The CLT panels were manufactured using grade C16 Irish Sitka spruce. The adhesives systems were applied and cured as recommended by the manufacturers. Edge bonded specimens had a bonded area of 30mm thick by 50mm wide. Solid wood specimens of the same dimensions were also prepared. CLT specimens were cut-out of three layer panels having a total thickness of 90mm (30mm per layer). The panels were face-bonded only with no edge bonds.

The results showed that for CLT produced using Irish Sitka spruce and the lowest manufacturing pressure, 0.4 N/mm^2, produced CLT with sufficient shear strength to meet the requirements outlined in the British CLT standard, prEN 16351 (BSI, 2011), for edge bonding.

2.4 Behaviour of Structural Wood Elements under Simulated and Actual Blast Loads

Investigation into the behaviour of lumber, engineered wood products, and timber substructures subjected to blast loads has increased over the last few years. Several research projects have been completed using the University of Ottawa' shock tube to establish dynamic response in a variety of wood structural members.

2.4.1 Influence of High Strain-Rates on the Dynamic Flexural Material Properties of Spruce–Pine–Fir Wood Studs (Jacques et al., 2014)

The objective of this study was to investigate the high strain-rate flexural behaviour of wood studs. More specifically, the researchers aimed to determine the DIF for the flexural modulus of elasticity (MOE) and modulus of rupture (MOR) of lumber and to compare the obtained DIF with the values provided in the CSA S850. Testing was performed on a total of 30 stud grade 38mm x 140mm x 2440mm SPF lumber specimens. Specimens of this size and species were selected as they represent typical North American light-frame wood construction. Twelve specimens were subjected to low strain-rate loading (i.e. static loads), while 18 were subjected to high strain-rates using the University of Ottawa's shock tube. The authors noted that the static tests had strain-rates ranging from 10-5 to 10-3 s^{-1} while ''high strain-rate'' tests had strain-rates exceeding 10^{-2} s^{-1}. All specimens were tested under simply supported four-point bending. The specimens' length was 2440mm with a clear span of 2235mm. Lateral restraints were provided at the supports in order to prevent lateral buckling.

The researchers used an SDOF iterative solution procedure to compute the high strain-rate MOR and MOE and, through comparison with static and dynamic testing results, concluded that the behaviour of the wood could be accurately predicted with an SDOF model. Based on the experimental results, they observed a DIF of 1.41, 1.14, and 1.18 for the MOR, MOE and strain at rupture (ε_d), respectively, for strain-rates ranging from 0.1 – 1 ε/s. For this range of strain-rates, the flexural stress-strain relationship is best represented by a linear elastic curve with the DIF applied to the MOR. The rupture strain was taken as proportional to the dynamic MOR and static MOE. The authors indicated that although the MOR is significantly affected by high strain-rate effects, these same effects do not seem apparent for the dynamic MOE or strain at rupture. This was primarily attributed to the large scatter of results within a small sample set. Furthermore, the authors compared the obtained results with the DIF prescribed by the design code (CSA S850) and concluded that the code factor applied to timber strength was appropriate.

2.4.2 Investigation of Dynamic Increase Factors in Light-Frame Wood Stud Walls Subjected to Out-of-Plane Blast Loading (Lacroix and Doudak, 2015)

This study presented the results of a research project undertaken at the University of Ottawa having as a primary objective to establish the behaviour and flexural response of light-frame timber wall systems (i.e. stud walls) under high strain rate loading. The research was limited to the wall assembly itself and therefore excluded possible influence from boundary connections between wall and floor subsystems. Being that the intent of this research was to determine that dynamic increase in the flexural failure, the authors recognized that potential failures could occur in the connections between subsystems in actual structures. A total of 20 wall specimens were tested statically and dynamically. The composition of the walls consisted of six 38 x 140mm MSR studs spaced at 406mm c/c and included a single top and bottom plate. Two variations of sheathing were tested: 11mm OSB and 18.5mm plywood. The OSB sheathing was fastened with 64mm long nails having a diameter of 3.5mm while the plywood sheathing was fastened with 89mm long nails having a diameter of 4.2mm. The nails were spaced at 150mm c/c in order to reduce potential nail withdrawal under dynamic loading. The overall dimensions of the walls were 2,159mm in height (clear span) by 2,032mm in width. These dimensions were chosen to be slightly larger than the opening of the shock tube in order to ensure that only the response of the studs and sheathing were observed and to ensure that the top and bottom plates were not engaged. The walls were loaded both statically and dynamically under four-point bending with idealized pinned end conditions. In order to observe a dynamic increase in flexure, the specimens tested were subjected to three different pressure-impulse combinations. The first combination was to incite an elastic response, the second was to produce an equivalent maximum load as that observed statically, and the third was to achieve failure in the specimen.

The researchers observed that the displacement of the studs occurred in unison up to the point of maximum displacement, at which point the displacement of the studs would be out of phase. In some cases, it was noted that following the inbound phase, undamaged studs failed during the rebound, which was caused by the negative pressure phase. Although the observed failure mode for both static and dynamic tests was flexural, differences were noted regarding the type of flexural failure. Splintering tension failure was observed under static loads whereas brash tension was observed under dynamic loads. The researchers observed a dynamic increase of 1.40 and 1.18 in the resistance and stiffness, respectively. These were determined by developing an SDOF model and comparing it to the experimental results obtained. Finally, the authors proposed an equation, DIF = 1.46 + 0.1 x log10ὲ, relating the dynamic increase factor to the strain rate for strain rates ranging from 1.67 – 1.65 x 10 s-1.

2.4.3 Numerical Analysis of Behaviour of CLT in Blast Loading (Šliseris et al., 2017)

This study presents a numerical simulation of a CLT wall element developed using explicit dynamic and a transversally isotropic composite damage model which was then compared with classical beam theory. The model was utilized on three-, five-, and seven-layer CLT panels. Blast loading was applied using a triangular impulse function with an impulse duration time ranging from 1 ms to 100 ms. The results showed that impulse duration time has a significant effect on the strength of CLT. It was observed that the overpressure impulse cause stress waves in the CLT panels which excited the first three vibration modes. They concluded that a significant part of the vibration amplitude was caused by shear deformation of the center shear layers. As such, the authors recommend that theories which incorporate shear deformation, such as Timoshenko's beam theory, be used when designing CLT.

2.4.4 Effects of High Strain Rates on the Response of Glulam Beams and Columns (Lacroix and Doudak, 2018)

A research project was undertaken at the University of Ottawa's structural laboratory to develop a model for the static and dynamic wood stress-strain response and a second model that accounts strain-rate effects and axial loading on glulam members subjected to out-of-plane blast loads. The predictive resistance curves generated from the models were subsequently compared to those obtained from experimental results. The first phase of experimental testing consisted of full-scale static testing of glulam members under four-point bending with simply supported boundary conditions and with no axial loading applied. The second phase of testing consisted of dynamic testing of glulam members with and without axial load. Specimens were loaded statically and dynamically using four-point bending with simply supported boundary conditions. Axial loading and dynamic reactions were measured directly with load cells. Columns were loaded axially through a range of 15%-75% of their design compression capacity. Specimens tested statically and dynamically without axial loading also served as validation for the predictive model.

The proposed material model developed by the researchers, which used input tensile and compressive stress-strain relationships from coupon tests, proved effective at capturing the flexural behaviour (no axial loads applied) of glulam subjected to out-of-plan static and dynamic loads when modified for high-strain rate effects. In addition, the authors indicated that the implementation of variable axial loading into the resistance function accurately captured the behaviour of the glulam specimen. The model accurately incorporated the projected shortening analogy to capture the loss in axial load at the point of maximum flexural resistance.

In addition, the researchers also concluded that an equivalent SDOF approach, which also accounted for an equivalent lateral load, could effectively be applied to obtain a glulam column's resistance with the use of experimentally measured time histories for displacement, pressure, reaction, and axial loading. This type of analysis also proved effective in predicting the dynamic response of glulam members subjected to blast loads with no axial loads.

Chapter 3 – Experimental Program

3.1 General

An experimental program was developed to investigate the effects of high strain rate on the flexural capacity of CLT with the intent to determine the dynamic increase factor (DIF). The experimental program involved testing CLT panels under four-point bending with simply supported boundary conditions. Panels were tested both statically as well as dynamically, through simulated blast loading.

A total of eighteen CLT panels (six statically and twelve dynamically) were tested to destruction. All specimens were tested statically within their elastic range prior to being tested to failure. A full overview of the testing schedule is presented below.

Two different CLT cross-sections and layup combinations were considered, including eleven 3-ply and seven 5-ply. The CLT specimens consist of grade E1, where the layers in the major axis direction consisted of 35mm by 80mm lumber with machine stress grade 1950Fb and Spruce-Pine-Fir (SPF) lumber species group. The transverse layers (minor direction) consist of No.3 / Stud grade SPF lumber. Finger joints were used to join lumber pieces in the major direction. Thicknesses for 3-ply and 5-ply panels were 105mm and 175mm, respectively. The panels had a width of 445mm and a length of 2500mm. However, the test span for each specimen was limited to 2235mm to accommodate the end frame opening of the shock tube apparatus.

3.2 Test matrix

An overview of the specimens tested and the type of test performed is summarized in Table 3.1. The nomenclature of the specimens is such that the first number indicates the number of plies and the second number is the specimen number. For example, CLT3-2 refers to specimen number 2 of the 3-ply CLT layup.

Table 3.1: Summary of Tests

Specimen Type	Loading Type			
	Static Elastic	Static Destructive	Dynamic Elastic	Dynamic Destructive
3-Ply	CLT3-1	CLT3-1	-	-
	CLT3-2	CLT3-2	-	-
	CLT3-3	CLT3-3	-	-
	CLT3-4	-	CLT3-4	CLT3-4
	CLT3-5	-	-	CLT3-5
	CLT3-6	-	-	CLT3-6
	CLT3-7	-	CLT3-7	CLT3-7
	CLT3-8	-	CLT3-8	CLT3-8
	CLT3-9	-	CLT3-9	CLT3-9
	CLT3-10	-	CLT3-10	CLT3-10
	CLT3-11		CLT3-11	CLT3-11
5-Ply	CLT5-1	CLT5-1	-	-
	CLT5-2	CLT5-2	-	-
	CLT5-3	CLT5-3	-	-
	CLT5-4	-	-	CLT5-4
	CLT5-5	-	-	CLT5-5
	CLT5-6	-	CLT5-6	CLT5-6
	CLT5-7	-	CLT5-7	CLT5-7

3.3 Static Testing

A total of eight CLT panels were tested statically to failure under four-point bending with simply supported boundary conditions, as shown in Figure 3.1. Idealized pin supports were provided by affixing metal plates to the specimen and resting them on rollers. The clear span between supports was 2235 mm, which is a limitation imposed by the end frame opening of the shock tube apparatus.

The metal plates served to provide a larger bearing area to mitigate localized crushing effects at the supports. Loading was applied at the third points via a combination of a hydraulic jack and a pump. The hydraulic jack was connected to a load cell, which served to measure the applied force, and subsequently attached to a steel I-beam which allowed for even load distribution to the two application points. Semi cylindrical wooden blocks were affixed to the steel I-beam and served to transfer the load to the specimen.

The mid-span deflection was measured using a wire gauge attached on the tension side. Compressive and tensile strains were measured using strain gauges affixed at mid-span. Applied force, displacement and strain measurements were recorded using a data acquisition system (DAS) with a sampling rate of 10 samples per second.

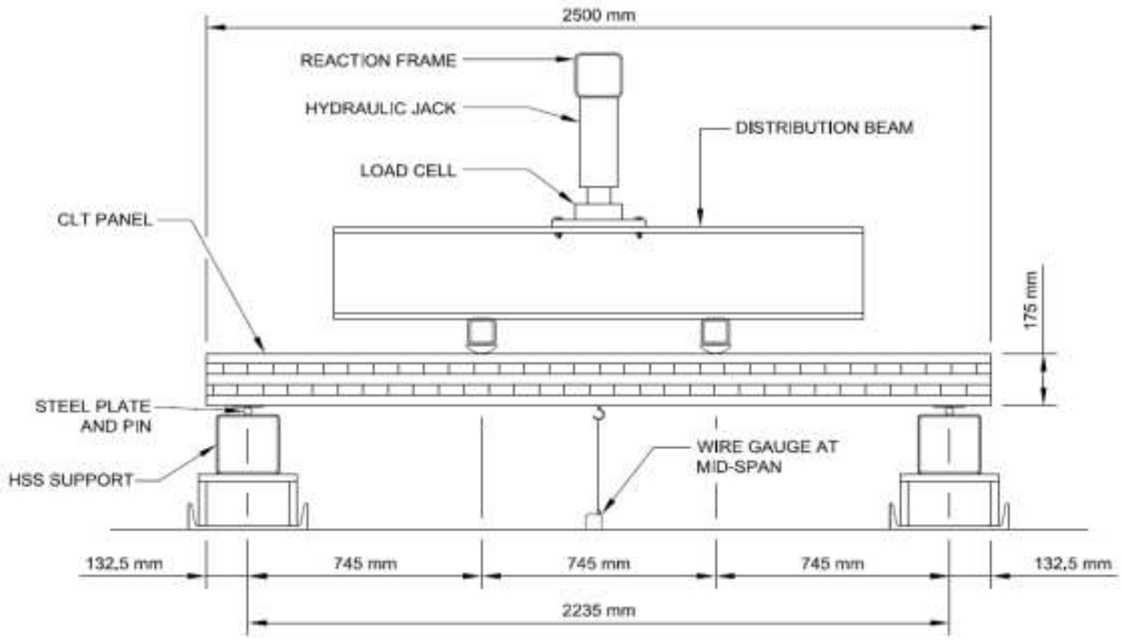

(a) Sketch

(b) Actual Test Setup

Figure 3.1: Static Test Setup: (a) Sketch; (b) Actual Test Setup

3.4 Dynamic Testing

Dynamic testing was conducted using the University of Ottawa's Shock Tube facility. The Shock Tube is an apparatus which generates shock waves in order to simulate high-pressure waves similar to those originating from a far-field detonation of high explosives.

3.4.1 Description of the Shock Tube

The Shock Tube simulates blast loads by compressing air and releasing it nearly instantaneously. The Shock Tube is made up of three major components that are used to achieve this: the driver section, the spool section, and the expansion section. The different sections and components are shown in Figure 3.3.

The driver serves as the main chamber for the compressed air, which when released a shock wave is created. The driver length ranges from 305mm to 5185mm and can be varied with increments of 305mm. Changing the driver length changes the impulse but does not affect pressure capacity, allowing for different pressure-impulse combinations. Several pressure-impulse combinations based on a range of available driver length configuration have been obtained through passed testing and calibration of the shock tube, of which the data is readily available to researchers. Based on preliminary analysis, it was determined that a 273mm (9ft) driver section would be suitable to obtained the desired pressure and impulse ranges required in this research project.

The spool serves as the detonation trigger and is referred to as a double diaphragm firing system. It is a relatively small section located between the driver and expansion sections. The spool section is bounded by sheets of aluminium foils at the interface of each adjacent section. The sheets of aluminium foil have a predetermined pressure-rupture capacity rating based on their thicknesses, which was obtained through previous testing and is available to researchers, and are installed and layered such that the desired pressure is achieved in the driver section. While the driver is being filled with air, the spool is simultaneously being partially filled in order to provide an equalizing pressure between the driver pressure and the atmospheric pressure in the expansion section. Therefore, the combination of foils between each section needs to be greater than the anticipated differential pressure to ensure that no premature trigger occur. Once the desired driver pressure is attained, the pressure in the spool is reduced by draining the air through a control nozzle until the foils rupture.

This nearly instantaneous release of compressed air forms the shock front which travels down the 6096mm long expansion section, where it eventually interacts with the specimens mounted at the Shock Tube's end frame. Twelve pressure relief vents are located near the end frame to allow for a negative pressure phase to develop once the shock wave dissipates. The rigid end frame's opening is 2032mm x 2032mm, which allows for testing of large scale specimens.

Specimens can be mounted directly to the end frame, in which case loading is applied directly, otherwise a load transfer device (LTD) can be installed in order to transfer the load to narrower specimens. The LTD used in this research project consisted of three steel panels that covered the entire opening of the end frame. The panels were connected together with hinges that allowed the panels to freely move outwards from the Shock Tube and transfer load to a test specimen without contributing to the stiffness of the system. Steel I-beams with welded rollers at the one-third points served as load application points allowing for four-point bending loading consistent with the static test conditions. This type of loading configuration has been successfully used in a variety of research projects investigating high strain rate responses of timber elements (Jacques et al. 2014; Lacroix et al. 2014; Lacroix and Doudak 2015; Viau 2016; Viau and Doudak 2016a, b; Lacroix 2017; Cote 2017) as well as reinforced concrete elements (Lloyd 2010; Jacques 2011; Burrell 2012; Aoude et al. 2015; Barreiro 2016).

The maximum reflected pressure and impulse that can be produced is 100 kPa and 2200 kPa-ms, respectively. The positive phase of the shock wave can vary from 5 ms to 70 ms. In the current study, a driver length of 2745 mm was used throughout testing.

(a) Driver Section (b) Expansion Section (c) End Frame

Figure 3.2: University of Ottawa's Shock Tube

3.4.2 Description of the Test Setup

The dynamic test setup, as show in Figure 3.3, was constructed to replicate the same simply supported boundary conditions and loading pattern as those used in the static testing. Loading consisted of four-point bending with idealized pin supports. Similarly to the static testing, the clear span of the specimen was 2235 mm. This span length had been based on the limitations of the Shock Tube.

The CLT panel specimens were installed flush against the LTD and their supports consisted of two HSS members with welded rollers placed on both sides of the tested specimens. The HSS sections were used to clamp the panels to the Shock Tube. Care was exercised when tightening the bolts for the HSS section to avoid introducing clamping effects during testing and to allow for free rotation of the panel. The HSS members were attached to the end frame with threaded rods and were held in place vertically using shims and adjustable steel column sections.

The first phase of dynamic testing was meant to directly measure the dynamic reactions in order to estimate the DIF. For these tests, four load cells, two at each support, were used to measure the dynamic reactions (Figure 3.4). They were held in place using an HSS member clamped to the end frame. Steel plates were placed at all loading and support points in order to mitigate localized crushing effects of the wood.

The mid-span deflection was measured using linear variable displacement transducer (LVDT), which was attached to a steel column member which was isolate from the test setup. Similar to the static testing, strain gauges were installed on the compression and tension face of the panel at mid-span to measure the corresponding strains. The reflected pressure-time history of the shock wave was recorded using two piezoelectric sensors (i.e. pressure gauges) located on the bottom and side wall near the opening of the end frame. All measurements were recorded using a DAS having a sampling rate 100,000 samples per second. In addition, a high speed camera with a recording rate of 500 frames per second was employed to capture the behaviour of the specimen and to help determine the prevailing failure mode.

It should be noted that the LTD was not fastened to the specimen. Thus, the negative phase of the shock wave only affected the LTD and did not have any effect on the specimen. However, this proved to be of little significance as the specimen would have already failed before any reverse loading took place.

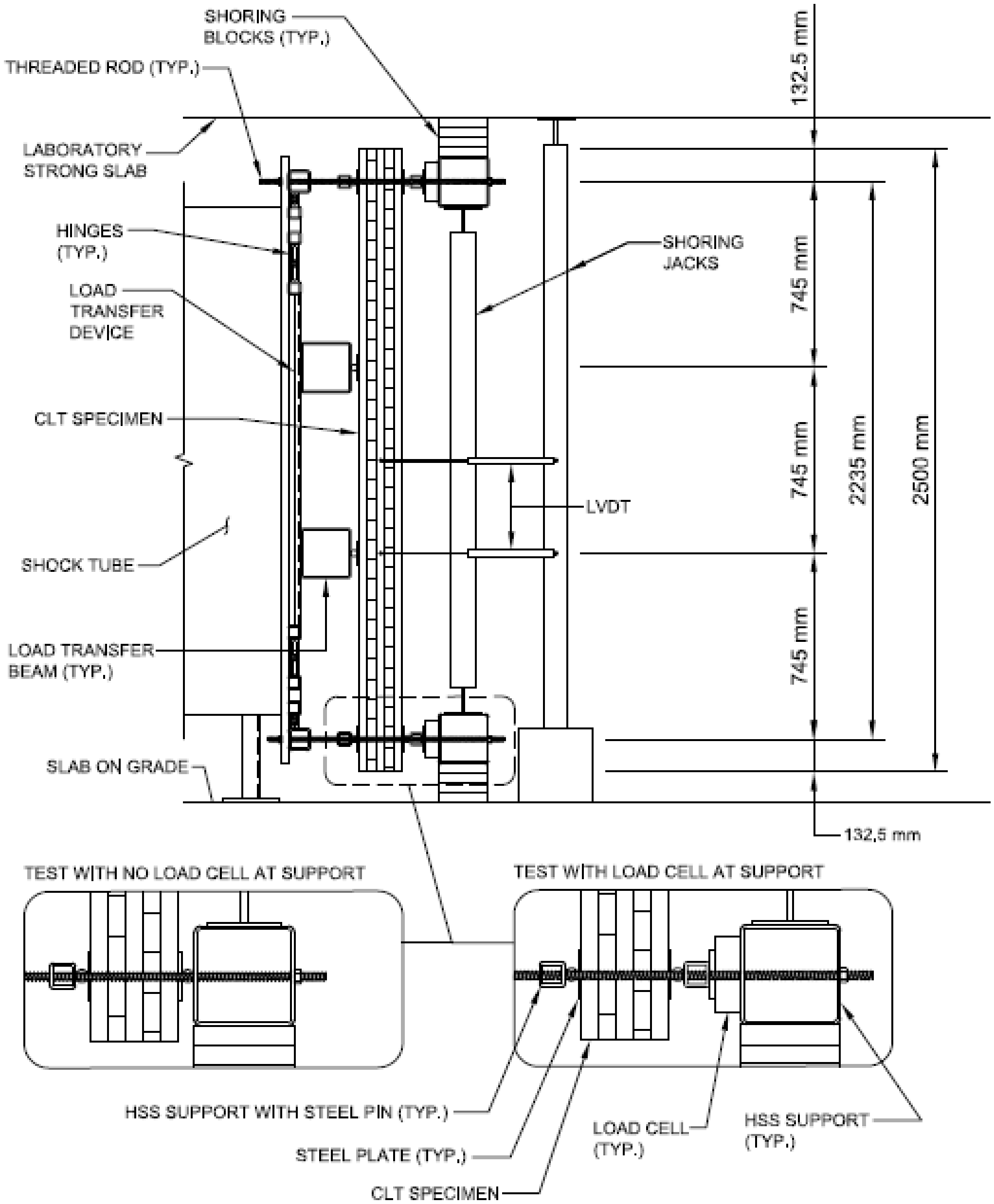

Figure 3.3: Sketch of Dynamic Test Setup

Figure 3.4: Actual Dynamic Test Setup

(a) Support with load cell

(b) Support without load cell

Figure 3.5: Dynamic Supports: (a) Support with load cell; (b) Support without load cell

Chapter 4 – Experimental Results

4.1 General

The experimental results of the static and dynamic testing are presented in this chapter. Some specimens were tested statically to destruction in order to determine the strength properties of the investigated material. All the specimens that were tested dynamically were also loaded statically to a point below their elastic limit in order to determine their initial stiffness. The strength and stiffness values are used to directly compare with those obtained through dynamic loading. The failure mode for each specimen tested to destruction are also presented in this chapter. Further details on the results of each test can be found in Appendix A and B.

4.2 Static Test Results

4.2.1 Static Destructive Testing

A total of six CLT panels were tested destructively under static loading, including three 3-ply and three 5-ply. Table 4.1 presents the results for theses specimens. Presented results include the maximum resistance (R_{max}), deflection at the maximum resistance (Δ_{Rmax}), maximum deflection at failure (Δ_{max}), ductility ratio (μ), stiffness (K), time to failure ($t_{f\text{-}max}$), strain-rate ($\dot{\varepsilon}$), and maximum moment (M_{max}). The nomenclature for the static test specimens is identical to that used in Table 3.1.

The ductility ratio, μ, is defined as the maximum displacement, Δmax, divided by the elastic displacement, ΔRmax. It is well established that most failure mechanism in wood are brittle in nature and therefore ductility in wood should not be thought of as plastic deformation before failure, such as the behaviour typically observed in steel, but rather as a post-peak resistance once outer laminates have failed. The stiffness, K, is defined as the maximum resistance, Rmax, divided by its associated elastic deflection, ΔRmax.

Table 4.1: Static Destructive Test Results

Panel Type	Specimen	R_{max} (kN)	Δ_{Rmax} (mm)	Δ_{max} (mm)	μ	K (kN/mm)	$t_{f\text{-}max}$ (min)	$\dot{\varepsilon}$ (s^{-1})	M_{max} (kNm)
CLT3	CLT3-1	65.7	34.3	67.7	2.0	2.05	6.48	6.92×10^{-6}	24.5
	CLT3-2	75.7	37.4	56.2	1.5	2.12	6.38	7.70×10^{-6}	28.2
	CLT3-3	63.8	32.3	58.7	1.8	2.06	3.77	1.05×10^{-5}	23.8
	Average	68.4	34.7	57.7	1.8	2.1	-	-	25.5
	St. Dev.	5.2	2.1	1.4	0.2	0.03	-	-	2.0
	COV	0.08	0.06	0.02	0.11	0.01	-	-	0.08
CLT5	CLT5-1	130.8	25.2	47.8	1.9	5.62	5.03	7.62×10^{-6}	48.7
	CLT5-2	132.6	24.3	49.1	2.0	5.92	4.22	2.39×10^{-5}	49.4
	CLT5-3	122.3	21.4	60.4	2.8	6.01	3.78	1.09×10^{-5}	45.6
	Average	128.6	23.6	52.3	2.2	5.9	-	-	47.9
	St. Dev.	4.5	1.6	5.6	0.4	0.17	-	-	1.7
	COV	0.03	0.07	0.11	0.19	0.03	-	-	0.03

The experimental resistance curves for all the statically tested CLT panels are shown in Figure 4.1. Figure 4.1(a) shows the behaviour of the 3-ply panels. The panels were observed to behave in a linear-elastic manner up to the maximum resistance corresponding to an initial flexural failure in the tension laminates. Rolling shear occurred at approximately the same time as the flexural failure. The 3-ply panels' post-peak resistance equates to approximately 20% of their maximum resistance. Observable damage was similar for the three panels. Initial flexural failure in the tension laminates generally occurred in locations having finger joints (FJ). In some cases there was clear separation of the joint, and in others there was shearing of the 'fingers', as seen in Figures 4.2 and 4.3, respectively. Failure would then propagate across the panel width before ultimate failure is attained. Some panels also exhibited signs of longitudinal shear following the initial flexural failure, as can be seen in Figure 4.4.

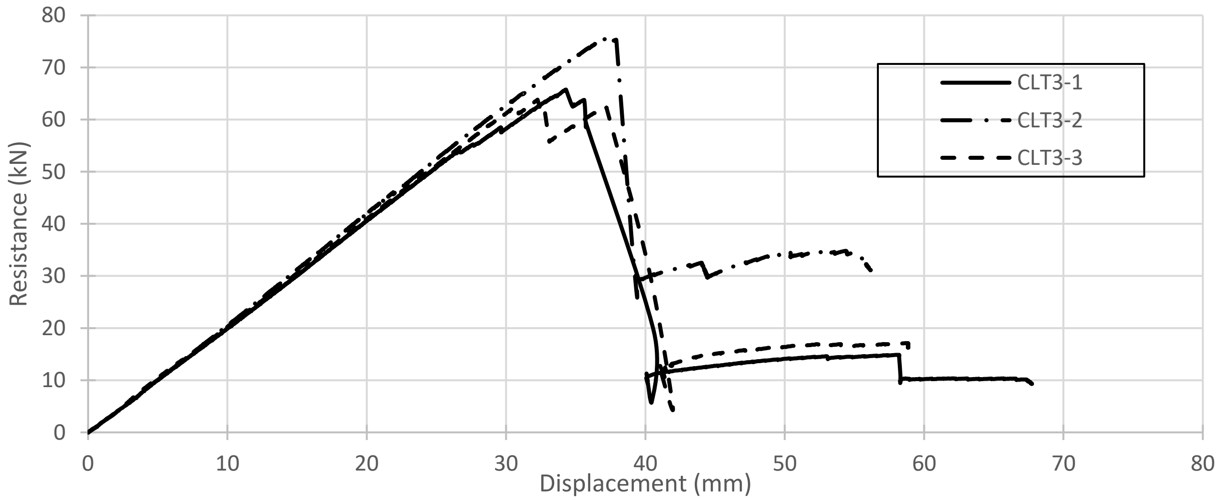

(a) 3-ply

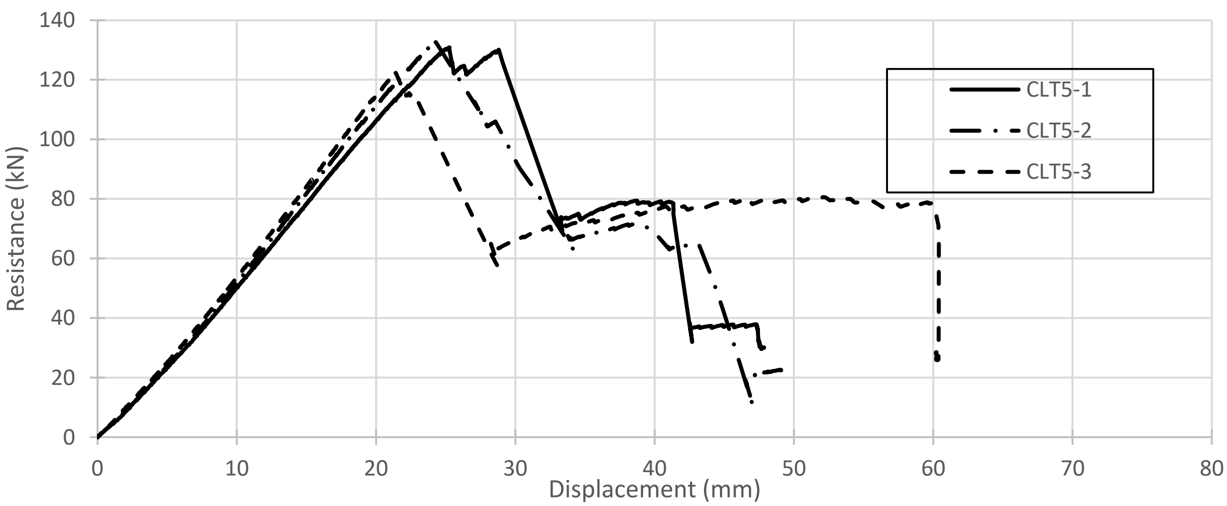

(b) 5-ply

Figure 4.1: Static loading resistance curves for CLT panels: (a) 3-ply; (b) 5-ply

Figure 4.2: Finger Joint Separation in Tension Laminates

Figure 4.3: Shearing of Finger Joints in Tension Laminates

Figure 4.4: Longitudinal Shear in Tension Laminates

The 5-ply panels behaved similarly to the 3-ply panels (Figure 4.1(b)), where the initial failure at the peak resistance was observed to be in at the outer tension laminates ultimately causing flexural failure. In addition, there was no apparent sign of rolling shear prior to the initial flexural failure. Similar to the 3-ply panels, flexural failure generally originated in areas having FJ and then propagated along the width of the panel. Separation of the FJ was common (Figure 4.5). Progressive failure of the layers across the depth of the panel is represented by the plateaus shown in Figure 4.1(b). The first plateau following the peak resistance, indicating failure of the first longitudinal laminate layer, is approximately 55% of the peak resistance and also corresponds to the peak resistance of a 3-ply panel. A second plateau is observed following the failure of the second longitudinal laminate layer, representing approximately 20% of the peak resistance.

The displacements measured at the post peak capacity for the 3-ply and 5-ply panels were on average 1.8 and 2.2 times larger than those corresponding to the ultimate capacity, respectively.

Figure 4.5: Multiple Finger Joints Separating in Tension Laminates of a 5-ply Specimen

4.2.2 Static Elastic Testing

All specimens tested dynamically to destruction were tested statically within their elastic limit to determine the specimens' initial static stiffness. Applied loading was limited to approximately one third of the expected ultimate capacity of the specimens. This was limit was based on the observed behaviour and results obtained during destructive static testing. This information was gathered in order to allow for a direct comparison between these values and those obtained through dynamic loading. The specimens were inspected for any minor cracks and initial signs or rolling shear that may have occurred during this non-destructive phase.

Twelve specimens that were tested dynamically were investigated in this phase, including eight 3-ply and four 5-ply panels. Table 4.2 presents the results for the specimens tested elastically, including the maximum applied load (P), the deflection at the maximum resistance (Δ_P), the stiffness (K), and the strain-rate ($\dot{\varepsilon}$).

Table 4.2: Static Elastic Test Results

Panel Type	Specimen	P (kN)	Δ_P (mm)	K (kN/mm)	$\dot{\varepsilon}$ (s^{-1})
	CLT3-4	22.9	14.4	1.59	1.43×10^{-5}
	CLT3-5	23.3	11.1	2.10	1.13×10^{-5}
	CLT3-6	23.5	12.2	1.88	1.33×10^{-5}
	CLT3-7	23.5	13.2	1.77	8.88×10^{-6}
	CLT3-8	21.6	12.9	1.66	1.10×10^{-5}
CLT3	CLT3-9	22.8	13.0	1.76	6.94×10^{-6}
	CLT3-10	24.6	11.8	2.10	1.53×10^{-5}
	CLT3-11	23.4	11.4	2.09	9.27×10^{-6}
	Average	23.2	12.5	1.87	-
	St. Dev.	0.8	1.0	0.20	-
	COV	0.03	0.08	0.10	-
	CLT5-4	48.4	8.7	5.64	5.30×10^{-6}
	CLT5-5	45.2	8.9	5.14	5.91×10^{-6}
	CLT5-6	46.8	8.7	5.53	5.12×10^{-6}
CLT5	CLT5-7	46.7	9.4	5.07	7.26×10^{-6}
	Average	46.8	8.9	5.34	-
	St. Dev.	1.1	0.3	0.24	-
	COV	0.02	0.03	0.05	-

4.3 Dynamic Test Results

Twelve CLT panels were subjected to simulated blast loads, including eight 3-ply panels and four 5-ply panels. The results are summarized in Table 4.3, and include the reflected pressure (P_R) and impulse (I_R), maximum dynamic resistance (R_{max}), displacement at maximum resistance (Δ_{Rmax}), maximum mid-span displacement (Δ_{max}), ductility ratio (μ), time-to-maximum displacement (t_{f-max}), strain-rate ($\dot{\varepsilon}$), static stiffness (K_{Static}), and observed dynamic failure mode. The nomenclature for dynamic test specimens has an added number which indicates the number of shots to which the panel was subjected (e.g., specimen CLT5-4.2 is a 5-ply specimen, was the fourth specimen to be tested in its group, and was subjected to a second shot). The term 'shot' in this instance refers to one test in which a specimen is dynamically loaded using the shock tube. Additional details of the results can be found in Appendix B.

Table 4.3: Dynamic Test Results

Panel Type	Specimen / Test	P_R (kPa)	I_R (kPa · ms)	R_{max} (kN)	Δ_{Rmax} (mm)	Δ_{max} (mm)	μ	$t_{f\text{-}max}$ (ms)	$\dot{\varepsilon}$ (s^{-1})	K_{Static} (kN/mm)	Failure Mode
CLT3	CLT3-4.1	11.6	90.0	-	-	16.1	-	26.8	5.00 x 10-2	1.59	Elastic
	CLT3-4.2	38.7	379.3	82.1	37.7	105.2	2.8	48.8	1.61 X 10-1	1.59	Rolling Shear
	CLT3-5.1	48.2	442.3	80.7	40.5	88.6	2.2	25.6	1.44 x 10-1	2.10	Flexural
	CLT3-6.1	52.6	613.7	88.3	45.8	143.7	3.1	35.0	1.52 x 10-1	1.88	Flexural
	CLT3-7.1	6.5	79.1	-	-	11.8	-	30.6	2.86 x 10-2	1.77	Elastic
	CLT3-7.2	52.8	439.9	-	-	119.2	-	47.2	1.58 x 10-1	1.77	Rolling Shear
	CLT3-8.1	5.8	59.4	-	-	10.1	-	28.0	2.16 x 10-2	1.66	Elastic
	CLT3-8.2	49.0	467.7	-	-	89.5	-	26.0	1.79 x 10-1	1.66	Rolling Shear then Flexural
	CLT3-9.1	12.2	131.2	-	-	18.7	-	31.2	5.22 x 10-2	1.76	Elastic
	CLT3-9.2	30.9	322.4	-	-	58.4	-	38.8	1.32 x 10-1	1.76	Rolling Shear
	CLT3-10.1	9.1	92.6	-	-	12.3	-	26.2	3.61 x 10-2	2.10	Elastic
	CLT3-10.2	34.0	374.4	-	-	99.4	-	79.6	1.58 x 10-1	2.10	Flexural
	CLT3-11.1	9.2	106.5	-	-	11.7	-	26.5	3.52 x 10-2	2.09	Elastic
	CLT3-11.2	32.9	345.4	-	-	72.5	-	35.2	1.19 x 10-1	2.09	Flexural
	Average	-	-	83.7	41.3	112.5	2.7	-	-	-	-
	COV	-	-	0.04	0.08	0.21	0.14	-	-	-	-
CLT5	CLT5-4.1	53.7	610.4	176.7	32.4	80.7	2.5	34.2	2.05 x 10-1	5.64	Flexural
	CLT5-5.1	58.6	690.7	171.7	29.6	58.2	2.0	26.2	1.80 x 10-1	5.14	Rolling Shear
	CLT5-6.1	7.2	81.7	-	-	6.5	-	22.4	2.56 x 10-2	5.53	Elastic
	CLT5-6.2	55.8	602.4	-	-	77.9	-	31.4	2.13 x 10-1	5.53	Flexural
	CLT5-7.1	7.3	81.8	-	-	6.4	-	22.8	3.28 x 10-2	5.07	Elastic
	CLT5-7.2	51.2	481.2	-	-	37.0	-	24.2	2.12 x 10-1	5.07	Flexural
	Average	-	-	174.2	31.0	69.5	2.3	-	-	-	-
	COV	-	-	0.01	0.04	0.16	0.11	-	-	-	-

Prior to being subjected to destructive dynamic tests, eight of the specimens were subjected to a low pressure-impulse combination loading in order to generate an elastic response. Careful consideration was taken when subjecting the specimen to these small dynamic loads as to prevent premature rolling shear or other damage. Following each elastic test, specimens were examined to ensure no visible damage was observed. The results of these tests were helpful in determining whether there was an increase in stiffness and also to aid in model validation. The results of the elastic dynamic shots is also included in Table 4.3. Figure 4.6 presents an example of an elastic shot for specimen CLT3-7.1, where Figure 4.6(a) presents the pressure- and impulse-time histories and Figure 4.6(b) presents the displacement- and strain-time histories.

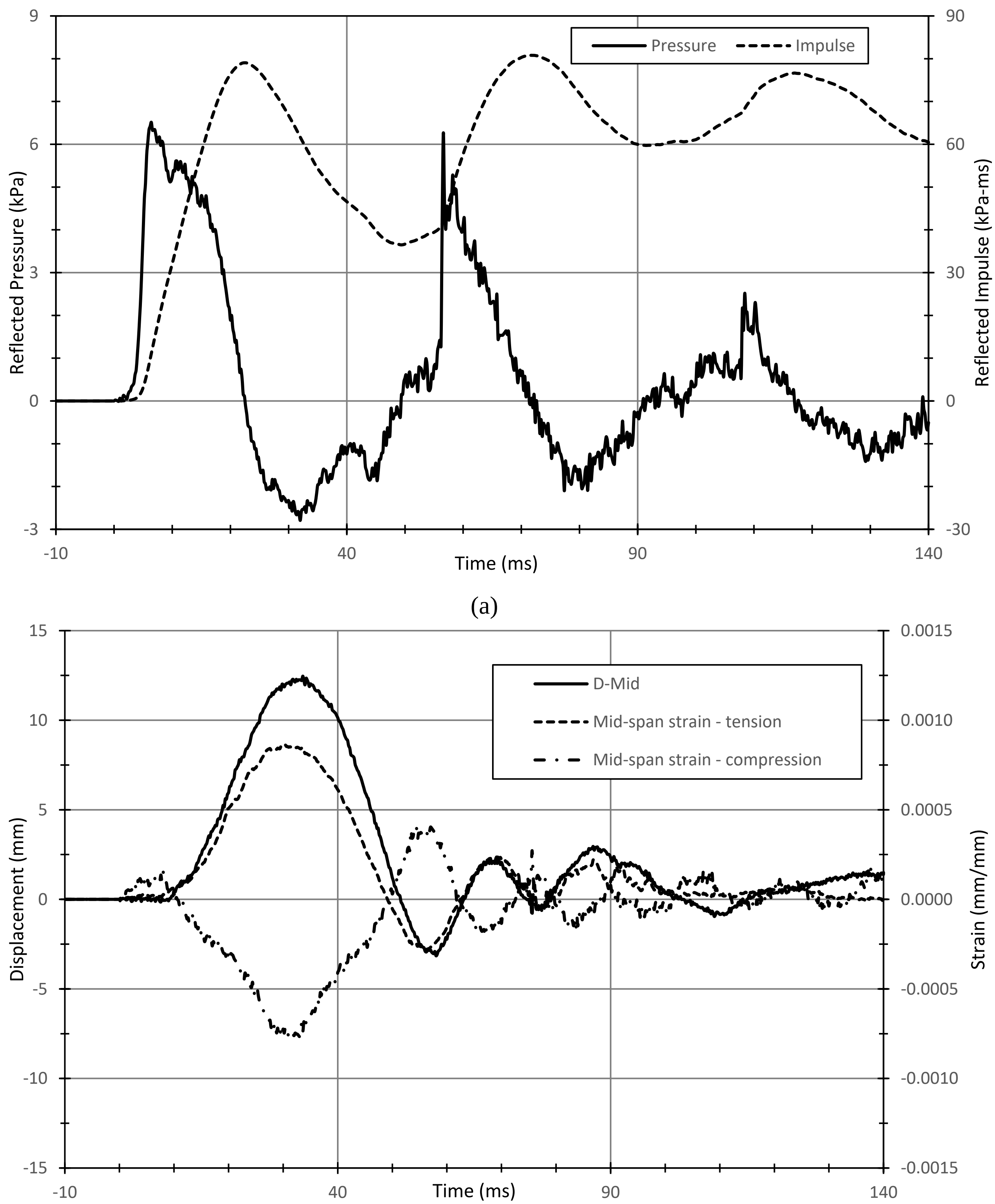

(a)

(b)

Figure 4.6 Dynamic elastic loading for CLT3-7.1: (a) presure- and impulse-time histories; (b) displacement- and strain-time histories

The observed failure modes under dynamic loading differed from those observed under static loading. Whereas the typical failure mode under static conditions for 3-ply and 5-ply panels consisted of flexural failure with observed rolling shear occurring near peak resistance, some specimens experienced significant rolling shear without necessarily failing in flexure. Typical pressure- and impulse-time histories and displacement- and strain-time histories of a rolling shear failure (panel CLT3-7.2) and flexural failure (CLT3-8.2) is present in Figure 4.7 and Figure 4.8, respectively. Figures 4.9 and 4.10 present examples of typical rolling shear failure (panel CLT3-4.2) and flexural failure (CLT3-5.1) taken from the test videos when the maximum displacement is reached.

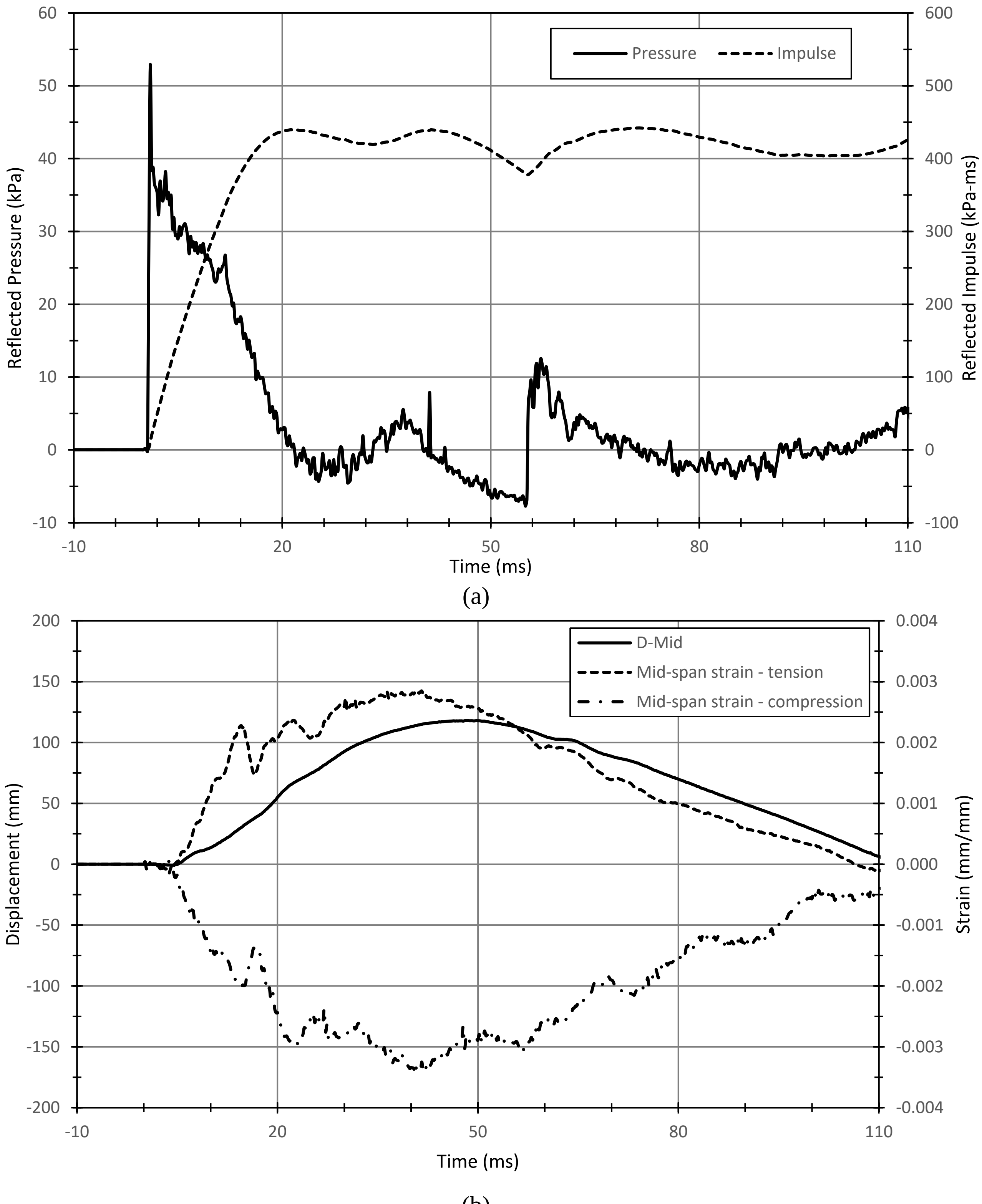

Figure 4.7 Dynamic loading for CLT3-7.2 (rolling shear failure): (a) presure- and impulse-time histories; (b) displacement- and strain-time histories

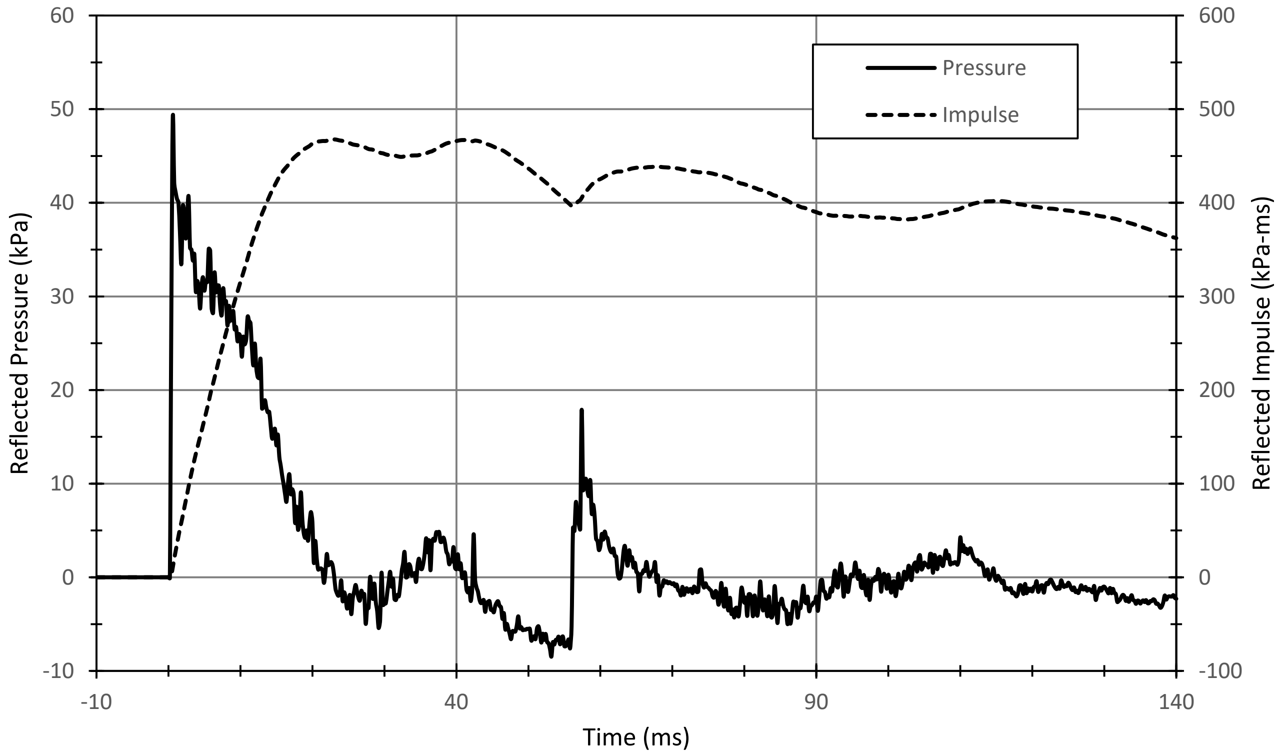

(a)

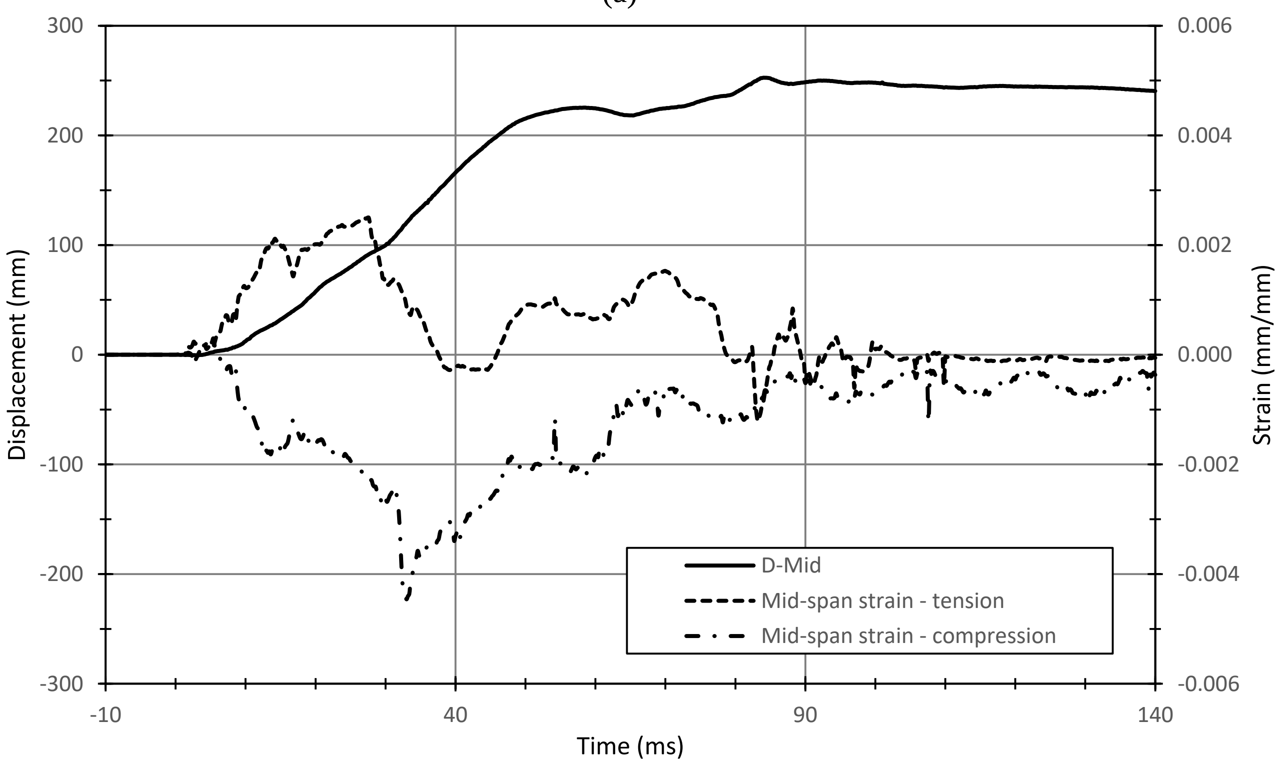

(b)

Figure 4.8 Dynamic loading for CLT3-8.2 (flexural failure): (a) presure- and impulse-time histories; (b) displacement- and strain-time histories

(a) (b) (c)

Figure 4.9: Rolling shear failure (CLT3-4.2): (a) rolling shear at maximum displacement; (b) outline of rolling shear damage on left side of panel; (c) outline of rolling shear damage on right side of panel

(a) (b) (c) (d)

Figure 4.10: Flexural failure (CLT3-5.1): (a) maximum displacement prior to failure; (b) flexural failure in the tension laminates; (c) failed panel post-test; (d) flexural failure through a series of finger joints

In general, the specimens that experienced rolling shear often saw minimal or no flexural damage. Furthermore, once rolling shear occurred, the composite action was ineffective and the longitudinal laminates deflected as individual studs. This allowed for larger deflections to be recorded prior to flexural failure relative to the specimens in which composite action had not been lost. Flexural failures were similar to those observed in static loading with little rolling shear observed. Similar to static loading, tension-side flexural failure originated in areas having finger joints or wood defects, followed by a propagation of the failure across the width of the panel along other joints or defects. The following presents a brief description of observed damage for each panel.

4.3.1 CLT3-4

Panel CLT3-4 was subjected to two different pressure and impulse combinations. The first shot resulted in a reflected pressure of 11.6 kPa and a reflected impulse of 90.0 kPa-ms over a positive phase of 18.0ms. The maximum recorded displacement was 16.1 mm, which occurred at an average time of 26.8ms. An inspection of the specimen post shot showed that the panel had no signs of rolling shear or other damage.

The second shot resulted in a reflected pressure of 38.7 kPa and a reflected impulse of 379.3 kPa-ms over a positive phase of 21.7ms. The maximum recorded displacement was 105.2 mm, which occurred at an average time of 48.8ms. The maximum dynamic resistance was determined to be 82.1 kN. The specimen experienced significant rolling shear near the supports and no observable flexural damage in the tension laminates was noted.

4.3.2 CLT3-5

Panel CLT3-5 was subjected to a single destructive shot. The shot resulted in a reflected pressure of 48.2 kPa and a reflected impulse of 442.3 kPa-ms over a positive phase of 19.8ms. The maximum recorded displacement was 88.6 mm, which occurred at an average time of 25.6ms following the initial reflected shock wave. The maximum dynamic resistance was determined to be 80.7 kN. The specimen failed in flexure along finger joints located in the tension laminates. Little to no rolling shear damage was observed at or near the supports. Most rolling shear was located at mid-span in the area of flexural failure. Based on video review, it was noted that rolling shear occurred after the flexural failure of the tension laminates.

4.3.3 CLT3-6

Panel CLT3-6 was subjected to a single destructive shot. The shot resulted in a reflected pressure of 52.6 kPa and a reflected impulse of 613.7 kPa-ms over a positive phase of 30.3ms. The maximum recorded displacement was 143.7 mm, which occurred at an average time of 35.0ms following the initial reflected shock wave. The maximum dynamic resistance was determined to be 88.3 kN. This specimen was retrofitted to eliminate potential failure in rolling shear and to induce a flexural failure. The specimen failed in flexure along finger joints located in the tension laminates. No rolling shear damage was observed.

4.3.4 CLT3-7

Panel CLT3-7 was subjected to two different pressure and impulse combinations. The first shot was meant to generate an elastic response and resulted in a reflected pressure of 6.5 kPa and a reflected impulse of 79.1 kPa-ms over a positive phase of 22.5ms. The maximum recorded displacement was 11.8 mm, which occurred at an average time of 30.6ms following the initial reflected shock wave. An inspection of the specimen post shot showed that the panel had no signs of rolling shear or other damage. This was further confirmed by reviewing the recorded video.

The second shot was intended to load the panel destructively and resulted in a reflected pressure of 52.8 kPa and a reflected impulse of 439.9 kPa-ms over a positive phase of 21.7ms. The maximum recorded displacement was 119.2 mm, which occurred at an average time of 47.2ms following the initial reflected shock wave. The specimen failed in a combination of rolling shear and flexural damage, which occurred near two finger joint locations on the tension layer.

4.3.5 CLT3-8

Panel CLT3-8 was subjected to two different pressure and impulse combinations. The first shot was meant to generate an elastic response and resulted in a reflected pressure of 5.8 kPa and a reflected impulse of 59.4 kPa-ms over a positive phase of 18.5ms. The maximum recorded displacement was 10.1 mm, which occurred at an average time of 28.0ms following the initial reflected shock wave. An inspection of the specimen post shot showed that the panel had no signs of rolling shear or other damage. This was further confirmed by reviewing the recorded video.

The second shot resulted in a reflected pressure of 49.0 kPa and a reflected impulse of 467.7 kPa-ms over a positive phase of 23.0ms. The maximum recorded displacement was 89.5 mm, which occurred at an average time of 26.0ms. The panel failed in flexure which appears to have originated in a finger joint in the tension laminates and subsequently propagated across the panel width through adjacent finger joints and other defects. Based on video review, it was noted that rolling shear occurred near the panel supports just prior to the flexural failure of the tension laminates.

4.3.6 CLT3-9

Panel CLT3-9 was subjected to two different pressure and impulse combinations. The first elastic shot resulted in a reflected pressure of 12.2 kPa and a reflected impulse of 131.2 kPa-ms over a positive phase of 21.0ms. The maximum recorded displacement was 18.7 mm, which occurred at an average time of 31.2ms. An inspection of the specimen post shot showed that the panel had no signs of rolling shear or other damage. This was further confirmed by reviewing the recorded video.

The second destructive shot resulted in a reflected pressure of 30.9 kPa and a reflected impulse of 322.4 kPa-ms over a positive phase of 21.4ms. The maximum recorded displacement was 58.4 mm, which occurred at an average time of 38.8ms. The specimen experienced rolling shear without any observable signs of flexural damage in the tension laminates.

4.3.7 CLT3-10

Panel CLT3-10 was subjected to two different pressure and impulse combinations. The first shot resulted in a reflected pressure of 9.1 kPa and a reflected impulse of 92.6 kPa-ms over a positive phase of 18.6ms. The maximum recorded displacement was 12.3 mm, which occurred at an average time of 26.2ms. An inspection of the specimen post shot showed that the panel had no signs of rolling shear or other damage.

The second shot resulted in a reflected pressure of 34.0 kPa and a reflected impulse of 374.4 kPa-ms over a positive phase of 23.1ms. The maximum recorded displacement was 99.4 mm, which occurred at an average time of 79.6ms. The panel failed in flexure which appears to have originated in a finger joint in the tension laminates and subsequently propagated across the panel width through adjacent finger joints and natural wood defects. Based on video review, it was noted that rolling shear occurred after flexural failure of the tension laminates had begun. There was no evidence of rolling shear occurring at or near the supports.

4.3.8 CLT3-11

Panel CLT3-11 was subjected to two different pressure and impulse combinations. The first shot was meant to generate an elastic response and resulted in a reflected pressure of 9.2 kPa and a reflected impulse of 106.5 kPa-ms over a positive phase of 19.4ms. The maximum recorded displacement was 11.7 mm, which occurred at an average time of 26.5ms. An inspection of the specimen post shot showed that the panel had no signs of rolling shear or other damage.

The second shot was to load the panel destructively and resulted in a reflected pressure of 32.9 kPa and a reflected impulse of 345.4 kPa-ms over a positive phase of 21.4ms. The maximum recorded displacement was 72.5 mm, which occurred at an average time of 35.2ms. Observable damage was similar to that of panel CLT3-7. Several finger joints in the tension laminates were located at mid-span which lead to the flexural failure of the panel. Little to no rolling shear damage was observed at or near the supports. Most rolling shear was located at mid-span in the area of flexural failure. Based on video review, it was noted that rolling shear occurred after the flexural failure of the tension laminates.

4.3.9 CLT5-4

Panel CLT5-4 was subjected to a single destructive shot. The shot resulted in a reflected pressure of 53.7 kPa and a reflected impulse of 610.4 kPa-ms over a positive phase of 23.8ms. The maximum recorded displacement was 80.7 mm, which occurred at an average time of 34.2ms. The maximum dynamic resistance was determined to be 176.7kN. The panel failed in flexure which appears to have originated in a finger joint in the tension laminates and subsequently propagated across the panel width through adjacent finger joints and natural wood defects. There was relatively little rolling shear damage observed. The majority of the rolling shear damage was near the upper support and in the area of the flexural failure.

4.3.10 CLT5-5

Panel CLT5-5 was subjected to a single destructive shot. The shot resulted in a reflected pressure of 58.6 kPa and a reflected impulse of 690.7 kPa-ms over a positive phase of 22.6ms. The maximum recorded displacement was 58.2 mm, which occurred at an average time of 26.2ms. The maximum dynamic resistance was determined to be 171.7kN. The specimen failed in rolling shear. The majority of the noted rolling shear damage was near the upper support. No observable flexural damage in the tension laminates was noted.

4.3.11 CLT5-6

Panel CLT5-6 was subjected to two different pressure and impulse combinations. The first elastic shot resulted in a reflected pressure of 7.2 kPa and a reflected impulse of 81.7 kPa-ms over a positive phase of 19.9ms. The maximum recorded displacement was 6.5 mm, which occurred at an average time of 22.4ms following the initial reflected shock wave. An inspection of the specimen post shot showed that the panel had no signs of rolling shear or other damage.

The second shot was to load the panel destructively and resulted in a reflected pressure of 55.8 kPa and a reflected impulse of 602.4 kPa-ms over a positive phase of 24.5ms. The maximum recorded displacement was 77.9 mm, which occurred at an average time of 31.4ms. The panel failed in flexure along a series of finger joints located in the maximum moment region. Significant rolling shear damage was noted primarily near the lower support. Based on video review, it was noted that rolling shear occurred prior to flexural failure

4.3.12 CLT5-7

Panel CLT5-7 was subjected to two different pressure and impulse combinations. The first elastic shot resulted in a reflected pressure of 7.3 kPa and a reflected impulse of 81.8 kPa-ms over a positive phase of 21.1ms. The maximum recorded displacement was 6.4 mm, which occurred at an average time of 22.8ms. An inspection of the specimen post shot showed that the panel had no signs of rolling shear or other damage.

The second shot was to load the panel destructively and resulted in a reflected pressure of 51.2 kPa and a reflected impulse of 481.2 kPa-ms over a positive phase of 23.4ms. The maximum recorded displacement was 37.0 mm, which occurred at an average time of 24.2ms. The specimen failed in rolling shear. The majority of the noted rolling shear damage was near the lower support. No observable flexural damage in the tension laminates was noted.

4.4 Residual Stiffness Test Results

Panels that did not fully exhibit flexural failure were subsequently tested statically in order to determine their residual stiffness. It was found that the stiffness of the specimens that had rolling shear damage only varied between 20% and 35% of their original stiffness while the 5-ply panel that had flexural damage in the first tension laminate only had a residual stiffness of approximately 10% of its stiffness obtained in its original undamaged state. The residual testing results are presented in Table 4.4. The residual static load resistance curves for all three tested specimens are shown in Figure 4.11. These quantities represent the stiffness degradation which is a function of the pressure-time history and the extent of the damage in the transvers and longitudinal laminae due primarily to rolling shear, and therefore cannot be generalized. However, these values were still useful in modeling the behaviour of the panels that had failed in rolling shear.

Table 4.4: Residual Static Test Results

Panel Type	Specimen	R_{max} (kN)	Δ_{Rmax} (mm)	Δ_{max} (mm)	μ	K (kN/mm)	$t_{f\text{-}max}$ (min)	M_{max} (kNm)
CLT3	CLT3-9	32.5	86.9	138.6	1.6	0.59	5.02	12.1
CLT5	CLT5-6	37.7	75.6	233.0	3.1	0.51	4.65	14.0
	CLT5-7	43.3	58.7	87.4	1.5	0.72	4.65	16.1
	Average	40.5	67.1	160.2	2.3	0.61	-	15.1
	COV	0.07	0.13	0.45	0.35	0.18	-	0.07

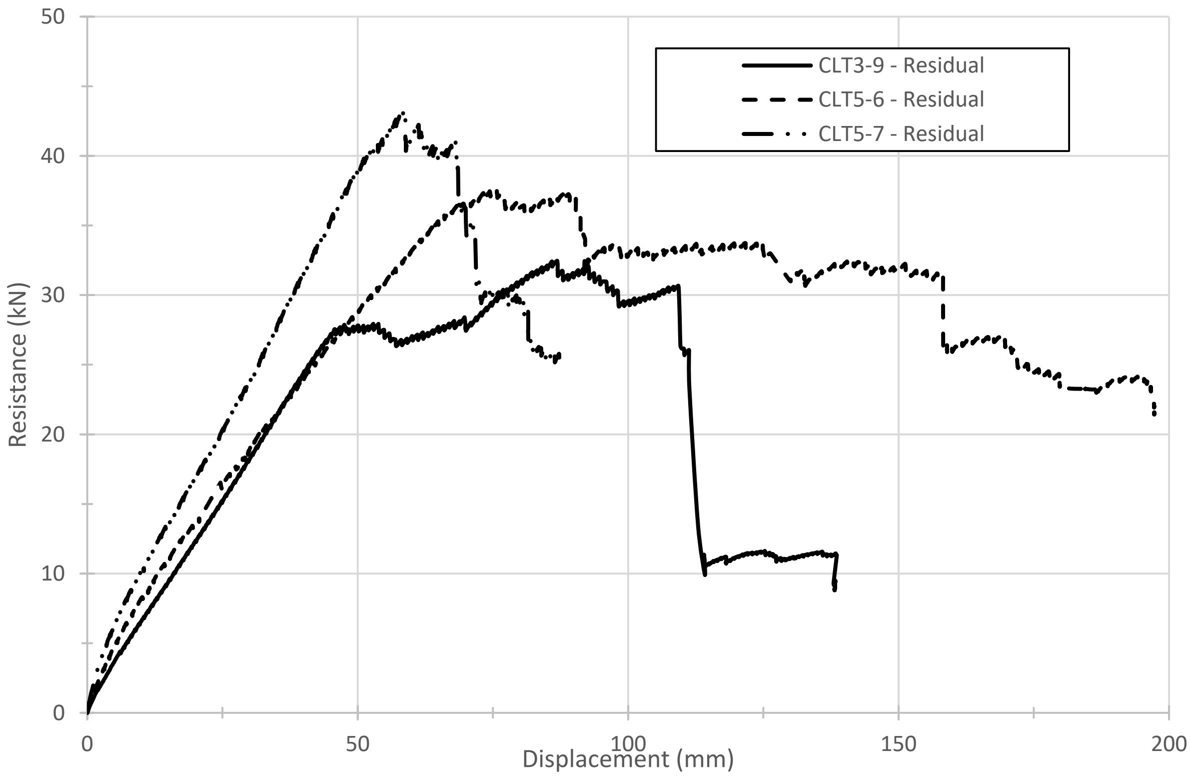

Figure 4.11: Residual static loading resistance curves for CLT panels

Chapter 5 – Analytical Modelling and Results

5.1 General

This chapter presents the methodology used to determine the dynamic increase factor (DIF) as well as the development of the material predictive model based on full scale testing and incorporating the predominant failure modes observed for CLT panels. The inputs used to develop the model are also presented below. It should be noted that the model developed during this research project is limited to slabs subjected to one-way bending with simply supported boundary conditions.

The dynamic displacement-time history predicted by the modeling procedure was obtained using the blast analysis software *RCBlast*® (Jacques, 2013). This software has been successfully used to model a variety of structural systems including reinforced concrete slabs (e.g. Jacques, 2011; Jacques et al., 2013), reinforced concrete columns (e.g. Lloyd, 2010; Burrell, 2012), light-frame wood stud walls (e.g. Lacroix, 2013; Viau, 2016), and glulam beams and columns (e.g. Lacroix, 2017).

5.2 Model Description and Inputs

The dynamic response of the CLT specimens was established through dynamic analysis using the SDOF methodology described in section 1.4. SDOF modelling requires that the structural system being analysed has a single independent coordinate used to describe the motion of the entire system. Therefore, the degree of freedom used in this modelling was the mid-span deflection. The assumed deflected shape for the analysis was that of a simply supported beam subjected to four-point bending. In this model, due to the short loading period and interest in the maximum dynamic response, damping was neglected (Biggs, 1964; Jansson, 1992; UFC, 2008) and the stiffness / displacement term was replaced with the resistance of the panel at a specific displacement, *R(y)*. For an undamped system, the SDOF equation of motion can be written as follows:

$$K_{LM} m\ddot{y}(t) + R(y) = AP_R\left(1 - \frac{t}{t_d}\right) \quad (5.1)$$

This equation and its terms are described in section 1.4. In equation 5.1, two different load-mass factors are required in order to account for the change in the assumed static shape from elastic to plastic mode. These load-mass factors are available in literature (Biggs, 1964; USACE, 2008), or can be determined using the assumed deflected shape along with equations 1.8, 1.9, and 1.11. In this case, the load-mass factors of 0.87 and 1.0 were used for the elastic and plastic regions, respectively. These load-mass factors are typical for concentrated mass. Whereas the CLT panel's mass is distributed, the LTD's mass is considered a concentrated mass, half of which is applied at each load application point. Some methods have been developed to reflect the actual position of the equivalent mass stemming from the mixed concentrated and distributed masses (Jacques, 2016; Lacroix, 2017). However, because the LTD offers significantly more mass to the system, especially when comparing to the 3-ply panels, it was deemed appropriate to approximate the system as a concentrated system for the purpose of using these factors. The mass of each specimen was measured prior to each test and adjusted based on the clear span of the members for the analysis. The participation of the mass located outside of the clear span was assumed to have negligible effects on the system. The average total system mass was 342.1 and 384.5 kg for the 3-ply and 5-ply systems, respectively.

Dynamic reactions at the supports were obtained with the use of load cells for a limited number of 3-ply and 5-ply panels in order to generate the experimental resistance curves for those specimens. Unlike static testing of specimens where the resistance of an element can be determined based on the total applied load, the inertial effects must be considered in the dynamic equilibrium (Biggs, 1964).

The dynamic reactions, *V(t)*, can be obtained by solving equation 5.2, which highlights its dependence on the experimentally measured beam resistance, *R(t)*, and the applied force, *F(t)*. This equation, provided in Biggs (1964), is derived by solving the internal dynamic equilibrium of the element at mid-span, which is done by taking the sum of moments about the inertia force. It was assumed that the LTD did not to contribute to the resistance. This analysis assumes that the inertia force has an identical distribution to that of the assumed deflected shape of the beam. As such, the intensity of the inertia force is proportional to the deflection.

$$V(t) = 0.525R(t) - 0.025F(t) \tag{5.2}$$

The forcing function is obtained by multiplying the pressure-time history, $P_r(t)$, and the loaded area, *A*. The loaded area was taken as 3.55 m^2, which is equal to the equivalent surface area of the LTD used to collect and transfer the pressure to the specimen. The forcing function used in all dynamic analyses was the actual pressure-time history.

The support reactions, *V(t)*, of the system is a function of the total mass provided by the specimen and the LTD. As the LTD formed a significant portion of the mass, equation 5.2 had to be modified in order to account for the significant influence on the inertia distribution. In addition, because the support reactions had been measured, it was desirable to solve the equation in order to determine the resistance of the specimen. Thus, the dynamic resistance can be determined using equation 5.3 (Jacques 2016, Lacroix 2017).

$$R(t) = \left(\frac{6}{L}\right)\left[V(t)x_{eq} + 0.5\left(\frac{L}{3} - x_{eq}\right)F(t)\right] \quad 5.3$$

$$x_{eq} = \frac{0.102\bar{m}L^2 + 0.290m_cL}{0.319\bar{m}L + 0.870m_c} \quad 5.4$$

where L is the clear span, x_{eq} is distance from the support to the point of application of an equivalent inertia force, $\bar{m}$ is the distributed mass of the specimen, and m_c is half of the mass of the load transfer device which is lumped at the load application point.

5.3 Determining the Dynamic Increase Factor

5.3.1 General

The dynamic increase factor (DIF) is the ratio of dynamic to static strength of a material, typically reported as a function of the strain rate as higher strain rates associated with dynamic loads lead to an increase of material strength. In timber design based on CSA O86 – Engineering Design in Wood, there is an additional increase factor called the load duration factor, K_D, which impacts the resistance of wood material based on the duration of the load. The CSA O86 (CSA 2014) allows for an increase of 15% in specified strength based standard load duration (two months) when subjected to short term loading defined as continuous or cumulative loading not exceeding seven days (CSA O86-09, 2009). Loading of this nature include wind and seismic loads. However, when calculating the blast load resistance, this load duration factor is assumed to be 1.0 in the blast design code (CSA S850-12, 2012).

5.3.2 Dynamic Increase Factor Results

The dynamic increase factors for both 3-ply and 5-ply panels were determined by comparing experimentally obtained static and dynamic resistance displacement relationships. The comparison of these relationships, as shown in Figure 5.1, demonstrates an increase in strength with no observable increase in stiffness. Increase factors for resistance were determined by dividing the peak dynamic resistance of each tested specimen by the average static resistance. The resulting increase factors were then averaged to obtain a single dynamic increase factor. Results of dynamic testing using ultimate pressure-impulse combinations only were used to determine the DIF. By plotting the peak static and dynamic resistance for each specimen, an average DIF of 1.28 was collectively observed for 3-ply and 5-ply panels, with a COV of 0.06, as shown in Figure 5.2.

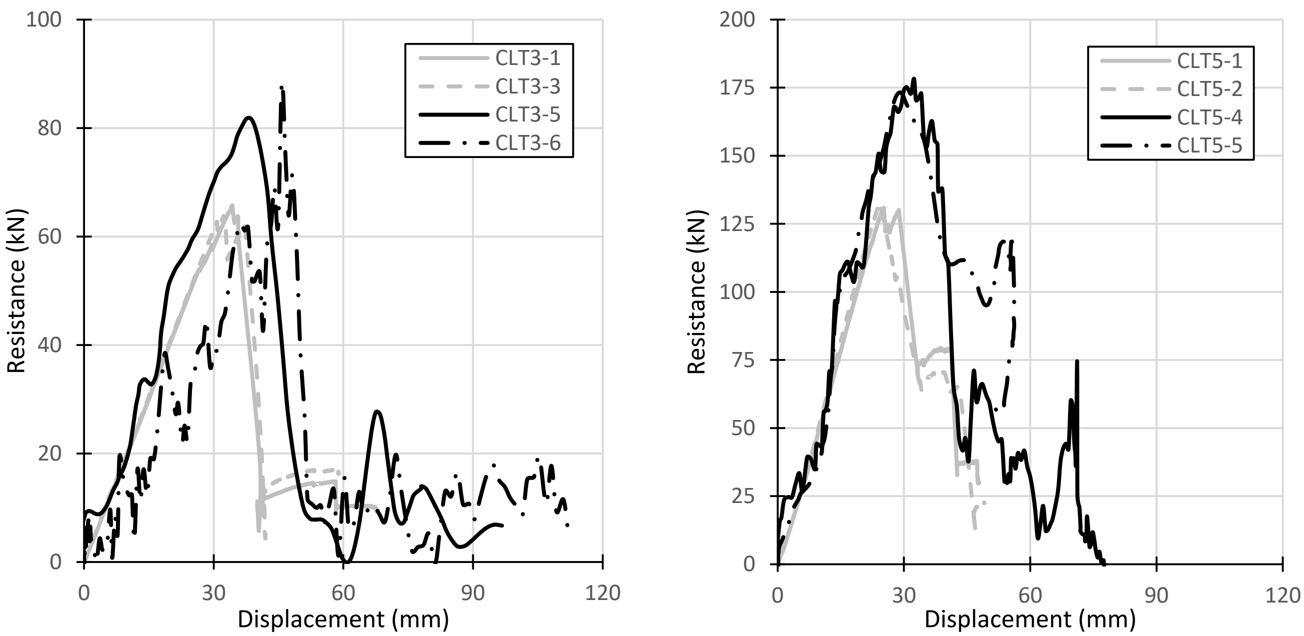

(a) 3-ply (b) 5-ply

Figure 5.1: Experimental static and dynamic resistance-displacement curves: (a) 3-ply; (b) 5-ply

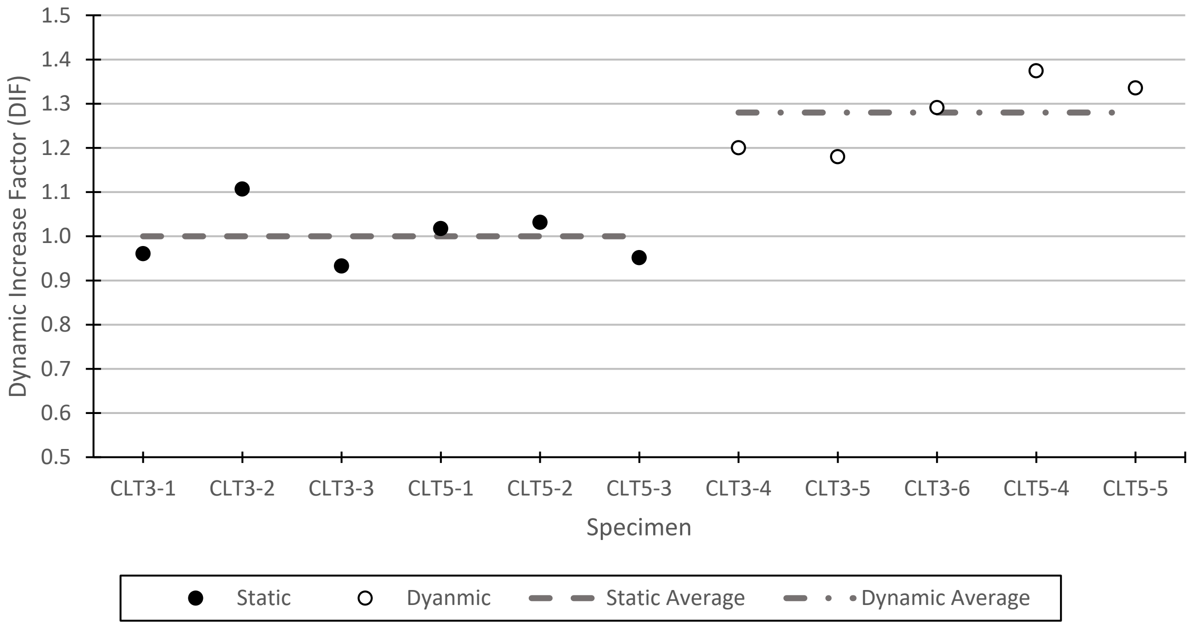

Figure 5.2: Dynamic Increase Factor in CLT Specimens

5.4 Material Predictive Model

5.4.1 General

The simplified approach described in section 5.2 to model the response of structural elements to blast loading has been shown to provide accurate predictions without resorting to resource-intensive finite element analysis (Jacques, 2011, Lacroix and Doudak, 2015, Barreiro, 2016, Viau and Doudak, 2016). Throughout dynamic testing, two predominant failure modes were noted, namely: flexure and rolling shear. When developing the appropriate resistance curves for the tested CLT specimens, it was important to take into consideration the type of failure mode, the post-peak residual behaviour, and ductility of the panels. Therefore, two different resistance curves were developed to properly reflect the type of failure mode observed. Development of the resistances will be discussed further in Chapter 6. Once the resistance curves were obtained, the displacement-time histories were generated using *RCBlast* (Jacques, 2013). Actual pressure-time histories from testing were inputed into the software, along with recorded deformation-time response and the developed resistance curves. The model was validated by comparing the predicted deformation-time response produced by the software to the experimentally obtained deformation-time history of CLT tests employing load cells.

5.4.2 Flexure Model

The ultimate dynamic resistance, R_u, and elastic limit, X_e, of the CLT panels failing in flexure were determined using Equations 5.5 and 5.6, respectively.

$$R_u = \frac{6 * DIF * M}{L} \qquad 5.5$$

$$X_e = \frac{R_u}{K} \qquad 5.6$$

where *DIF* is the average dynamic increase factor, *M* is the average experimental static moment capacity, *L* is the clear span of the panels, and *K* is the average static stiffness of the element. The static stiffness used in this model was based on the average stiffness calculated from the experimental resistance curves for each specimen type. The static stiffness was calculated by dividing the ultimate resistance by the mid-span deflection measured at that point. The clear span of the specimen remained constant at 2235 mm for all tests. The post peak behaviour was determined based on the observed post-peak resistance, ductility, and stiffness for both the 3-ply and 5-ply panels. The ultimate static resistance could be obtained through readily available static models such as those detailed in the CLT Handbook (FPInnovations, 2011), however the post peak resistance could not be obtained through this method.

For the 3-ply specimen, the post-peak behaviour was modelled as a sudden drop in resistance, which represents the loss of the outer longitudinal and transverse laminates. Similarly for the 5-

ply specimens, there is an initial drop in resistance post-peak which is explained through the loss of the outer longitudinal and transverse laminates. This failure mechanism implies that the specimen would then behave as a 3-ply panel. The observed behaviour confirmed that the initial drop in resistance would then equate to the ultimate resistance of a 3-ply panel. This can be seen in Figure 5.3, which overlays the experimental static resistance curves for the 5-ply and 3-ply panels tested. A second drop in resistance is then observed at an equivalent deflection equal to that of the elastic limit of the equivalent 3-ply panel. At this point, the resistance drops to a value equivalent to 20% of the ultimate resistance for the 5-ply specimen. This represents the continuing damage endured by the panel and the loss of the central longitudinal laminates. The value of resistance drop to 20% of ultimate resistance was determined through experimental testing and seemed to correlate well with the observed behaviour obtained during static testing. However, whether this observed 20% drop in resistance can be generalized for all CLT panels is unclear due to the relatively limited number of tests completed. The post-peak residual deflections were limited to a maximum ductility ratio of 2.5, based on experimental findings and previous research (Gromala, 1983, Liu and Bulleit, 1995, Lacroix and Doudak, 2015, Viau, et al., 2015, Viau, 2016).

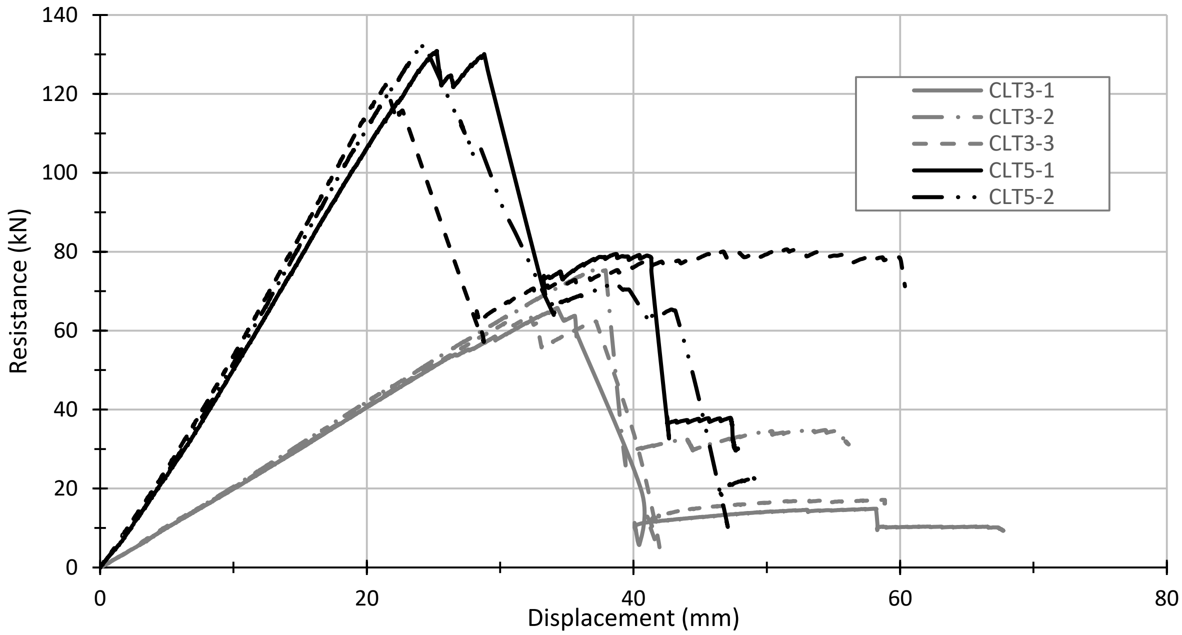

Figure 5.3: Comparison of 3-Ply and 5-Ply Load Resistance Curves

For the 5-ply panels, once the outer tension laminate had failed due to flexure, rolling shear had generally also occurred in the transverse laminate thus only allowing for partial composite action between the remaining two layers of tension laminates. This lead to a significant drop in stiffness, which seemed to align reasonably well with the stiffness of 3-ply panels, as can be seen in Figure 5.3. However, the post-peak resistance following the initial drop was modelled as a plateau up to the second drop in resistance, which was equivalent to the first drop in resistance observed in 3-ply specimens. Representative flexural resistance curves are shown in Figure 5.4 for the 3- and 5-ply specimens. The comparison between the experimental displacement-time history and the results by RCBlast utilizing the SDOF model is shown in Figure 5.5.

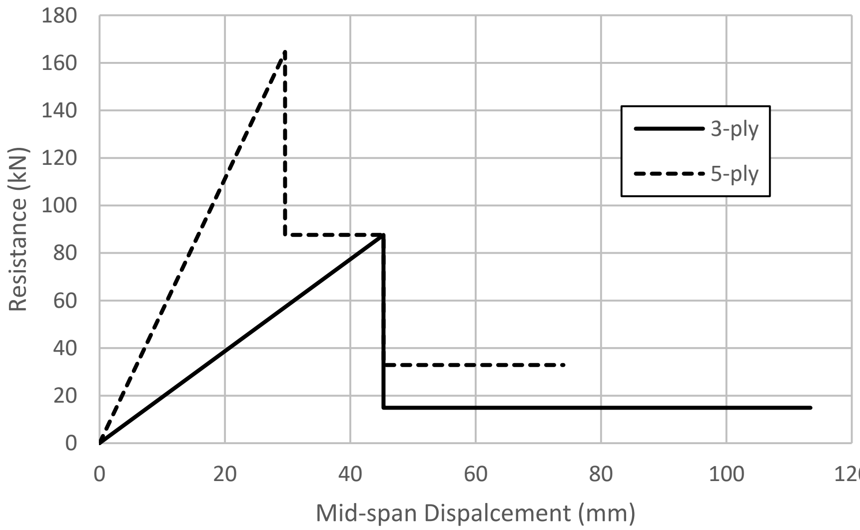

Figure 5.4: Dynamic Resistance Curves for Flexural Failure

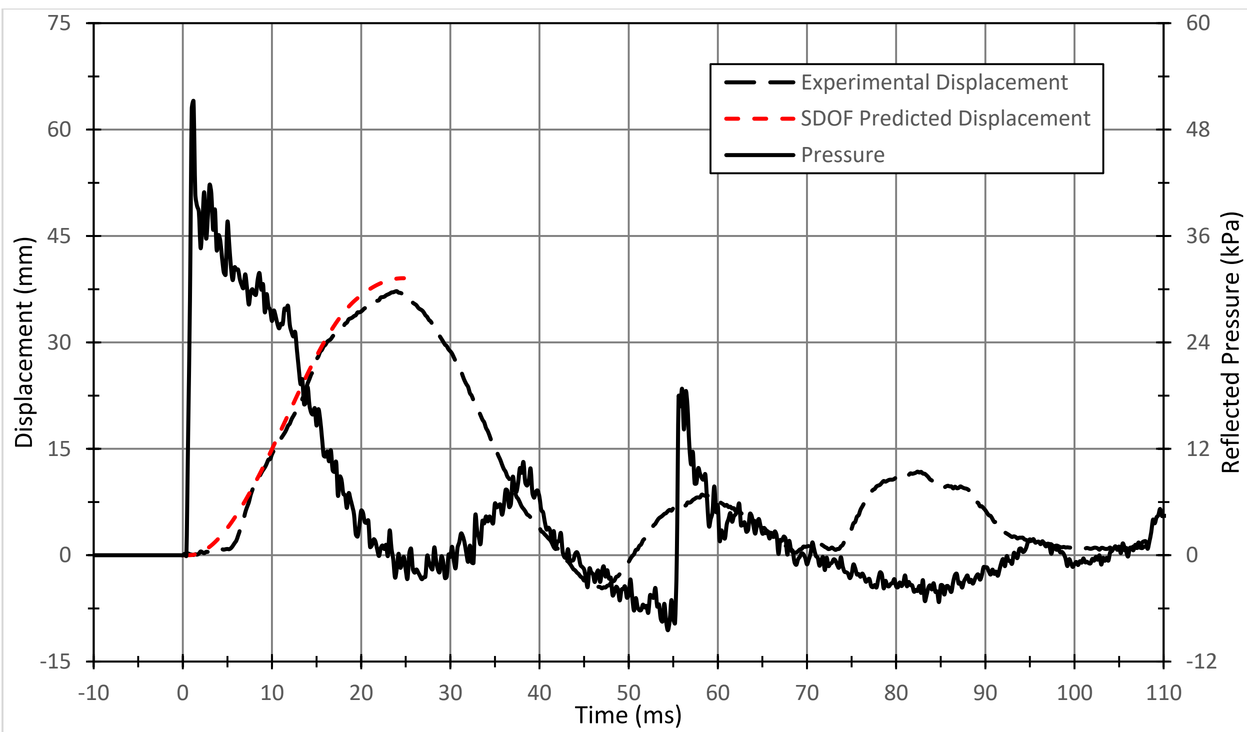

Figure 5.5: SDOF Model Results Compared to Experimental Displacement-Time History for Flexure Model (Specimen CLT3-4.2)

5.4.3 Rolling Shear Model

Specimens in which rolling shear failure occurred prior to flexural failure necessitated a modified approach in order to accurately capture this behaviour. In design, rolling shear is the governing failure mode for CLT bending elements. When rolling shear failure fully develops, the transverse layers experience heavy damage and provide weaker connectivity between longitudinal laminate layers. As such, the individual layers of the panel no longer behave as one rigid component, but rather as individual, largely undamaged elements. High speed video recordings were taken of dynamically tested specimens and were reviewed in order to determine which specimens failed in rolling shear, as well as to determine the time and displacement at which the rolling shear failure became apparent. By knowing the stiffness of the specimen and the displacement at which the rolling shear occurred, it was possible to determine the dynamic rolling shear resistance. The change from full composite to partial composite action between the laminates caused a reduction in stiffness on the order of 65% to 80%. This was determined through static testing of panels having already been tested dynamically in the attempt to determine their residual capacity and stiffness. A representative resistance curve modified for rolling shear failure is shown in Figure 5.6. The comparison between the experimental displacement-time history and analytical results utilizing this modified SDOF model is shown in Figure 5.7.

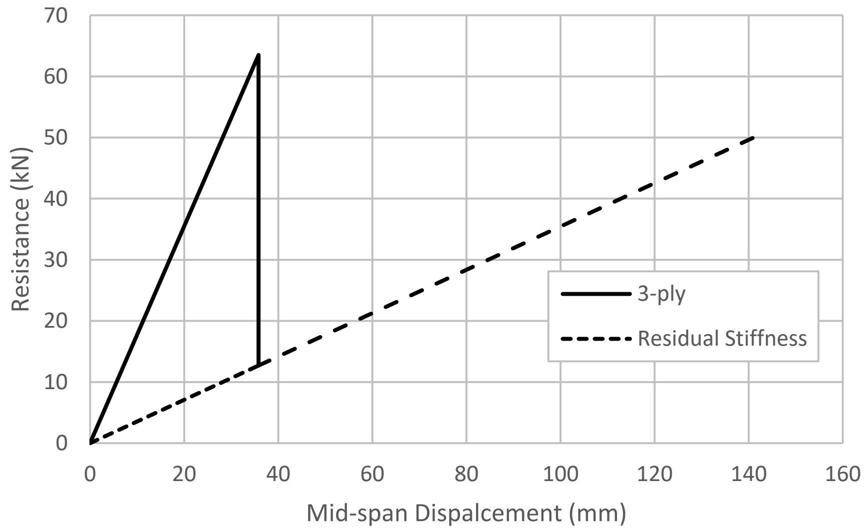

Figure 5.6: Dynamic Resistance Curves for Rolling Shear Failure

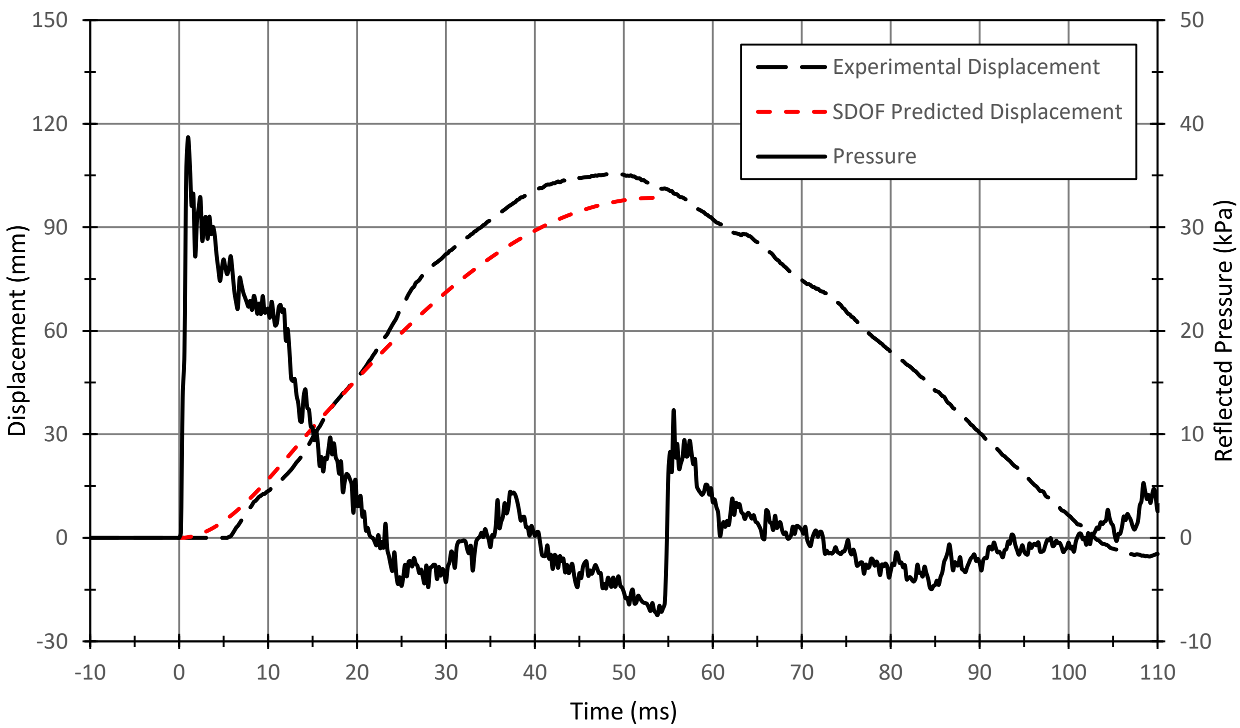

Figure 5.7: SDOF Model Results Compared to Experimental Displacement-Time History for Rolling Shear Model (Specimen CLT3-4.2)

Chapter 6 –Discussion

6.1 General

A total of eighteen CLT specimens were tested to failure under static and dynamic loading in order to investigate the effects of high strain rates and to determine the dynamic increase factor. The study was limited in scope to simply supported slab elements of constant span and width (aspect ratio). It should be noted that axial loading and its effects were not considered throughout this study. Although CLT panels in the lay-ups tested in this study (i.e. 3-ply and 5-ply) are routinely used as load bearing wall segments, and that axial load effects could have a significant impact on the behaviour of the panels, it was decided to omit these effects in order to establish a baseline panel response. It can be argued that establishing the strain rate effects, which is a material property, could be done independently of whether axial loads are present in the investigation. Future studies can build on the findings of the current study in order to investigate the myriad variety in loading conditions, boundary conditions, panel lay-ups and configurations, etc.

6.2 Observed Failure Modes

All CLT specimens tested had a consistent failure under static loading conditions. The elements failed in a combination of flexural failure, represented by failure in the tension laminates, and rolling shear failure in the transverse laminates. The flexural failure was clearly observed in the maximum moment zone (between the load application points), and the rolling shear failure occurred in the area of maximum shear (between the load application point and supports). Flexural failures in the tension laminates typically originated at a finger joints or other natural defects within the individual laminates. Failure would generally initiate within a narrow board along the edge of the panel and stagger across the tension laminates through adjacent finger joints or defects in the wood. Typical flexural failures of the tension laminates are shown in Figure 6.1. Typical rolling shear failure in the transverse laminates are shown in Figure 6.2.

(a)

(b)

(c)

(d)

Figure 6.1: Typical static flexural failures: (a) shearing of finger joint; (b) failure of tension layer along finger joints; (c) separation of finger joint; (d) rupture of tension laminate at wood defect

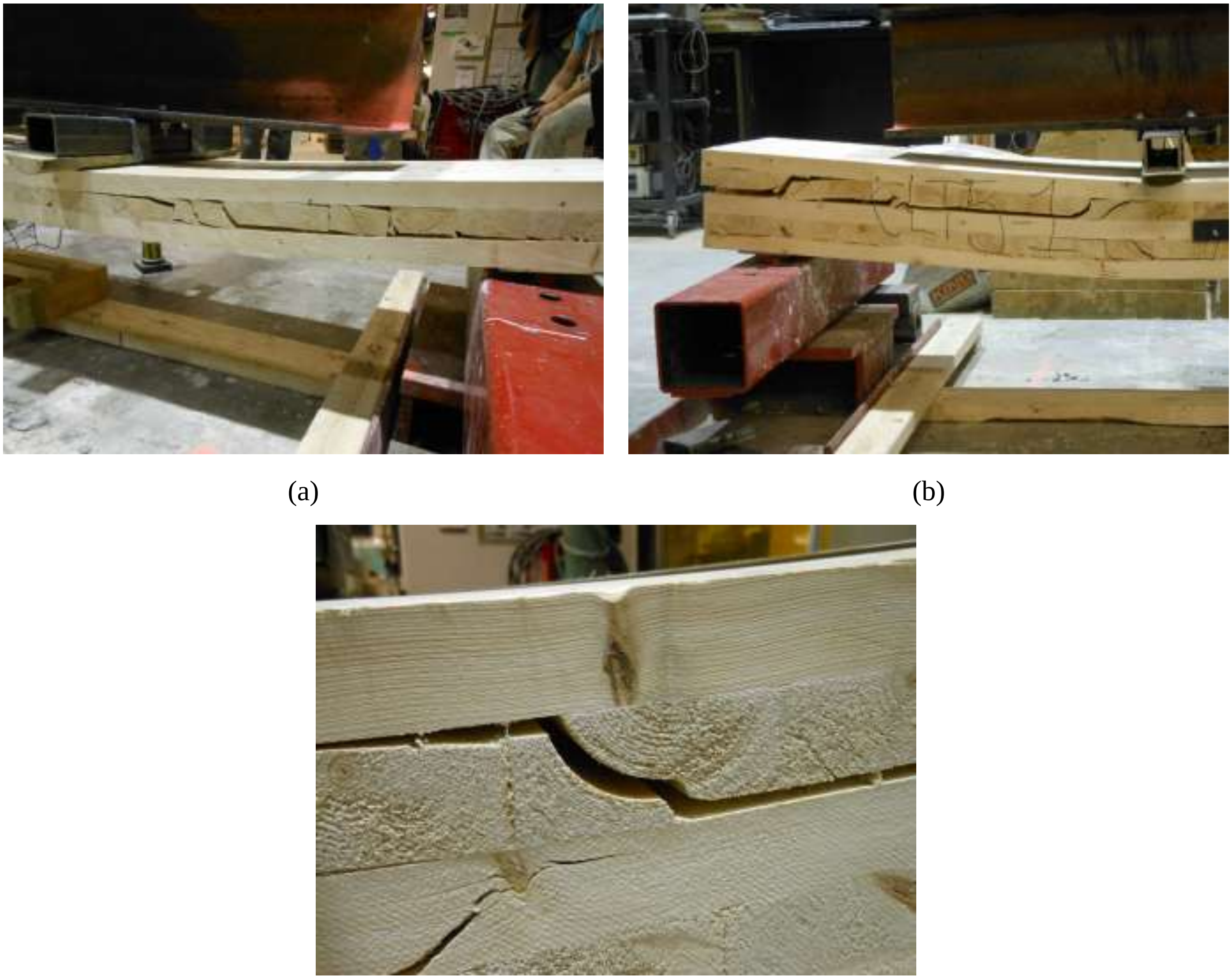

(a) (b)

(c)

Figure 6.2: Typical static rolling shear failures: (a) rolling shear in 3-ply panel; (b) rolling shear in 5-ply panel; (c) rolling shear at growth ring

During the dynamic testing two different failure modes were observed. The first consisted of flexural failure originating in the outer tension laminates of the panel in the maximum moment zone with rolling shear developing simultaneously in the maximum shear zones, similar to what was observed in the statically tested specimens. Specimens having fingers joints in the outer laminates within the high moment area consistently had failure initiated at the finger joint location. Interestingly, unlike the slow separation of fingers observed during static testing, finger joint failures in dynamic testing would typically consist of the fingers having been sheared off one of the jointed planks. This may be an indication that adhesives used in finger joint fabrication could experience their own dynamic increase factor independent of that found in wood. However, further testing would be required to examine and correlate these observations. Typical flexural failures in dynamic specimens are shown in Figure 6.3 and typical rolling shear failures in dynamic specimens are shown in Figure 6.4.


(a) (b)


(c) (d)

Figure 6.3: Typical dynamic flexural failures: (a) failure along finger joints; (b) failure at FJ and wood defects; (c) separation of finger joint; (d) rolling sheer following flexural failure

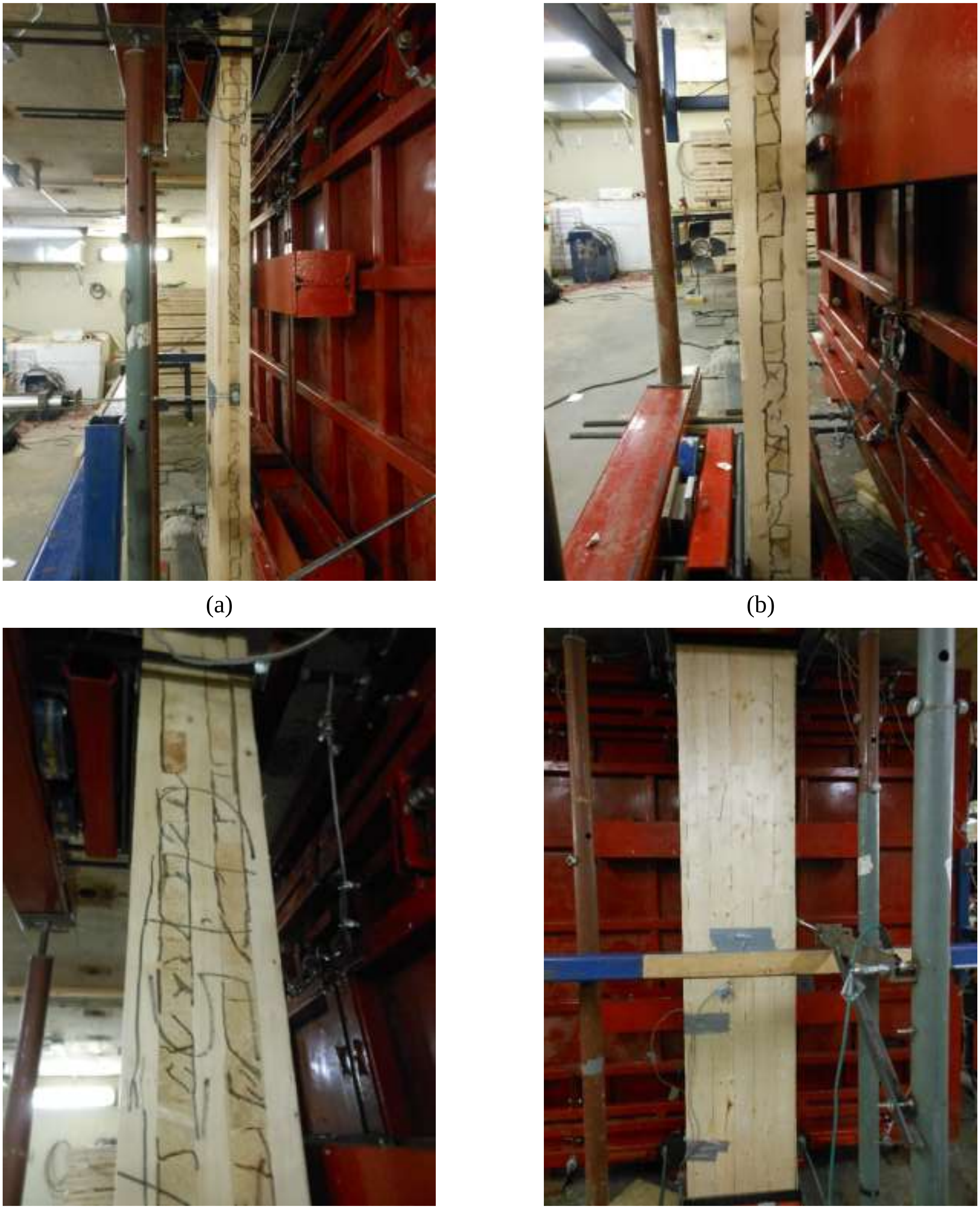

(a) (b) (c) (d)

Figure 6.4: Typical dynamic flexural failures: (a) rolling shear along full length of 3-ply panel; (b) rolling shear in shear zone; (c) rolling shear in 5-ply panel; (d) minimal flexural damage following rolling shear

The second failure mode observed was that of rolling shear occurring in the shear zone with no significant damage to the tension laminates. Significant reduction in the panel stiffness was observed and as described in section 5.4.3, the residual stiffness of the panels was reduced by 65% to 80%. In addition, the panels' peak residual resistance was approximately 40% to 50% lower than the average static peak resistance of their undamaged counterparts. This reduction in capacity was attributed to loss of composite action between layers between the longitudinal and transverse layers. Factors that can incite rolling shear to occur include overall panel dimensions, individual laminate dimensions, layups, and presence of edge glue. Rolling shear is a complex failure mode, incorporating tension forces perpendicular to grain, generally perpendicular to annual ring orientation, and shear forces (Nie, 2015).

6.3 Dynamic Increase Factor

Similarly to other materials, wood experiences an increase in capacity when subjected to high strain rate loading. This phenomenon has been demonstrated in solid sawn visually graded lumber (Jacques et al., 2013), machine stress rated (MSR) lumber (Lacroix, 2013), as well as glued-laminated timber (Lacroix, 2017). The dynamic increase factor is defined as the ratio of the dynamic to static strength. As demonstrated in section 5.3.2, the average increase in capacity was determined to be 1.28 for both 3-ply and 5-ply panels. This DIF can be applied when designing 3-ply and 5-ply CLT members for flexural strength subjected to strain rates in the range of 2.16×10^{-2} to 2.13×10^{-1} s^{-1}. At the time of writing this thesis, the provisions in the Canadian blast design standard (CSA, 2012) allow for a DIF of 1.4 to be applied to static strengths of Glulam and engineered wood products subjected to far-field blast loads. This value was proposed pending further testing. A recent research project conducted at the University of Ottawa by Lacroix (2017) suggested that a more appropriate DIF for glulam members in bending be 1.14, for members without continuous finger joints in the outer laminates, and 1.0 (i.e. no applicable DIF) for members where finger joint discontinuity cannot be guaranteed. In addition, the author suggested that a DIF of unity be used when considering stiffness. While there was no observed increase in stiffness from static to dynamic loading, the results from the current study suggest that there is an increase in capacity irrespective of the presence of continuous or non-continuous finger joints in the outer tension laminations. Contrastingly, the results of the present study points to an increase in capacity when designing with CLT. However, as there was no change in stiffness between static and dynamic loading conditions, a DIF of unity is also applicable when considering the stiffness of CLT.

Rolling shear failure was limited to only a few specimens. It is speculated that the reason for more rolling shear only failure under dynamic loading may be due to the increase in the flexural strength due to the high strain rate effects. It should be noted that due to the small number of tests performed, more investigation in the variation of strain rate effects as a function of load-to-grain direction would be required.

6.4 Material Predictive Model

An initial model was developed based on flexural failure, described in section 5.4.2, to predict the dynamic behaviour of all the CLT specimens. This model consisted of a series of peaks and plateaus in capacity correlating to the rupturing of the outer tension laminates as flexural failure progress. This model proved to be relatively accurate in predicting the peak displacement for specimens having failed in flexure. However, it proved to be significantly less accurate when used to predict dynamic displacements of specimens in which rolling shear failure had been observed, as seen in Figure 6.5, where the predicted displacement is overlaid on the recorded displacement-time history of specimen CLT3-4.2. A summary of the results is shown displayed in Figure 6.6, which shows the level of accuracy between the analytical and experimental displacements using the flexural model only. As can be seen in Figure 6.6, while there is a close correlation for the specimens that failed in flexure, there is significant scatter for the specimens that failed in rolling shear.

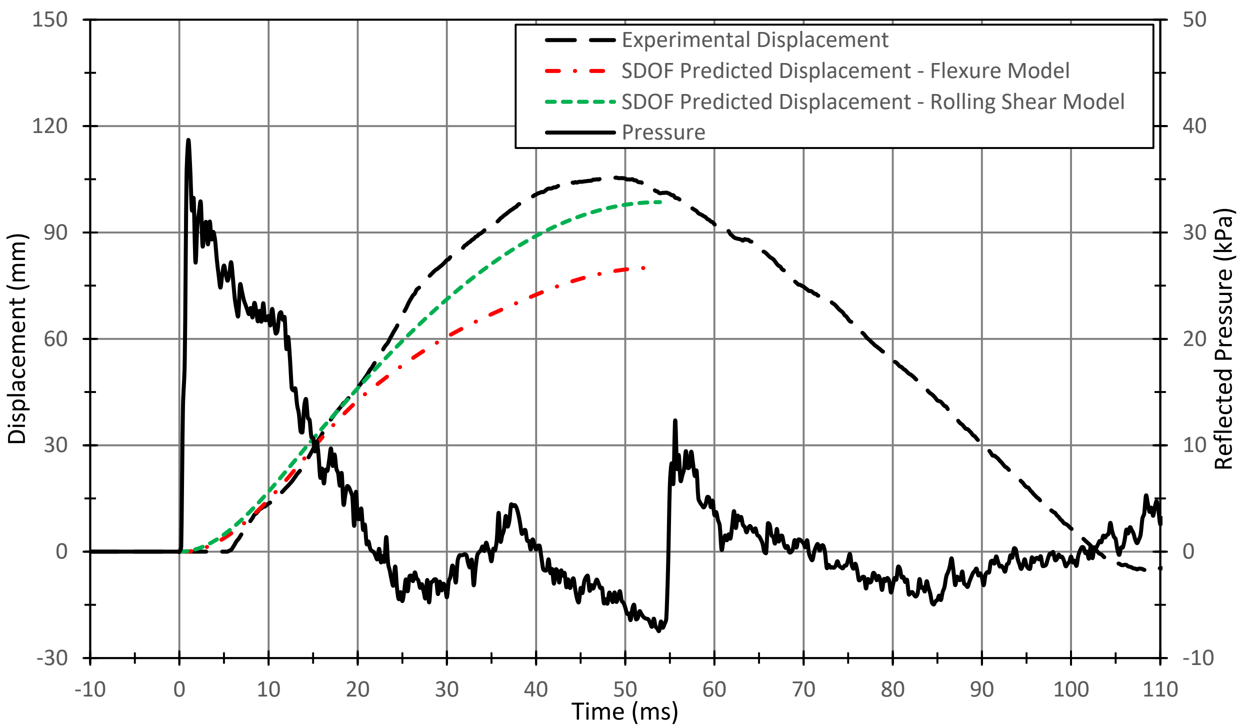

Figure 6.5 Poor Prediction of Displacement due to Rolling Shear Failure using Flexural Model (Specimen CLT3-4.2)

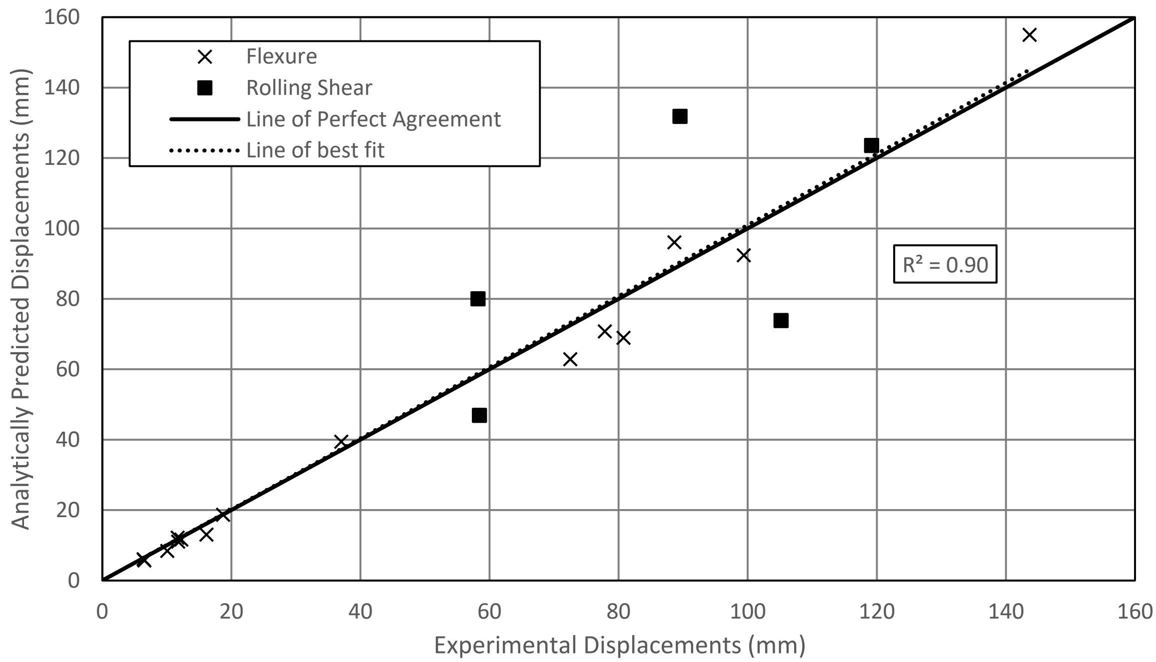

Figure 6.6: Comparison between Analytical and Experimental Displacements – Flexural Model Only

Therefore, it was necessary to develop a second model to account for the reduced stiffness and capacity which occurred once the member had experienced rolling shear. This secondary model, described in section 5.4.3, proved to be much more reliable in capturing these effects, as seen in Figure 6.5, where the predicted displacement from both the flexure and rolling shear models are overlaid on the recorded displacement-time history of specimen CLT3-4.2. This model consisted of panels having an initial stiffness up to a peak resistance, after which a drop in capacity and reduced stiffness was incorporated. The residual stiffness, obtained through static testing, was approximately 20% to 35% of the undamaged panel stiffness. Once specimens having failed by rolling shear were identified and this model used, there was a marked improve in prediction accuracy. A summary of these results is displayed in Figure 6.7, which shows the level of accuracy between the analytical and experimental displacements obtained by using both models.

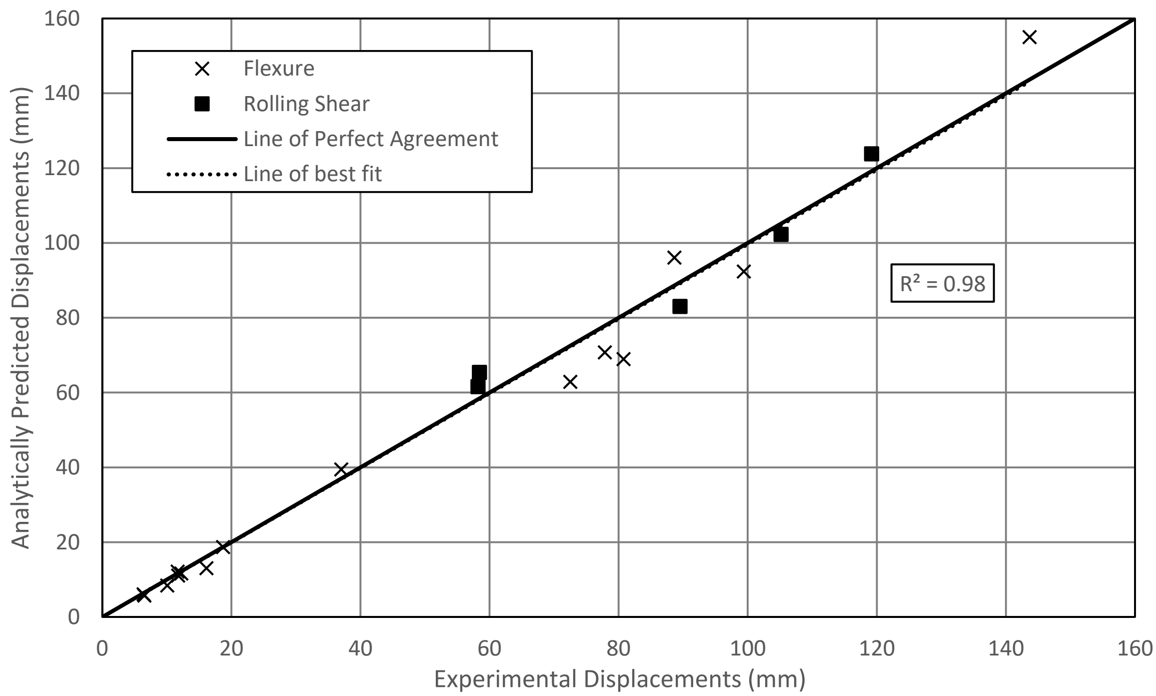

Figure 6.7: Comparison between Analytical and Experimental Displacements – Flexural and Rolling Shear Models

Despite the improved correlation between the analytical and experimental results, the flexure and rolling shear models seem to, on average, underpredict the maximum displacements by approximately 3%, with a COV of 0.09. Additionally, the time-to-maximum displacements are, on average, overpredicted by approximately 11%, with a COV of 0.17. The results of the analytical versus experimental displacement for each specimen is presented in Appendix B.

6.5 Code Consideration and Implication on Design

Blast design in Canada is governed by *CSA S850-12 – Design and Assessment of Buildings Subjected to Blast Loads* (CSA, 2012). This design code was developed with the intent of guiding designer with the design of new structures and to help assess existing structures that could potentially be exposed to blast events. This code is still in its relative infancy compared to other CSA standards, such as CSA O86 for the design of wood structures, and acknowledges that certain assumptions presented within still require validation.

In the standard it is stated that the dynamic bending resistance, S_D, can be determined based on static bending resistance, S_S, modified for high strain rate effects as per equation 6.1.

$$S_D = SIF \times DIF \times S_S \tag{6.1}$$

Where SIF is the strength increase factor and DIF is the dynamic increase factor. The static bending resistance is determined according to the appropriate material standards, which for design in wood is *CSA O86-14 – Engineering Design in Wood* (CSA, 2014).

When determining the SIF and DIF, the blast standard (CSA, 2012) lumps all engineered wood products into a single category. According to the standard, the DIF and SIF for engineered wood products is 1.4 and 1.2, respectively. However, as mentioned in section 6.3, the generalization of these factors, especially the DIF, across all engineered wood products is not accurate. Although the increase in dynamic resistance is a material property, the manufacturing process for various engineered wood products significantly alters the material and thereby its performance. The stacking of the laminates, effect of glue, presence of finger-joints all affect the behaviour and lead to significantly different increases under strain rate effects

According to the timber design standard (CSA, 2014), the static bending resistance of CLT panels can determined using equations 6.2 to 6.4. These equations are valid for panels with layup configurations that are symmetrical about the neutral axis, and have longitudinal laminates (bending in the major strength axis) with identical modulus of elasticity.

$$M_r = \varphi\ [f_b(K_D K_H K_{Sb} K_T)] S_{eff} K_{rb} \tag{6.2}$$

$$S_{eff} = \frac{2 \times I_{eff}}{h} \tag{6.3}$$

$$(EI)_{eff} = \sum_{i=1}^{n} E_i \cdot b_i \cdot \frac{h_i^3}{12} + \sum_{i=1}^{n} E_i \cdot A_i \cdot \frac{h_{total}}{2} \tag{6.4}$$

The load duration factor, K_D, the system factor, K_H, service condition factor, K_{Sb}, and treatment factor, K_T, are all taken as unity; f_b is the specified bending strength in the major direction.

The bending resistance outlined in the timber design standard (CSA, 2014) is based on the Shear Analogy Method (Kreuzinger, 1999), which is explained in detail in the CLT Handbook (FPInnovations, 2011).

The DIF was evaluated through static and dynamic testing of 3-ply and 5-ply CLT panels. The results showed an average increase in capacity by a factor of 1.28 when panels were subjected to high strain rate loading. No dynamic increase was observed for the stiffness. Therefore, for far field blast loading, a DIF of 1.28 on the capacity only seems appropriate.

Two material predictive models were proposed, the first for flexural failure and the second to account for rolling shear failure effects. The models were validated with experimental dynamic test results and showed reasonable fit.

Further testing is recommended to examine whether these models also function with a reasonable degree of accuracy for deeper members with an additional number of layers (e.g. 7-ply and 9-ply) and with varying loading conditions. Also, these models could be further refined through more sophisticated analysis techniques such as finite element modeling, which could aid in refining the proposed model.

Failure due to rolling shear is a key failure mechanism for CLT under static loading conditions. For this reason, and because the governing failure mode is relatively difficult to predict in dynamic loading conditions, the conservative approach in design applications would be to consider failure due to rolling shear effects first, and subsequently verify the design using the flexural model.

Chapter 7 – Conclusion

7.1 General Conclusions

This study was undertaken to assess the behaviour of cross-laminated timber panels subjected to simulated blast loading using a shock tube apparatus. More specifically, the aim of this study was to investigate the behaviour of CLT panels subjected to static and dynamic loads to determine a dynamic increase factor in order to quantify high strain rate effects on this material. Testing was limited to one-way bending with simply supported boundary conditions at the panel ends and free boundary conditions along the panel edges. Strain rates between 0.02 to 0.21 s^{-1} were generated using the shock tube corresponding to strain rates from far-field blast loading. Based on the results of this study, the following conclusions can be made:

- An average dynamic increase factor of 1.28 on the resistance was found, while no increase in the dynamic stiffness was observed.
- Differences in failure modes were observed between static and dynamic testing, where rolling shear was more prevalent in dynamic conditions.
- All specimens tested under static conditions failed in flexure with some rolling shear developing at the time of failure.
- Under dynamic loading, two distinct failure modes were observed: flexural failure with some rolling shear developing at the time of failure, and rolling shear failure with no notable flexural damage on the outer tension layers.
- Two material predictive models to capture the two distinct failure modes incorporating material properties, observed behaviors, and measured residual capacities were developed. The models were validated using experimental dynamic test results and

showed a reasonable correlation between predicted and experimentally obtained displacements.

- The results obtained in this study related to the dynamic increase factor can be considered in design standard development for far-field blast design.

7.2 Recommendations for Future Work

Based on the research work completed to date, the following areas have been identified for future work:

- Additional testing with larger sample sets is warranted in order to validate the trends observed during this study with regards to rolling shear and flexural failure.
- Refinement of the predictive models, possibly involving more sophisticated techniques, in order to produce a more generalized model.
- Testing of deeper sections, sections with different layup configurations, and with varying loading conditions in order to expand on the current model.
- Testing panels under varying boundary conditions, such as panels acting as two-way slabs, with connections or with continuous panels over multiple storeys.
- Testing of CLT panels fabricated using other wood species (e.g. Douglas fir) to determine if these have similar dynamic increase factors on the capacity and stiffness.
- Investigating axial load effects on the performance of CLT and incorporating these effects in the predictive model in order to simulate load bearing walls.

References

Aoude, H., Dagenais, F. P., Burrell, R. P., and Saatcioglu, M. (2015). “Behavior of ultra-high performance fiber reinforced concrete columns under blast loading.” Int. J. Impact Eng., 80(1), 185–202.

Baker, W. E., Explosions in Air. University of Texas Press, Austin, TX, 1973.

Barreiro, J. (2016). “Blast resistance of non-composite tilt-up sandwich panels and their connections.” Ph.D. dissertation, Univ. of Ottawa, Ottawa.

Biggs, J. M. (1964). *Introduction to structural dynamics*. New York,: McGraw-Hill.

Bill 9. (2009). Wood First Act. Retrieved 17/11/2017, from http://www.leg.bc.ca/39th1st/1st_read/gov09-1.htm

BSI. (2011). PREN 16351 - Timber Structures - Cross Laminated Timber. London, England: British Standards Institution.

Burrell, R. P. (2012). “Performance of steel fibre reinforced concrete columns under shock tube induced shock wave loading.” M.A.Sc. thesis, Univ. of Ottawa, Ottawa.

Chock, J. M. K. (1999). Review of Methods for Calculating Pressure Profiles of Explosive Air Blast and its Sample Application. Blacksburg, Virginia: the Virginia Polytechnic Institute and State University.

Christovasilis, I.P., Brunetti, M., Follesa, M., Nocetti, M., Vassallo, D. (2016). Evaluation of the Mechanical Properties of Cross Laminated Timber with Elementary Beam Theories. Construction and Building Materials, 122 (2016), pp. 202–213.

Ciornei, L. (2012). Performance of polyurea retrofitted unreinforced concrete masonry walls under blast loading. (M.A.Sc.), University of Ottawa, Ottawa, Canada.

Cote, D. (2017). “Effect of Realistic Boundary Conditions on the Behaviour of Cross-Laminated Timber Elements Subjected to Simulated Blast Loads” M.A.Sc. Thesis, Univ. of Ottawa, Ottawa.

CSA. (2012). CSA S850 - Design and assessment of buildings subjected to blast loads. Mississauga: Canadian Standards Association Group.

CSA. (2014). CSA O86 - Engineering design in wood. Mississauga: Canadian Standards Association.

Díaz Alonso, F., González Ferradás, E., Sánchez Pérez, J.F., Miñana Aznar, A., Ruiz Gimeno, J., Martínez Alonso, J., (2006). Characteristic overpressure–impulse–distance curves for the detonation of explosives, pyrotechnics or unstable substances. Journal of Loss Prevention in the Process Industries, 19 (2006), pp. 724–728.

Dickson, M., & Parker, D. (2015). *Sustainable Timber Design*. New York, Routledge.

Draganić, H., & Sigmund, V., (2012). Blast Loading on Structures. Technical Gazette, 19(3): 643-652.

Dumais, A.J.: “Optimized Wood Components and Subassemblies for Maximum Ductility.” University of Maine, 2008

Dusenberry, D.O. (2010). Handbook for blast-resistant design of buildings. Hoboken, N.J.: J. Wiley.

Florek, J. R. (2007). Study of Simplified Models of Aircraft Structures Subjected to Generalized Explosive Loading. New Brunswick, New Jersey: Rutgers, the State University of New Jersey

FPInnovations. (2011) CLT handbook: cross-laminated timber. Québec: FPInnovations, 6.

Habipi, B., Ajdinaj, D., (2015). “Wood Finger-Joint Strength as Function of Finger Length and Slope Positioning of Tips.” International Journal of Engineering and Applied Sciences, 12(2): 128-132, ISSN: 2394-3661.

Hopkins, R. (2011). Explosion Investigation and Analysis. Trace Fire Protection and Safety Consultants, Ltd., Retrieved 12/03/17 from http://www.tracefireandsafety.com/

Jacques, E. (2011). “Blast retrofit of reinforced concrete walls and slabs.” Ph.D. dissertation, Univ. of Ottawa, Ottawa.

Jacques, E. (2014). RCBLAST (Version. 0.5.1) [Computer program]

Jacques, E., Lloyd, A., and Saatcioglu, M. (2013). "Predicting reinforced concrete response to blast loads." Canadian Journal of Civil Engineering, 40(5), 427-444.

Jacques, E., Lloyd, A., Braimah, A., Saatcioglu, M., Doudak, G., Abdelalim, O., (2013). “Influence of High Strain-Rates on the Dynamic Flexural Material Properties of Spruce–Pine–Fir Wood Studs.” Can. J. Civ. Eng., 41: 56-64, DOI: 10.1139/cjce-2013-0141

Jansson, B. (1992). Impact Loading of Timber Beams. Vancouver, BC: University of British Columbia.

Karlos, V., & Solomos, G., (2013). Calculation of Blast Loads for Application to Structural Components. Luxembourg: Publications Office of the European Union

Keenan, F. 1986. Limit States Design of Wood Structures. Toronto, ON: Canada Morrison Hershfield Ltd.

Krauthammer, T. (2008). Modern protective structures. Boca Raton, FL: CEC Press.

Kreuzinger, H. (1999) Platten, Scheiben und Schalen. Ein Berechnungsmodell fur gangige Statikprogramme (German). Bauen mit Holz, 1:34-39

Lacroix, D. (2013). "Behaviour of Light-Frame Wood Stud Walls Subjected to Blast Loading" M.A.Sc. Thesis, Univ. of Ottawa, Ottawa.

Lacroix, D. (2017). Investigating the Behaviour of Glulam Beams and Columns Subjected to Simulated Blast Loading. Ottawa: University of Ottawa.

Lacroix, D. N., Doudak, G., and El-Domiaty, K. (2014). "Retrofit options for light-frame wood stud walls subjected to blast loading." J. Struct. Eng., 10.1061/(ASCE)ST.1943-541X.0000885, 04013104.

Lacroix, D., & Doudak, G. (2012). Behaviour of typical light-frame wood stud walls subjected to blast loading. World Conference on Timber Engineering: Strength and Serviceability - Extreme Events. Auckland, New-Zealand.

Lacroix, D., & Doudak, G. (2013). Modelling the Behaviour of Light-Frame Wood Stud Walls Subjected to Blast Loading. 3rd Specialty Conference on Material Engineering & Applied Mechanics (pp. 1-10). Montreal, QC: CSCE.

Lacroix, D.N. (2017). "Investigating the Behaviour of Glulam Beams and Columns Subjected to Simulated Blast Loading" Ph.D. thesis, Univ. of Ottawa, Ottawa.

Lacroix, D.N., Doudak, G. (2015). "Investigation of Dynamic Increase Factors in Light-Frame Wood Stud Walls Subjected to Out-of-Plane Blast Loading." J. Struct. Eng., 141(6), DOI: 10.1061/(ASCE)ST.1943-541X.0001139.

Lacroix, D.N., Doudak, G. (2018). "Effects of High Strain Rates on the Response of Glulam Beams and Columns." J. Struct. Eng., 144(5), DOI: 10.1061/(ASCE)ST.1943-541X.0002020.

Lam, F., Li, Y., Li, M. (2016). Torque loading tests on the rolling shear strength of cross-laminated timber. Journal of Wood Science, 62, pp. 407-415

Lloyd, A. (2010). "Performance of reinforced concrete columns under shock tube induced shock wave loading." Ph.D. dissertation, Univ. of Ottawa, Ottawa.

Maienschein, J.L. (2002). Estimating Equivalency of Explosives through a Thermochemical Approach. Submitted to the 12th International Conference Symposium, San Diego, California

Ngo, T., Mendis, P., Gupta, A., & Ramsay, J., (2007). Blast Loading and Blast Effects on Structures – An Overview. EJSE Special Issue: Loading on Structures: 76-91.

Nie, X. (2015). "Failure Mechanism of Rolling Shear Failure in Cross-Laminated Timber" M.Sc. Thesis, University of British Columbia, Vancouver.

Riyanto, D., & Gupta, R., (1996). Effect of Ring Angle on Shear Strength Parallel to the Grain of Wood. *Forest Products Journal*, *46*(7/8): 87-92.

Schafer, S., (2014) Pins vs. Tails. Lost Art Press, Retrieved 05/02/18, from https://blog.lostartpress.com/2014/12/23/pins-vs-tails/

Serrano, E. (2000). "Adhesive Joints in Timber Engineering – Modelling and Testing of Fracture Properties" Ph.D. thesis, Lund University, Lund.

Serrano, E., Gustafsson, P.J., (2014). "Influence of Bondline Brittleness and Defects on the Strength of Timber Finger-Joints." International Journal of Adhesion & Adhesives, 19: 9-17.

Sikora, K., McPolin, D., Harte, A. (2016). Effects of the Thickness of CLT Panels Made from Irish Sitka Spruce on Mechanical Performance in Bending and Shear. Construction and Building Materials, 116 (2016), pp. 141–150.

Sikora, K.S., McPolin, D.O., Harte, A.M., (2016). "Shear Strength and Durability Testing of Adhesive Bonds in Cross-laminated Timber", The Journal of Adhesion, 92:7-9, 758-777, DOI: 10.1080/00218464.2015.1094391

Sliseris, J., Gaile, L., Pakrastiņš, L. (2017). Numerical Analysis of Behaviour of Cross Laminated Timber (CLT) in Blast Loading. IOP Conference Series: Materials Science and Engineering, 251 (1), pp. 012105

Steiger, R., Gülzow, A., Czaderski, C., Howald, M.T., Niemz, P., (2012). "Comparison of Bending Stiffness of Cross-Laminated Solid Timber Derived by Modal Analysis of Full Panels and by Bending Tests of Strip-Shaped Specimens", Eur. J. Wood Prod., 70: 141-153, DOI: 10.1007/s00107-011-0521-7

Syron, W. (2010). Strain rate-dependent behaviour of laminated strand lumber. Orono, Maine: University of Maine.

Syron, W., Lopez-Anido, R., Nagy, E. (2010). High strain rate effects in composite wooden bolted connections. World Conference on Timber Engineering, Trentino, Italy.

Unified Facilities Criteria (UFC) 03-340-02. (2008). Structures to Resist the Effects of Accidental Explosions (pp. 1943). Washington, D.C.: United States of America Department of Defense.

USAF. (2006). Vehicle Bomb Mitigation Guide. Lackland AFB, Texas: United States Air Force.

Viau, C. (2016). “Investigating the response of light-frame wood stud walls with and without boundary connections to blast loads.” M.A.Sc. thesis, Univ. of Ottawa, Ottawa.

Viau, C., and Doudak, G. (2016a). “Investigating the behavior of light-frame wood stud walls subjected to severe blast loading.” J. Struct. Eng., 10.1061/(ASCE)ST.1943-541X.0001622, 04016138.

Viau, C., and Doudak, G. (2016b). “Investigating the behaviour of typical and designed wall-to-floor connections in light-frame wood stud wall structures subjected to blast loading.” Can. J. Civ. Eng., 43(6), 562–572.

Zhou, Q., Gong, M., Chui, Y.H., Mohammad, M., (2014). “Measurement of Rolling Shear Modulus and Strength of Cross Laminated Timber Fabricated with Black Spruce”, Construction and Building Materials, 64: 379-386, DOI: 10.1007/s00107-011-0521-7

Appendix A – Static Test Results

Destructive Static Tests

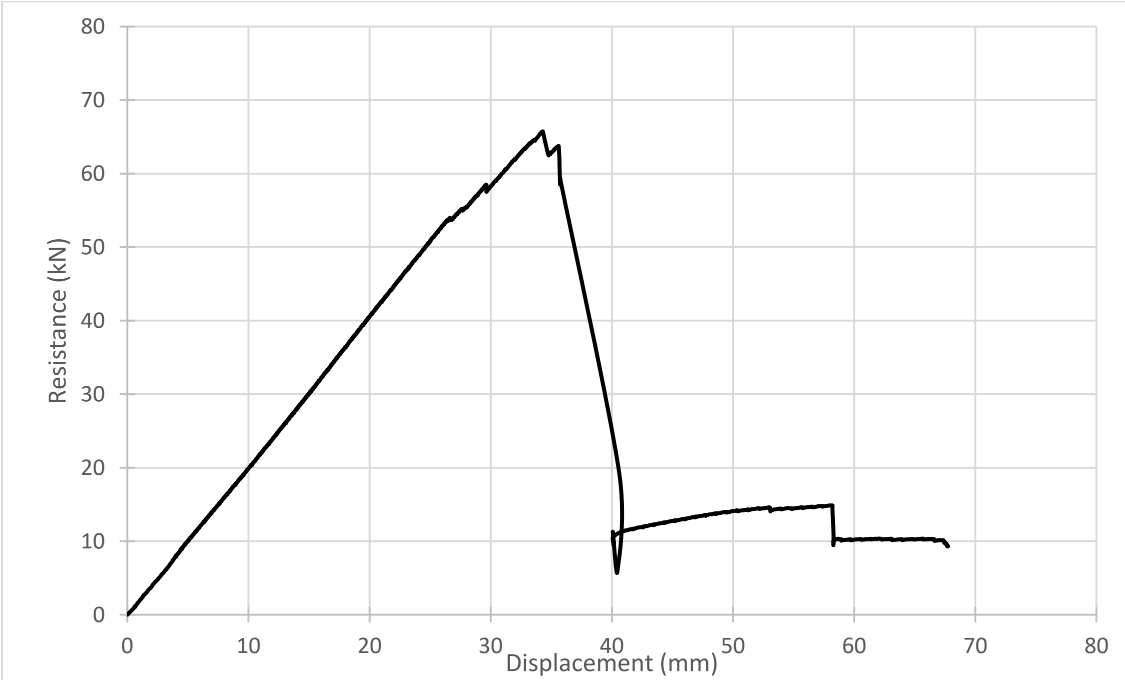

Figure A1.1: Experimental Force Displacement for CLT3-1

Figure A1.2: Flexural Failure in Tension Laminate and Rolling Shear in Transverse Laminate in CLT3-1

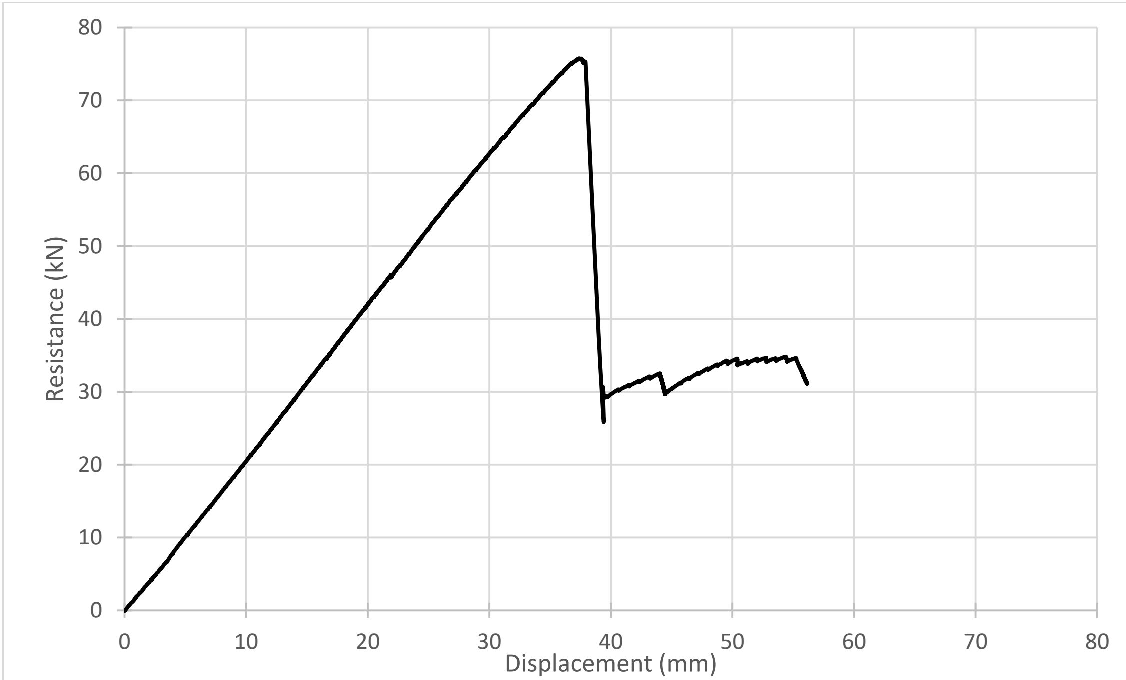

Figure A1.3: Experimental Force Displacement for CLT3-2

Figure A1.4: Rolling Shear Developed in Transverse Laminate in CLT3-2

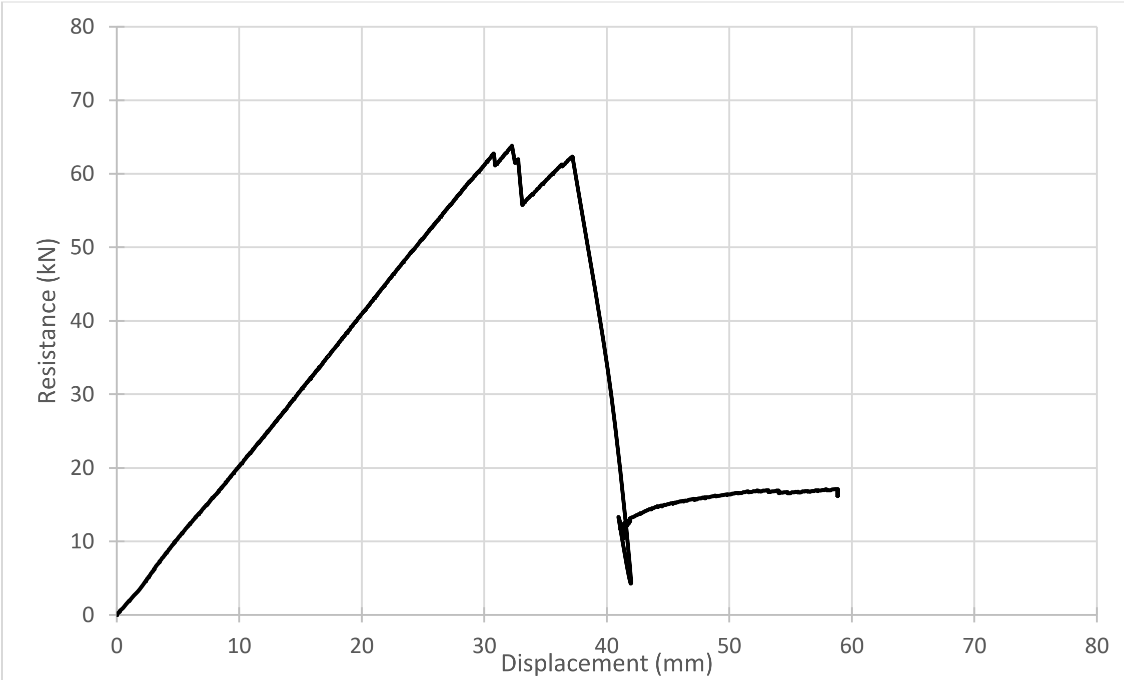

Figure A1.5: Experimental Force Displacement for CLT3-3

Figure A1.6: Flexural Failure along Finger Joints in CLT3-3

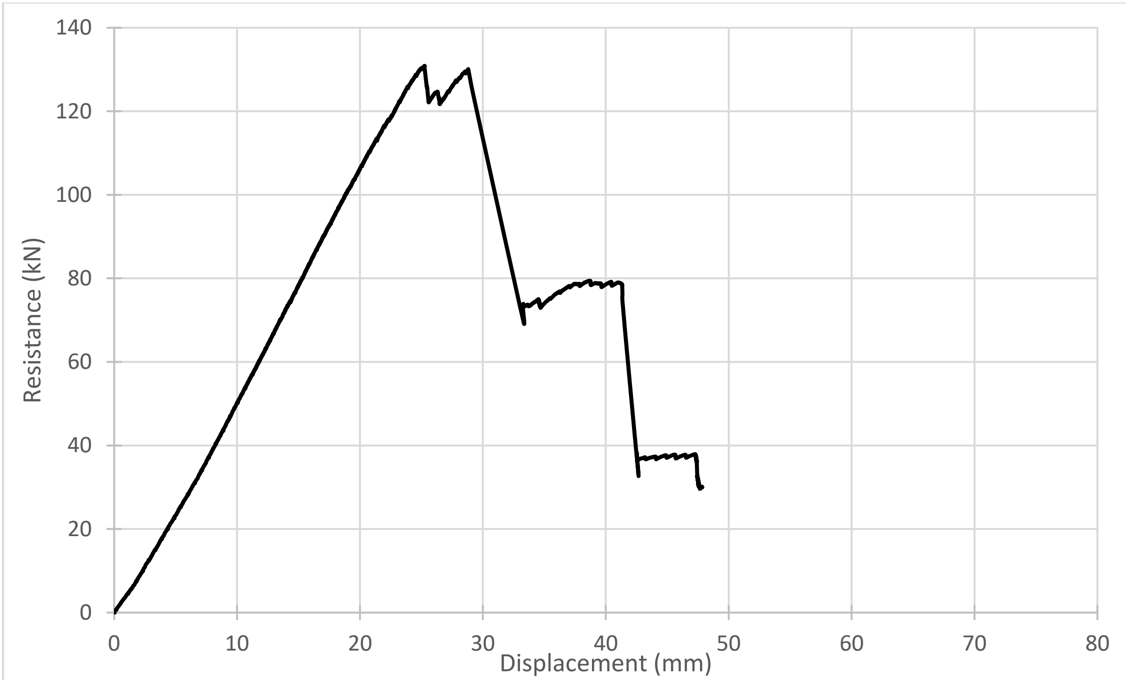

Figure A1.7: Experimental Force Displacement for CLT5-1

Figure A1.8: Development of Rolling Shear Post Flexural Failure in CLT5-1

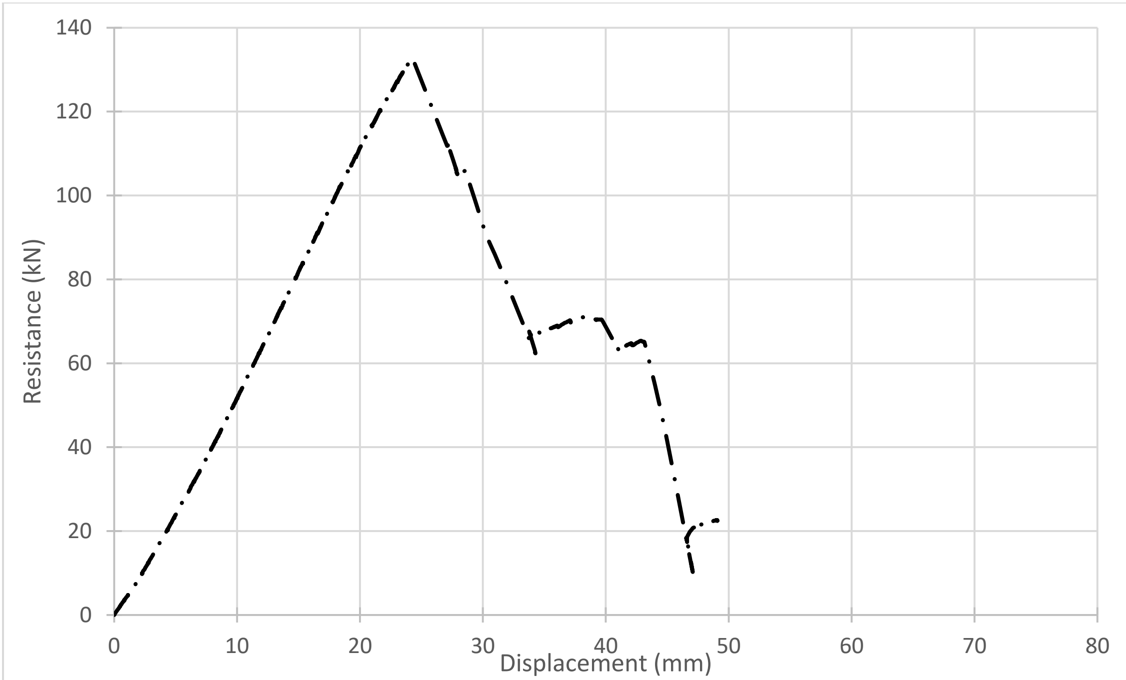

Figure A1.9: Experimental Force Displacement for CLT5-2

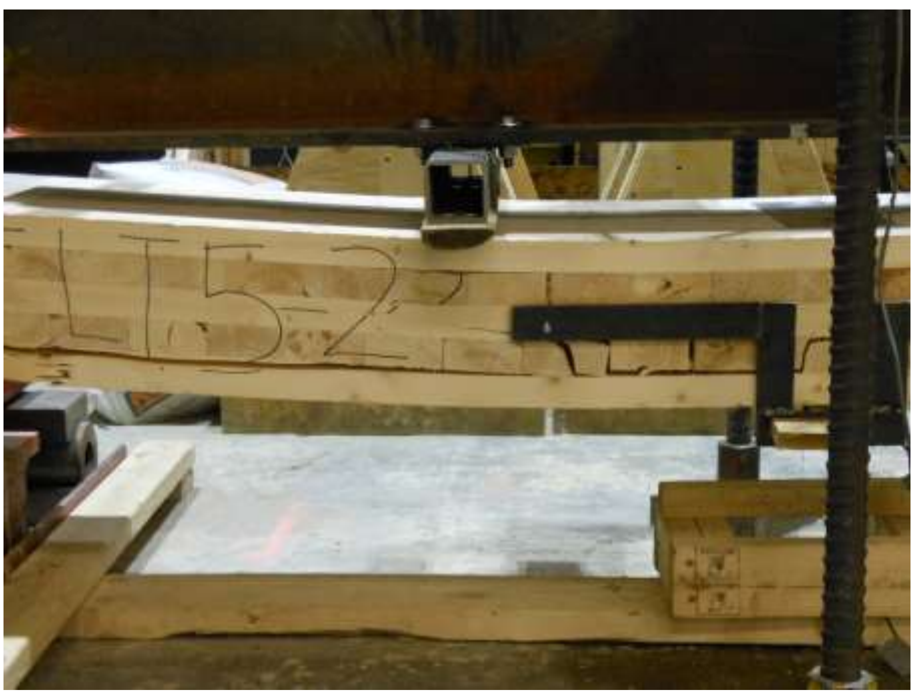

Figure A1.10: Development of Rolling Shear Post Flexural Failure in CLT5-2

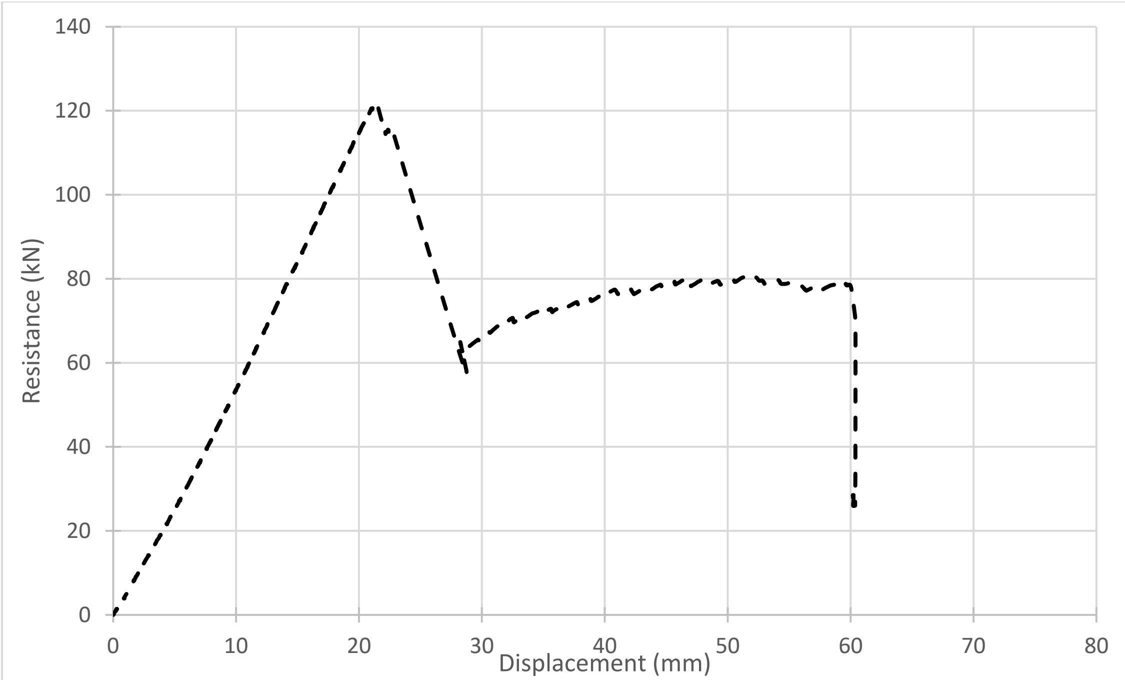

Figure A1.11: Experimental Force Displacement for CLT5-3

Figure A1.12: Separation of Finger Joints in CLT5-3

Residual Static Tests

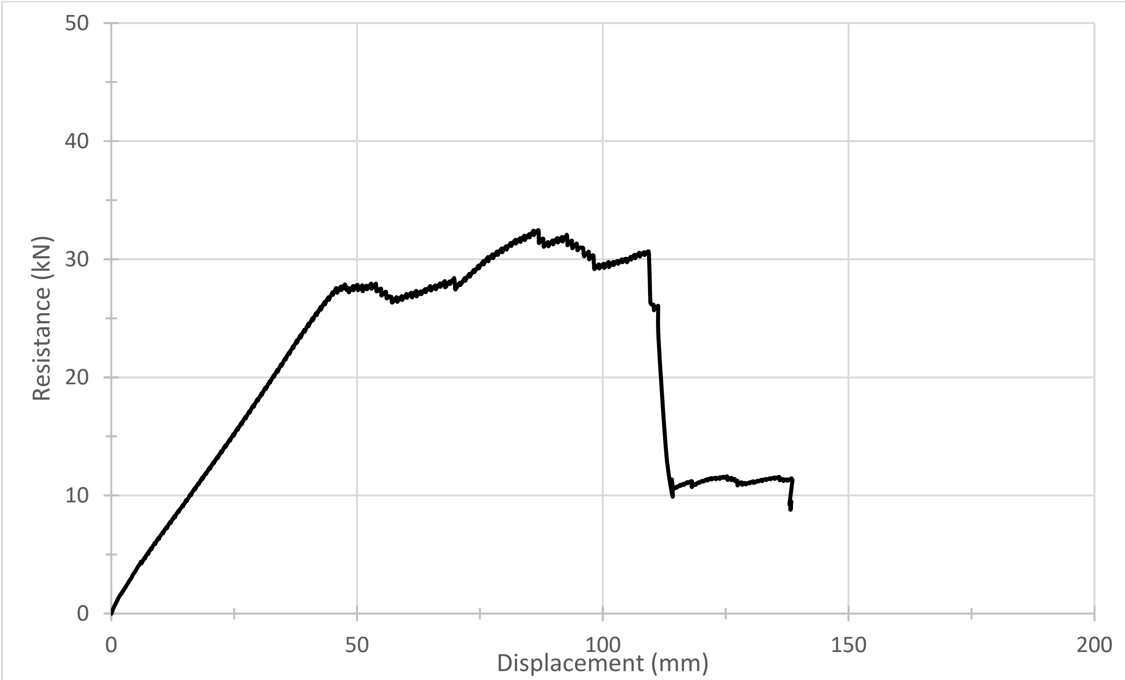

Figure A1.13: Residual Experimental Force Displacement for CLT3-9

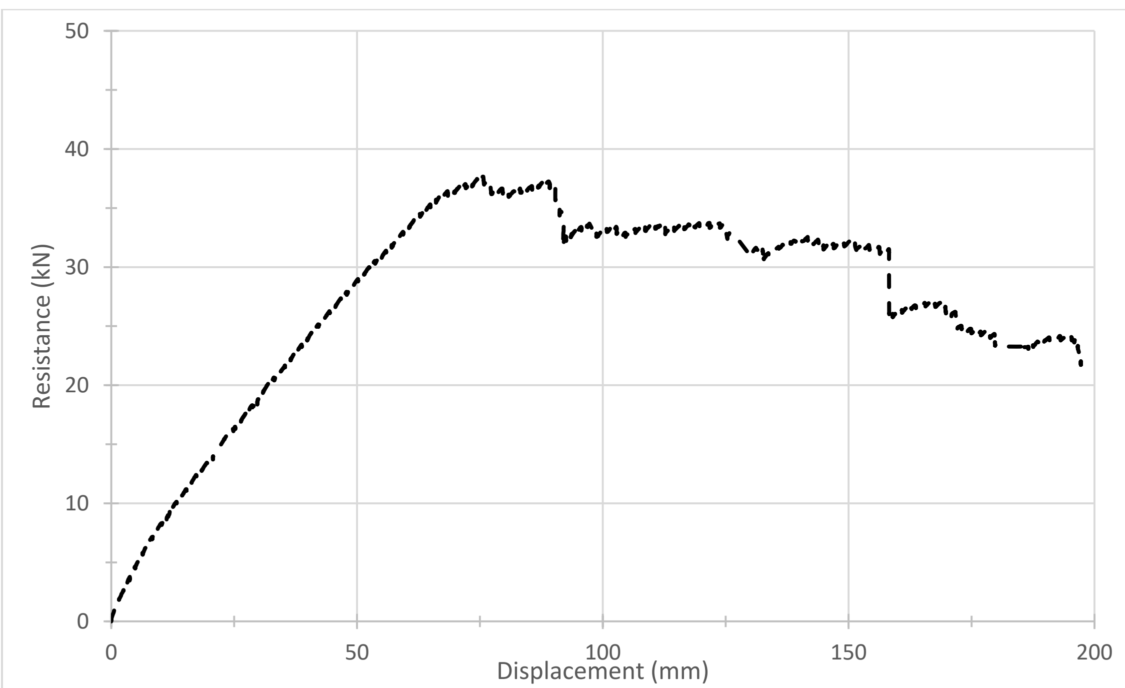

Figure A1.14: Residual Experimental Force Displacement for CLT5-6

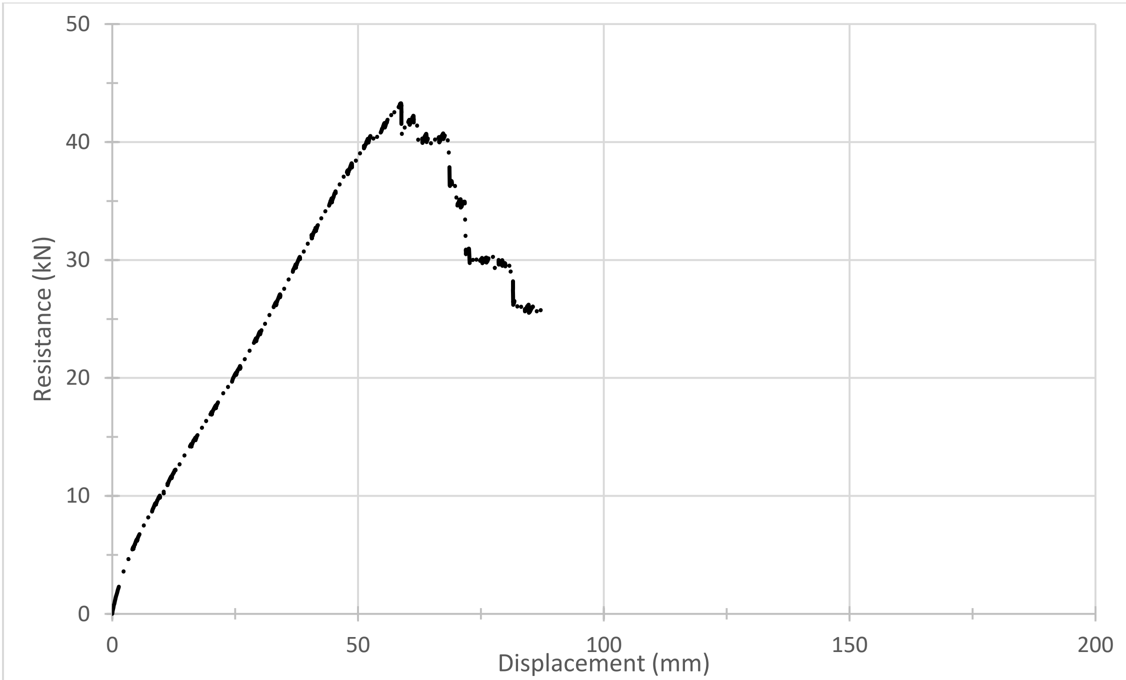

Figure A1.15: Residual Experimental Force Displacement for CLT5-7

Appendix B – Dynamic Test Results

Specimen: CLT3-4

Failure mode: Rolling Shear

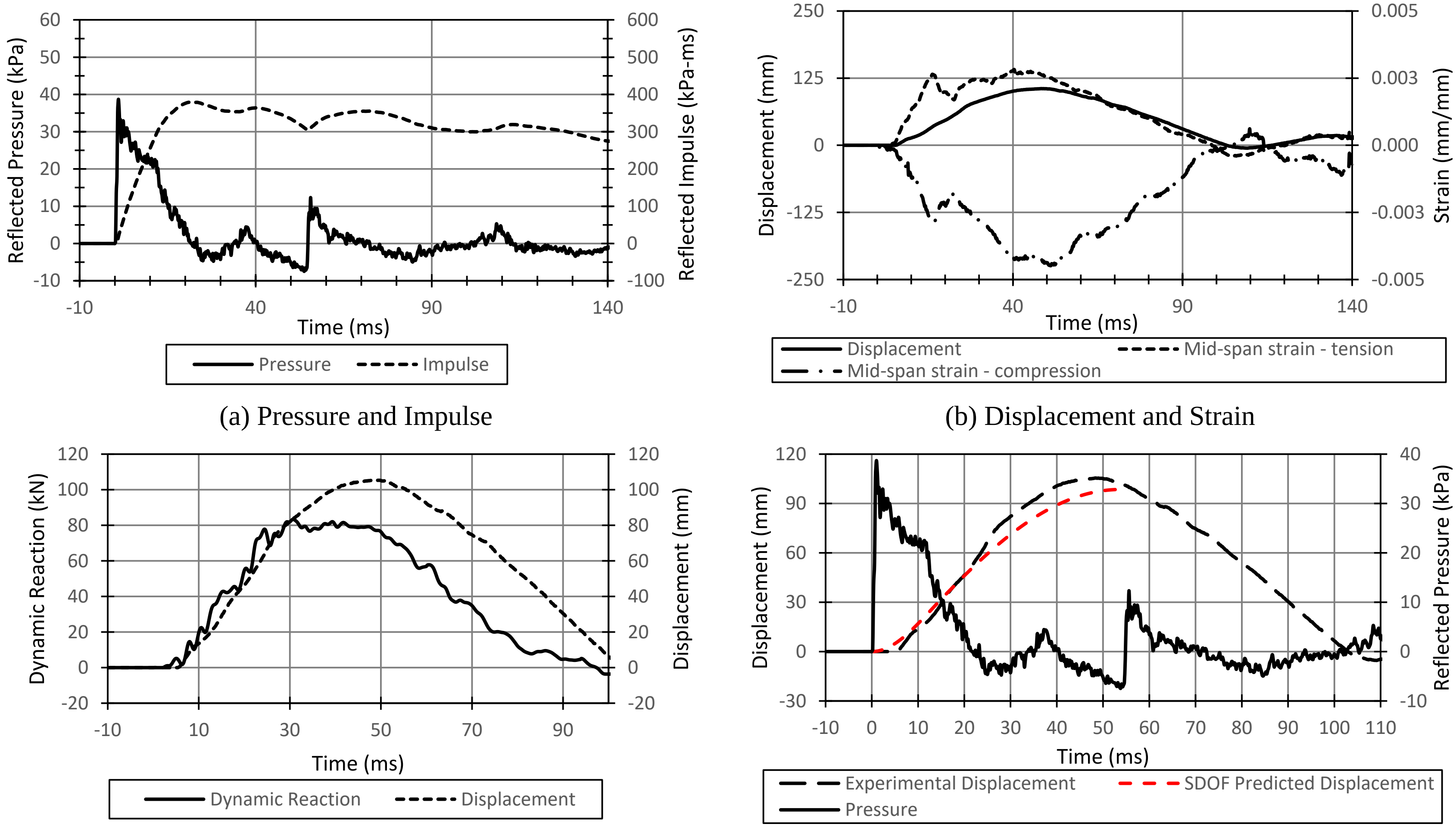

(a) Pressure and Impulse

(b) Displacement and Strain

(c) Reaction and Displacement

(d) SDOF Prediction

Figure B1.1: Dynamic Test Results for CLT3-4

(a) Rolling Shear on Left Side

(b) Rolling Shear on Right Side

Figure B1.2: Dynamic Test Damage for CLT3-4

Specimen: CLT3-5

Failure mode: Flexure

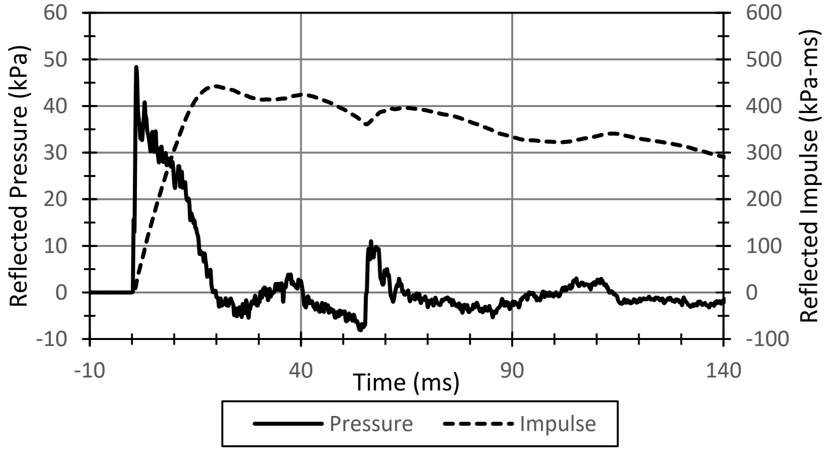

(a) Pressure and Impulse

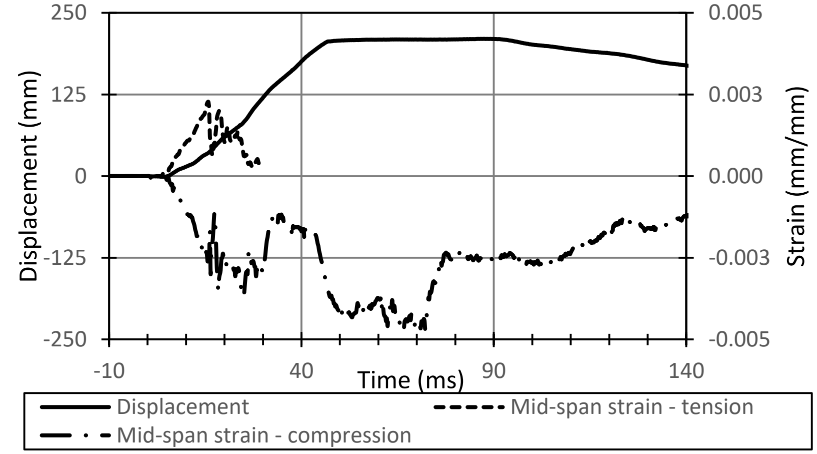

(b) Displacement and Strain

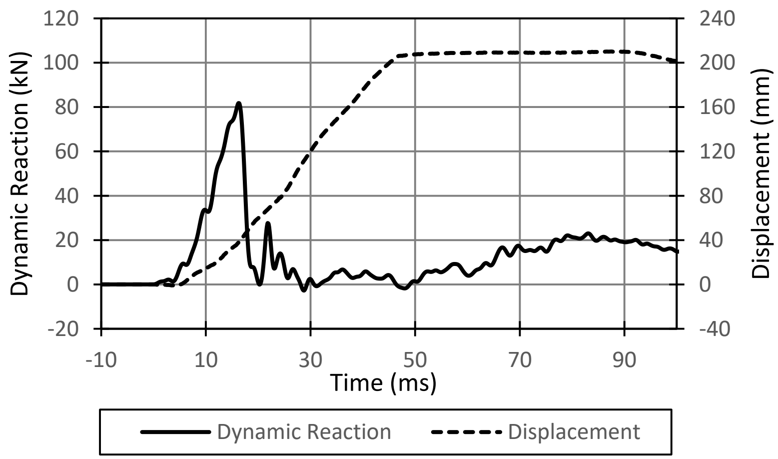

(c) Reaction and Displacement

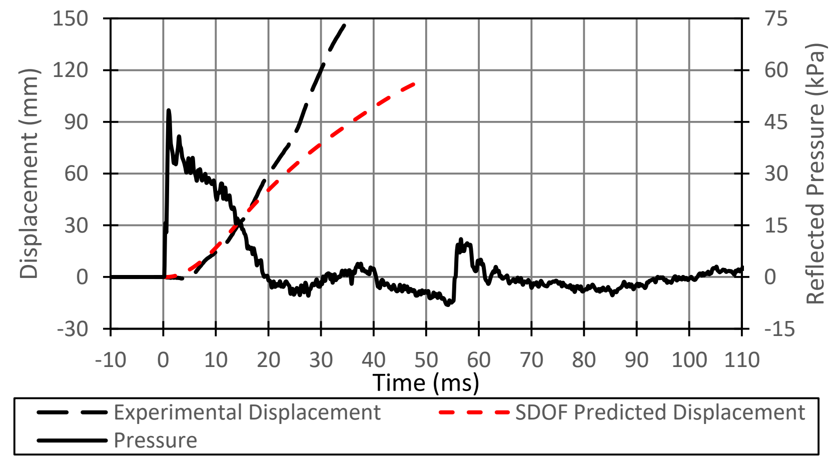

(d) SDOF Prediction

Figure B1.3: Dynamic Test Results for CLT3-5

(a) Front Face

(b) Left Side

Figure B1.4: Dynamic Test Damage for CLT3-5

Specimen: CLT3-6

Failure mode: Flexure

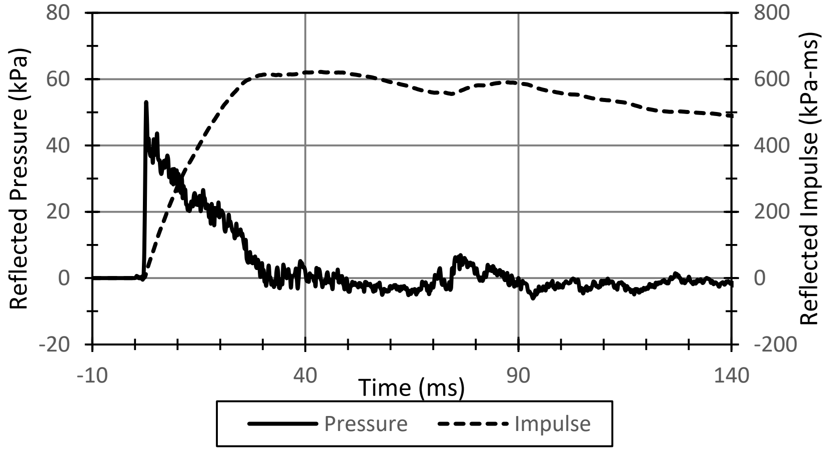

(a) Pressure and Impulse

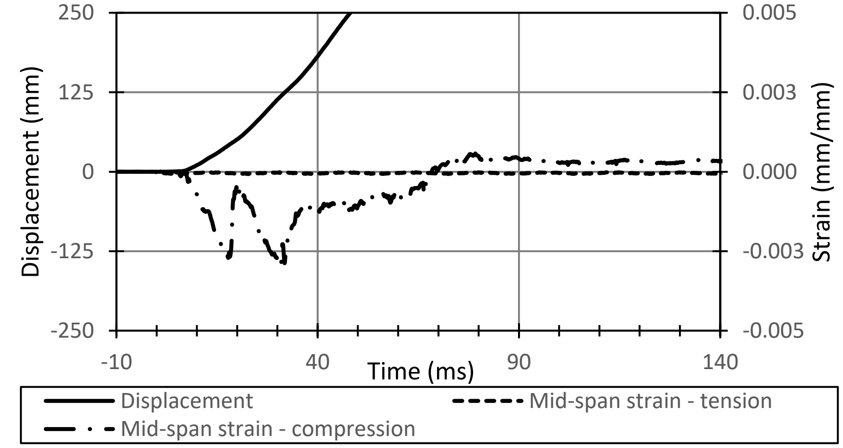

(b) Displacement and Strain

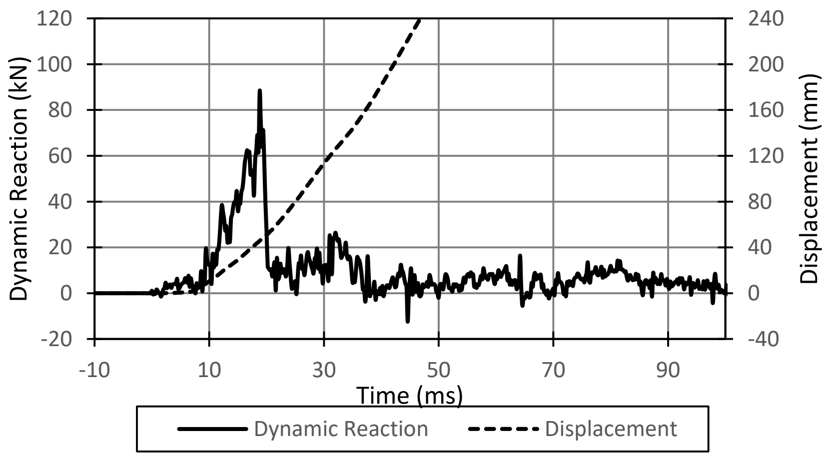

(c) Reaction and Displacement

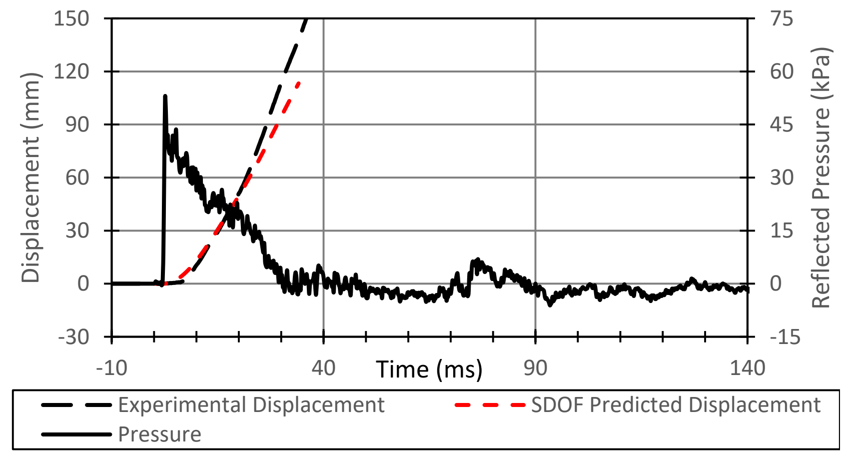

(d) SDOF Prediction

Figure B1.5: Dynamic Test Results for CLT3-6

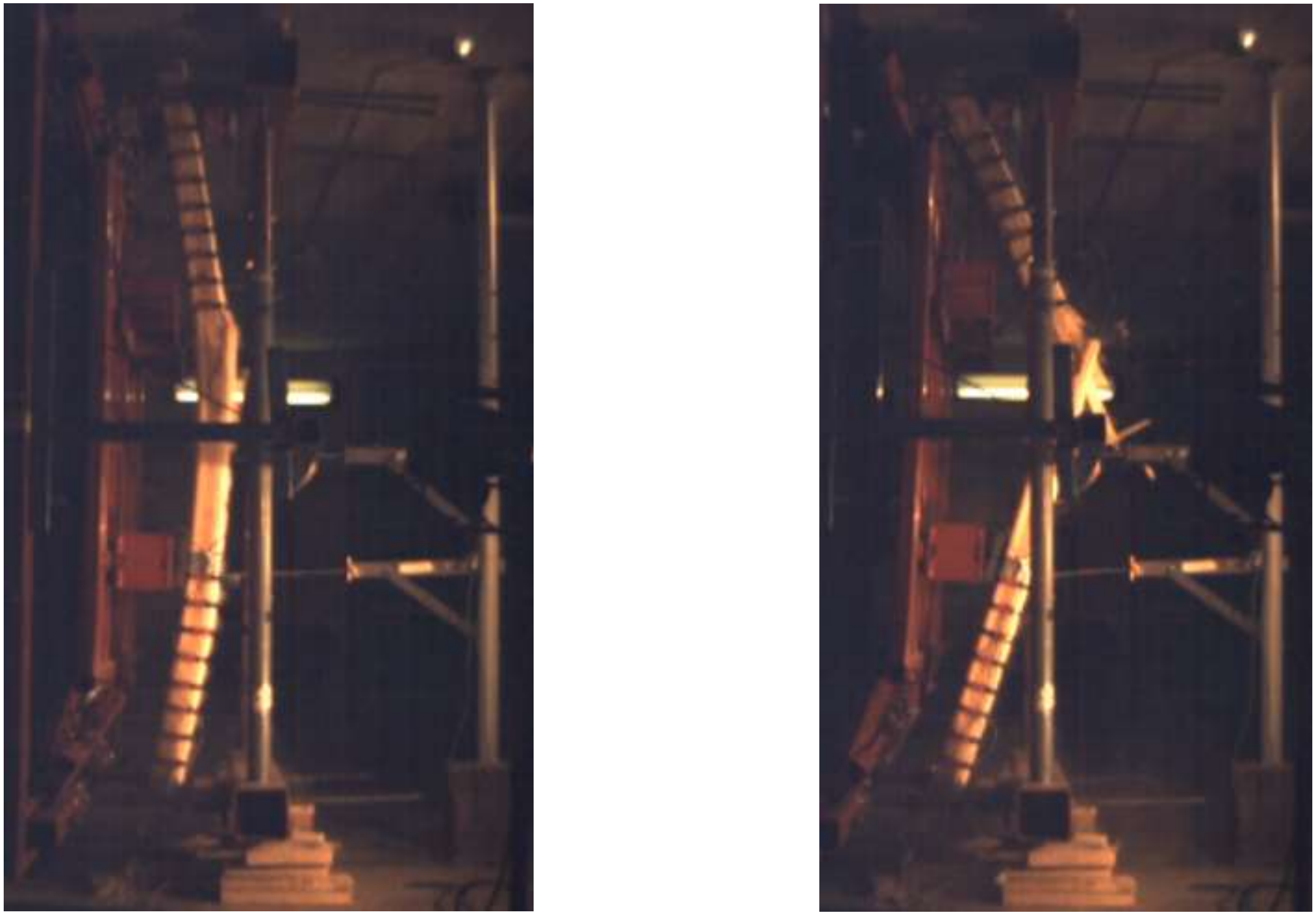

(a) Start of Flexural Failure (b) Complete Flexural Failure

Figure B1.6: Dynamic Test Damage for CLT3-6

Specimen: CLT3-7

Failure mode: Rolling Shear

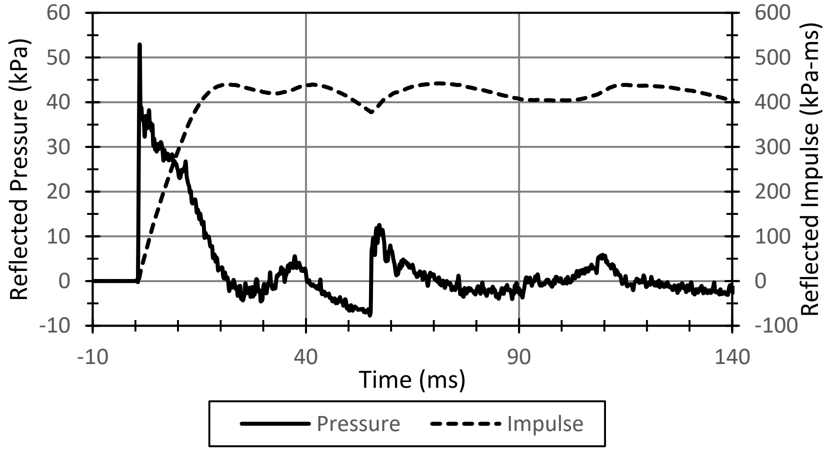

(a) Pressure and Impulse

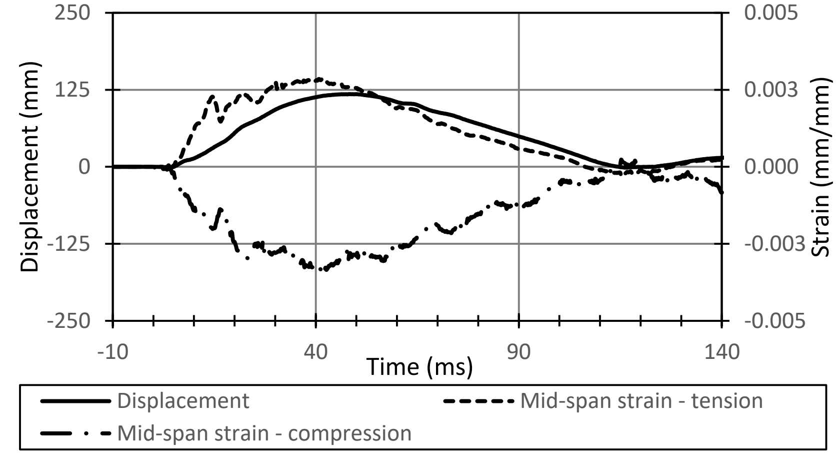

(b) Displacement and Strain

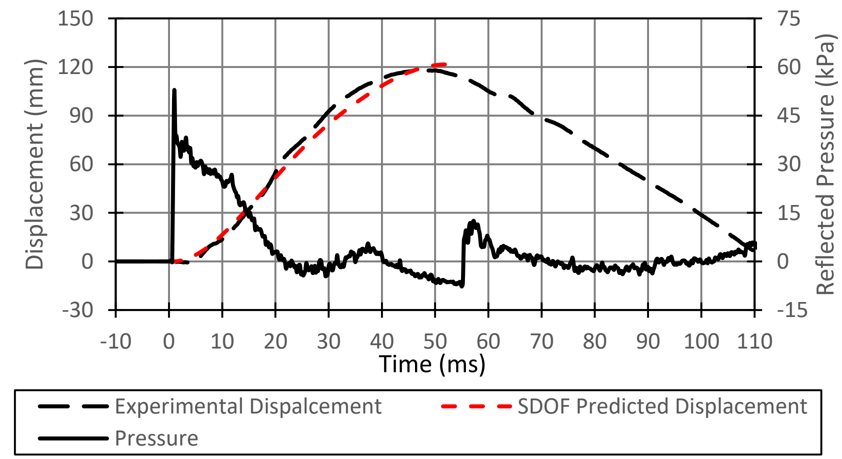

(c) SDOF Prediction

Figure B1.7: Dynamic Test Results for CLT3-7

(a) Rolling Shear on upper Left Side (b) Rolling Shear on Lower Right Side

Figure B1.8: Dynamic Test Damage for CLT3-7

Specimen: CLT3-8

Failure mode: Rolling Shear then Flexure

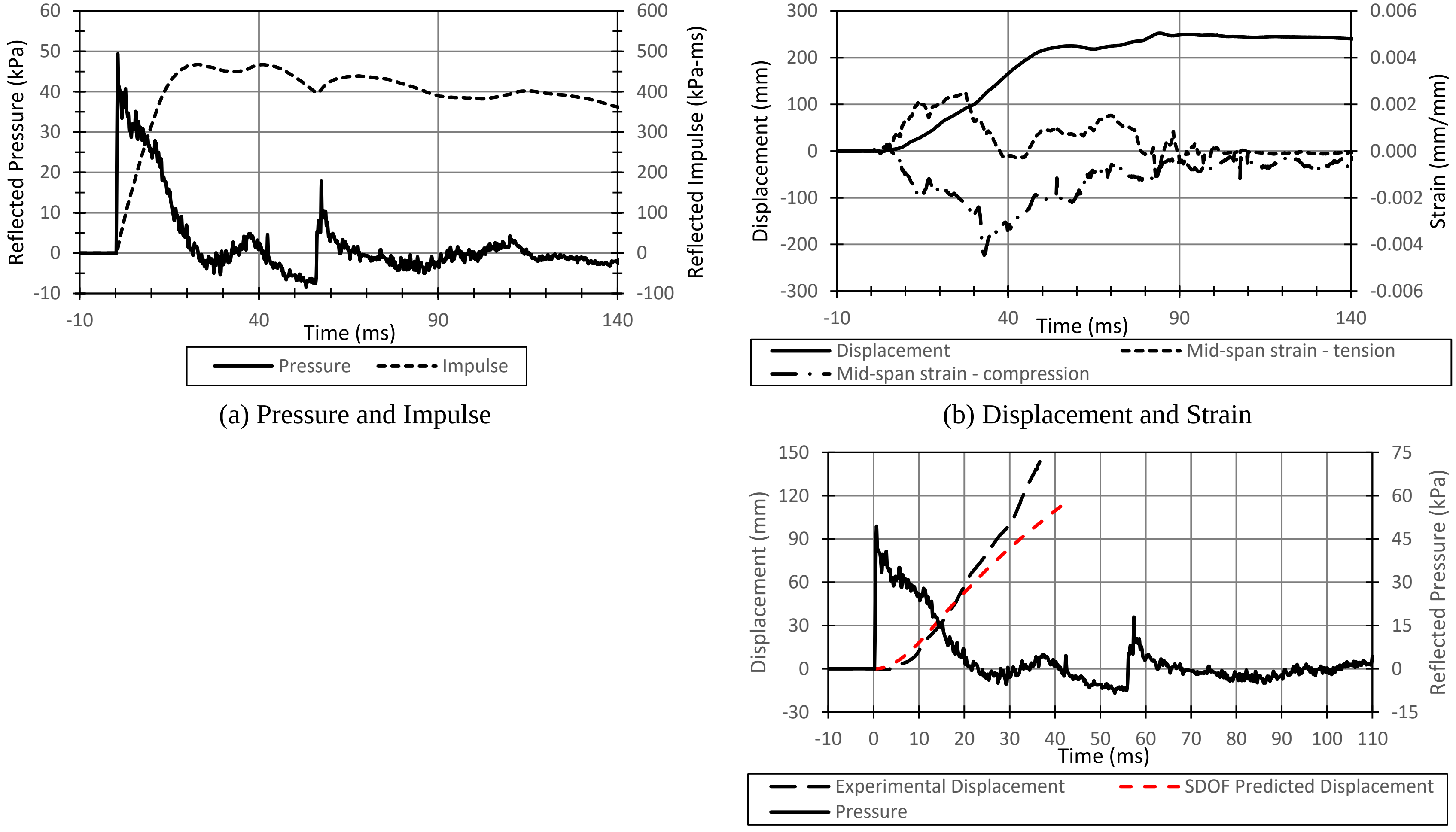

Figure B1.9: Dynamic Test Results for CLT3-8

(a) Flexural Failure – Front Face (b) Flexural and Rolling Shear on Right Side

Figure B1.10: Dynamic Test Damage for CLT3-8

Specimen: CLT3-9

Failure mode: Rolling Shear

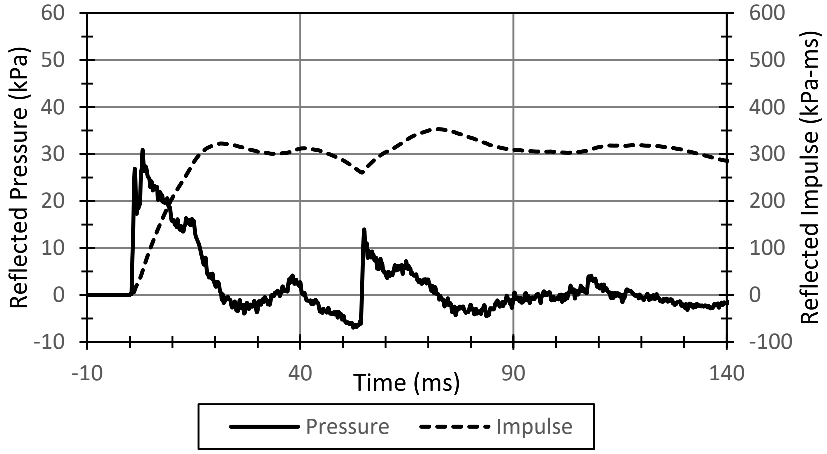

(a) Pressure and Impulse

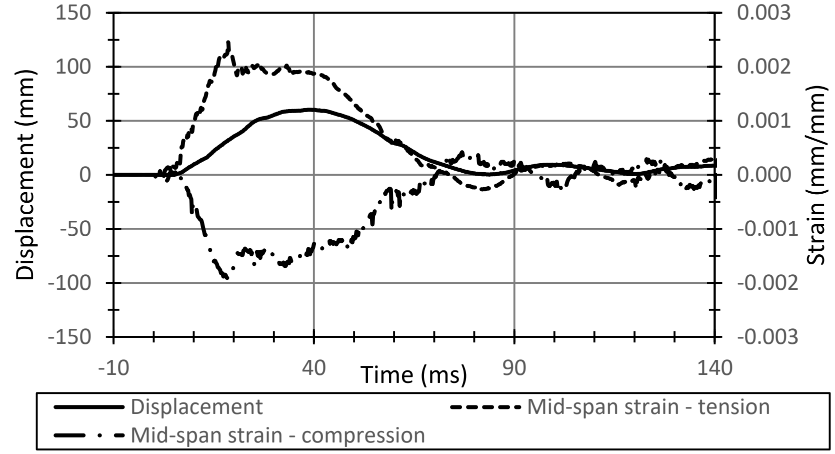

(b) Displacement and Strain

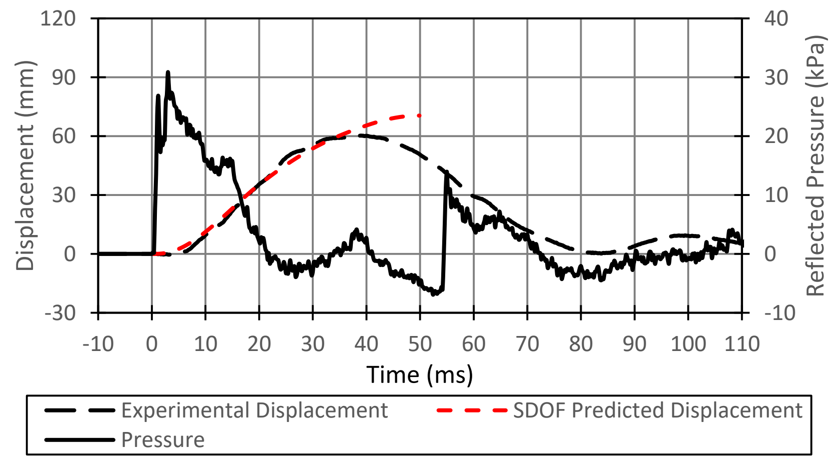

(c) SDOF Prediction

Figure B1.11: Dynamic Test Results for CLT3-9

(a) No Flexural Damage Post Test (b) Rolling Shear at Upper Left Side

Figure B1.12: Dynamic Test Damage for CLT3-9

Specimen: CLT3-10

Failure mode: Flexure

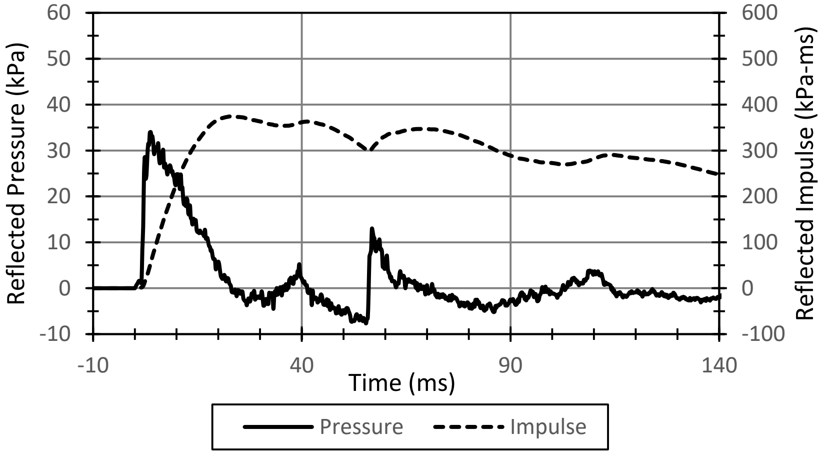

(a) Pressure and Impulse

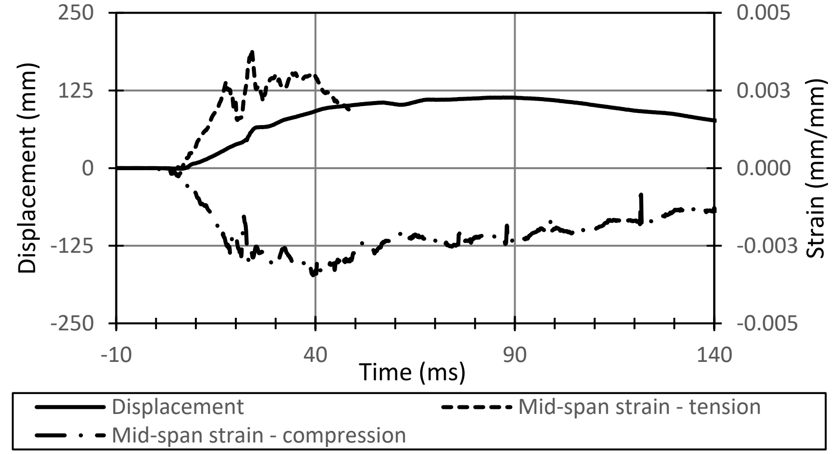

(b) Displacement and Strain

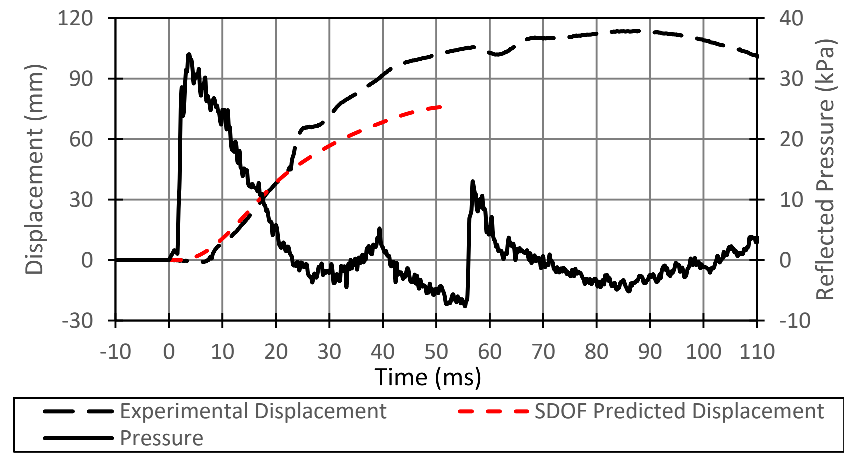

(c) SDOF Prediction

Figure B1.13: Dynamic Test Results for CLT3-10

(a) Flexural Failure Along Finger Joints – Front Face (b) Failure at Finger Joint – Right Side

Figure B1.14: Dynamic Test Damage for CLT3-10

Specimen: CLT3-11

Failure mode: Flexure

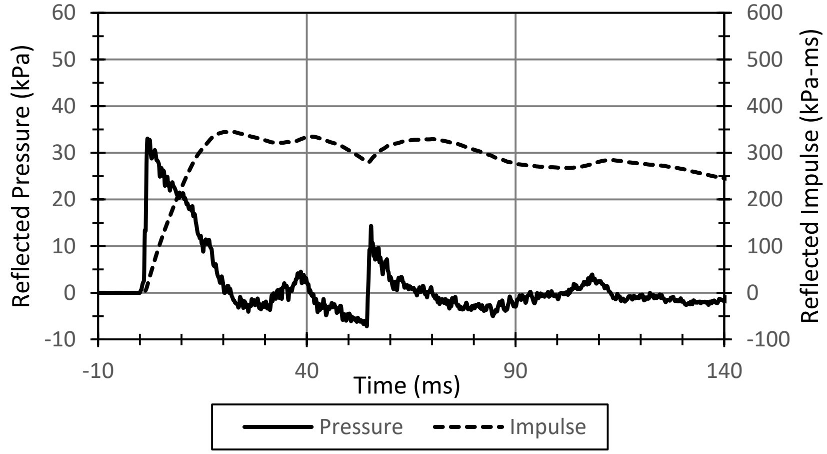

(a) Pressure and Impulse

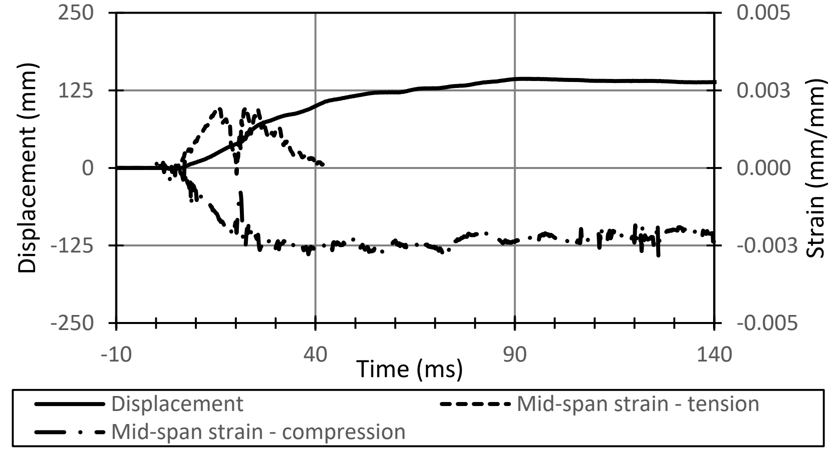

(b) Displacement and Strain

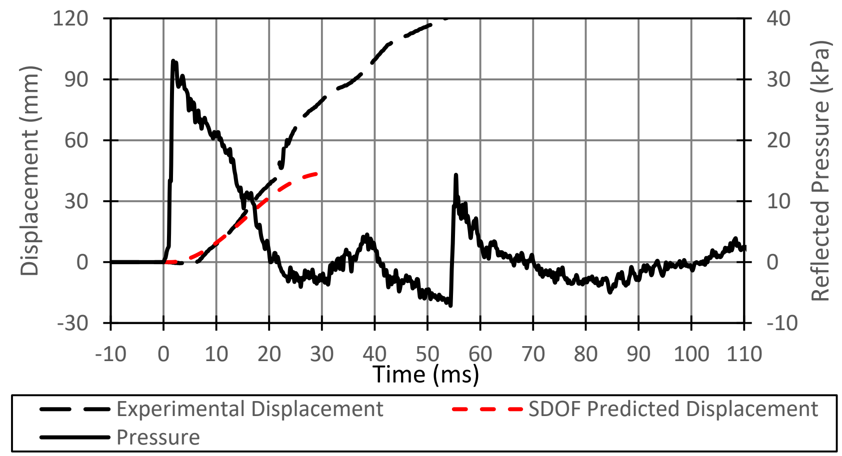

(c) SDOF Prediction

Figure B1.15: Dynamic Test Results for CLT3-11

(a) Flexural Failure along Finger Joints (b) Separation of Finger Joints - Right Side

Figure B1.16: Dynamic Test Damage for CLT3-11

Specimen: CLT5-4

Failure mode: Flexure

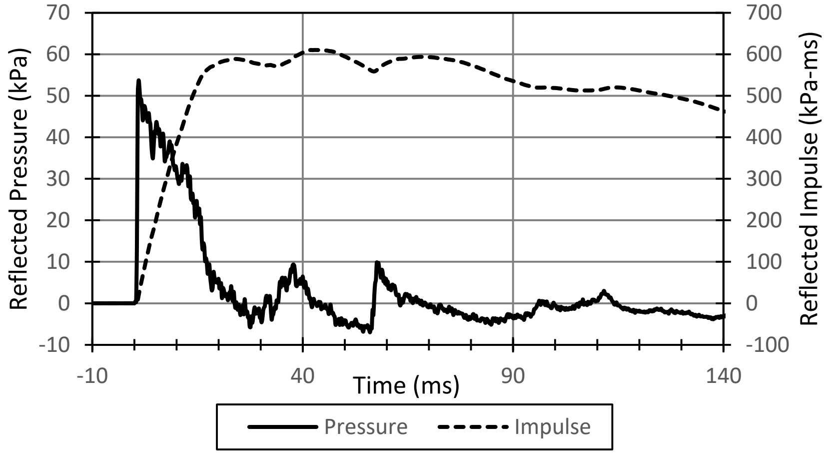

(a) Pressure and Impulse

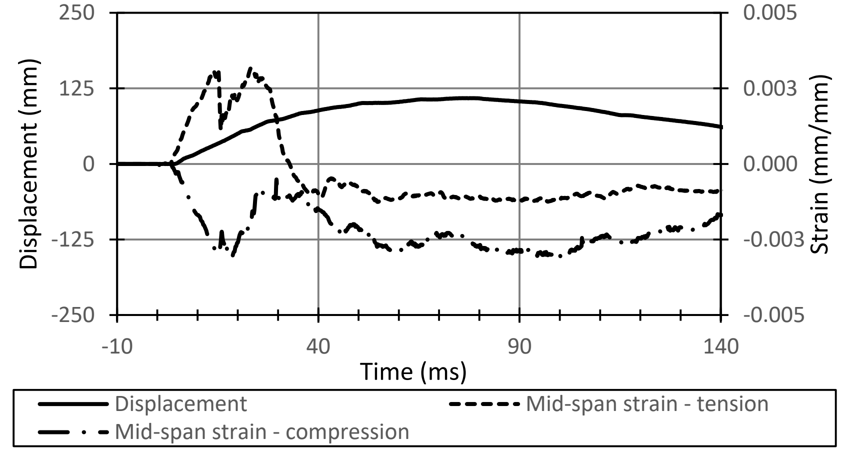

(b) Displacement and Strain

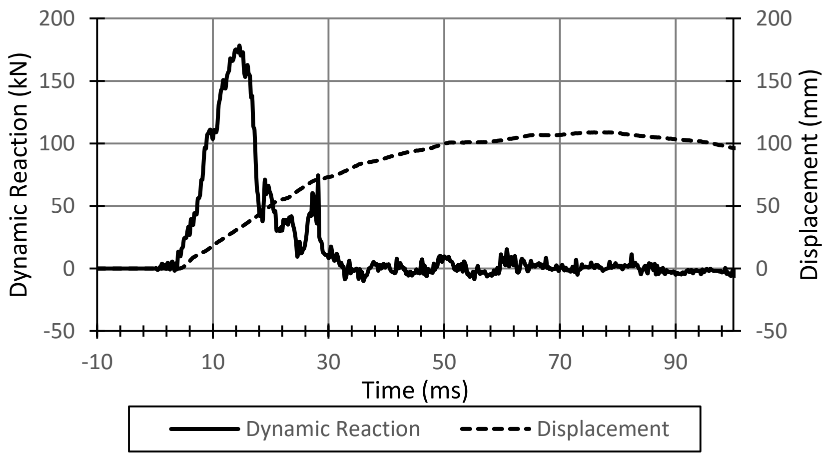

(c) Reaction and Displacement

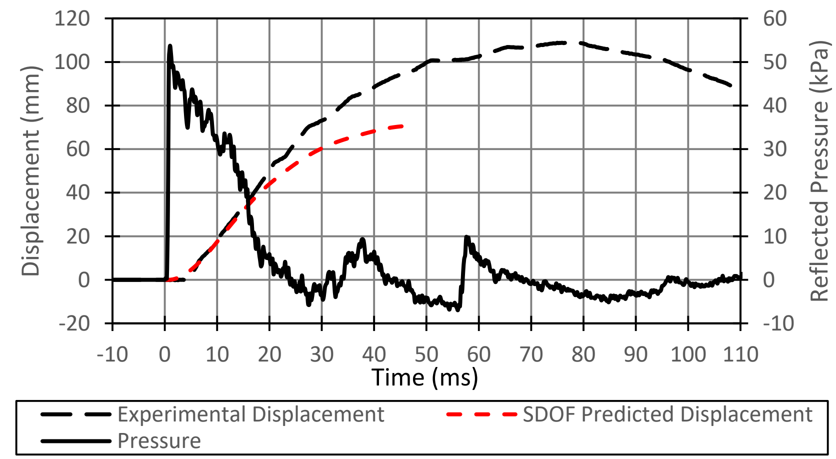

(d) SDOF Prediction

Figure B1.17: Dynamic Test Results for CLT5-4

(a) Start of Flexural Failure – Left Side (b) Full Flexural Failure – Left Side

Figure B1.18: Dynamic Test Damage for CLT5-4

Specimen: CLT5-5

Failure mode: Rolling Shear

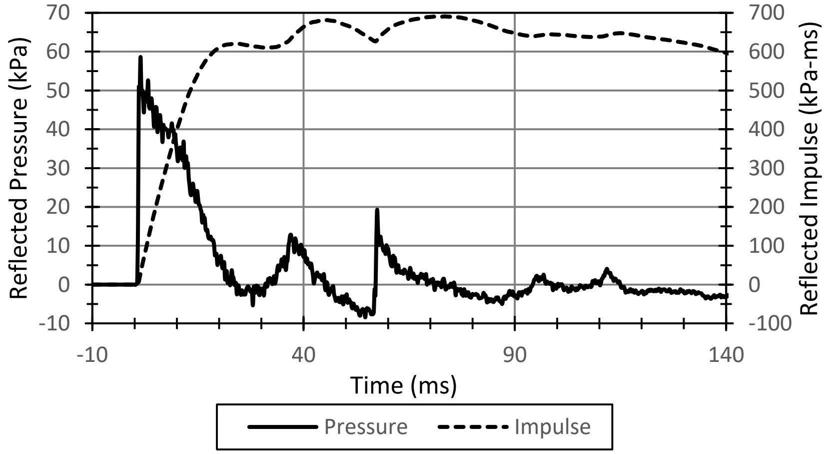

(a) Pressure and Impulse

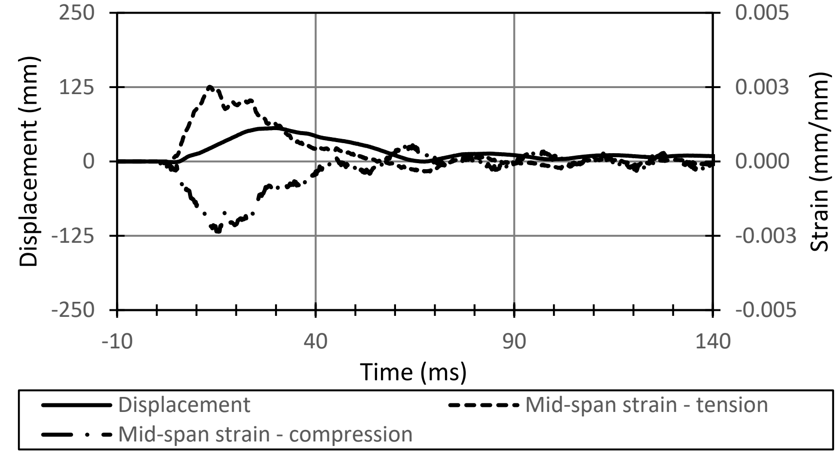

(b) Displacement and Strain

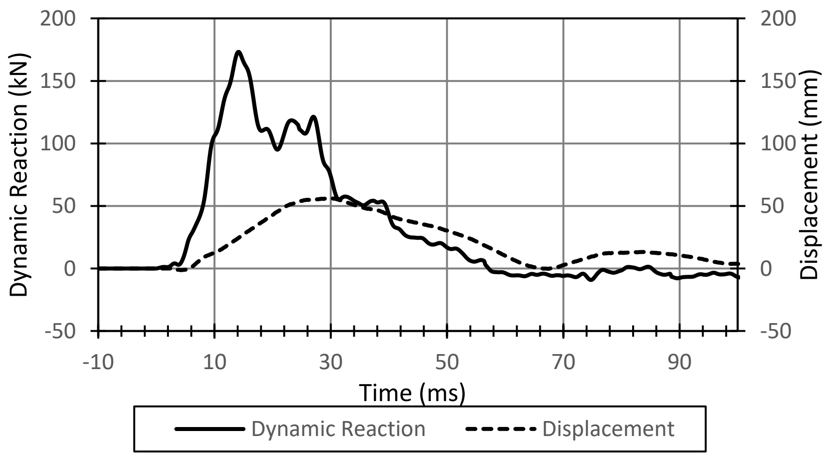

(c) Reaction and Displacement

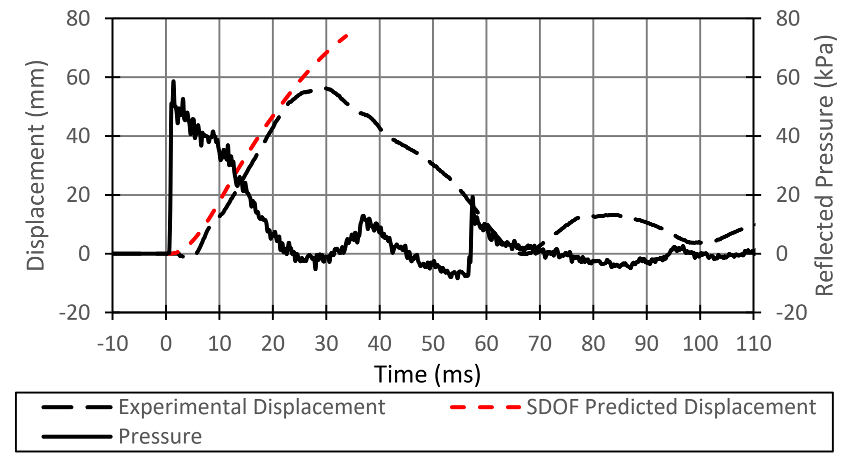

(d) SDOF Prediction

Figure B1.19: Dynamic Test Results for CLT5-5

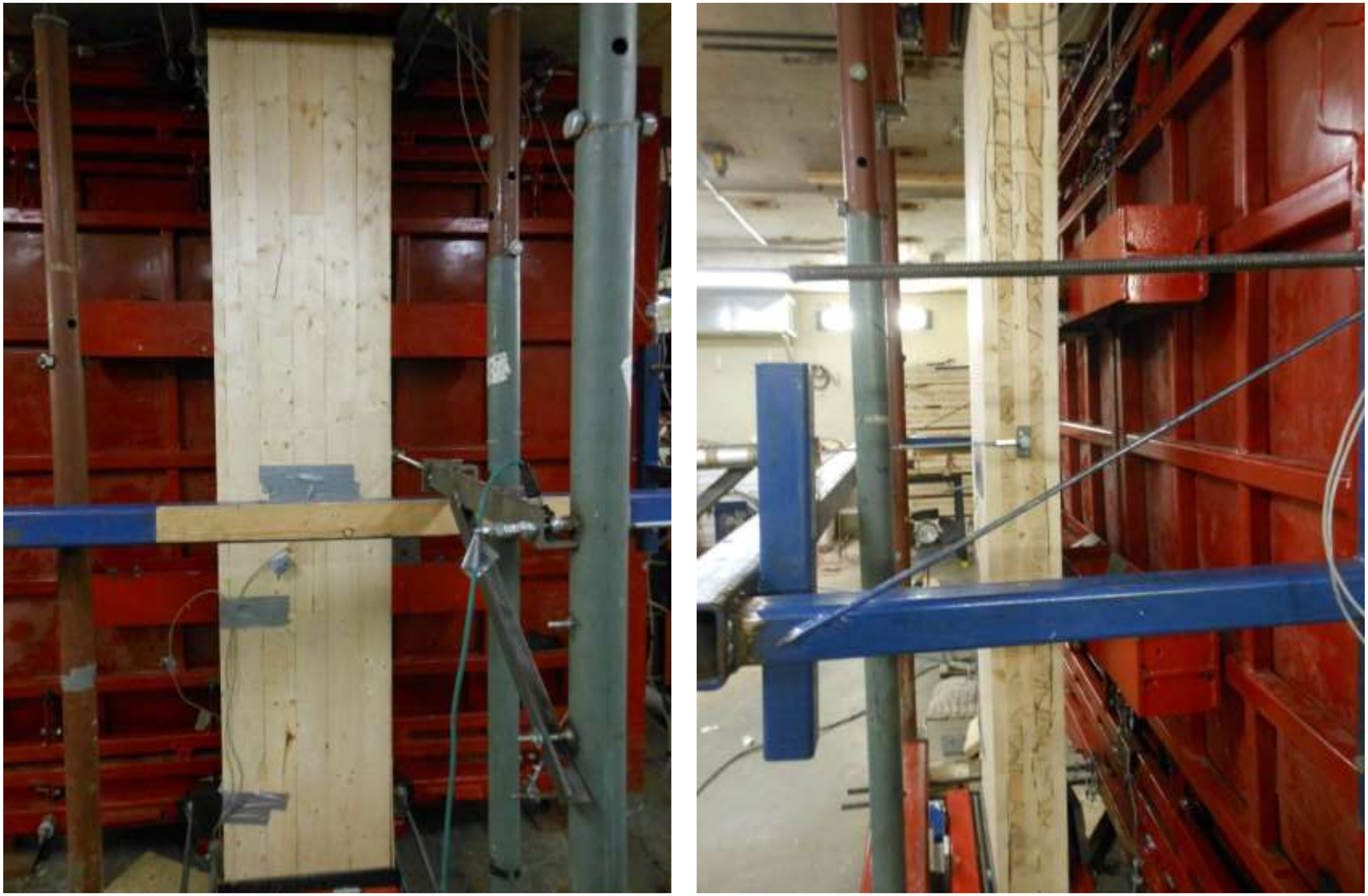

(a) No Significant Flexural Damage Post Test – Front Face (b) Rolling Shear along Full Height of Panel - Right Side

Figure B1.20: Dynamic Test Damage for CLT5-5

Specimen: CLT5-6

Failure mode: Flexure

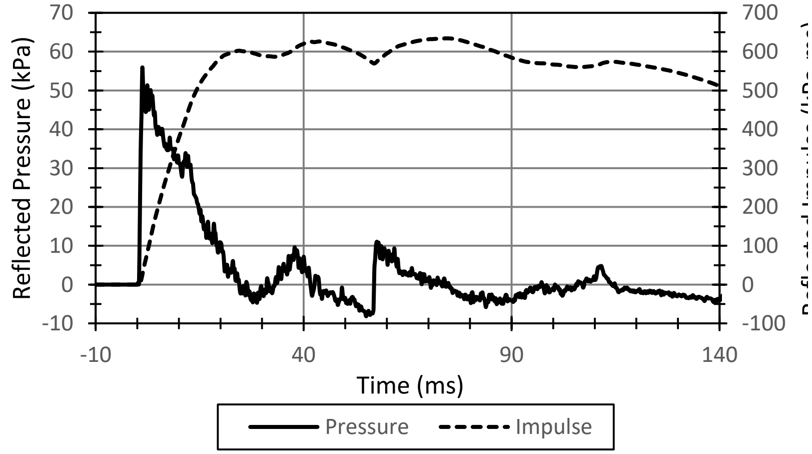

(a) Pressure and Impulse

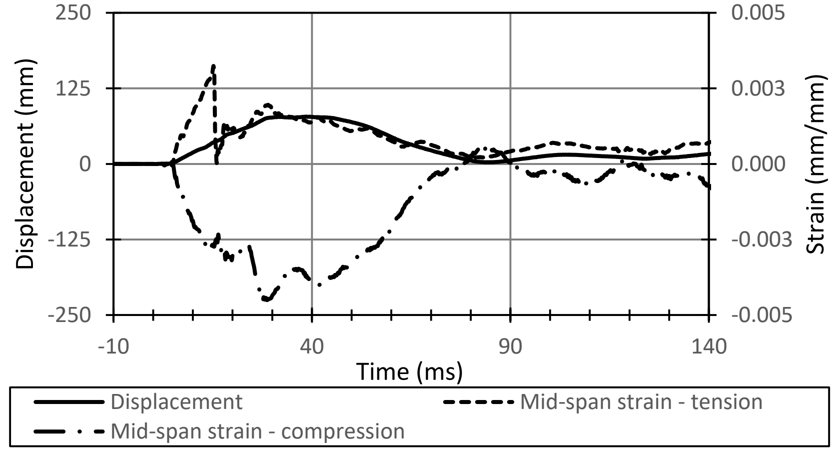

(b) Displacement and Strain

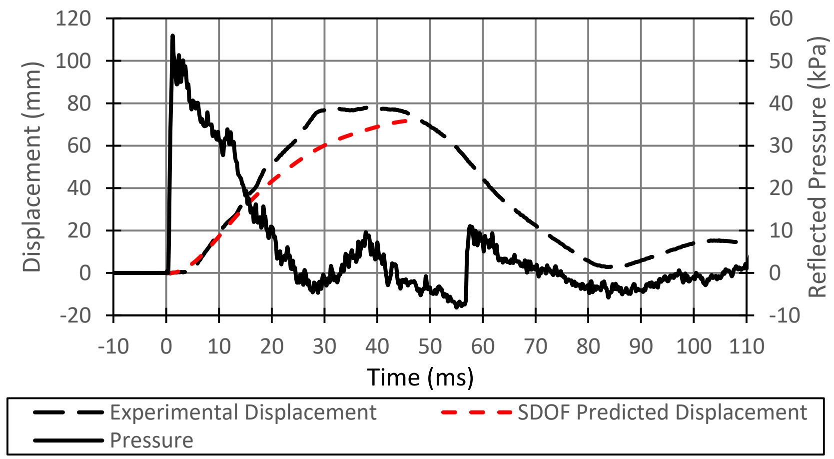

(c) SDOF Prediction

Figure B1.21: Dynamic Test Results for CLT5-6

(a) Flexural Damage in Tension Laminates (b) Rolling Shear on Lower Right Side of Panel

Figure B1.22: Dynamic Test Damage for CLT5-6

Specimen: CLT5-7

Failure mode: Flexure

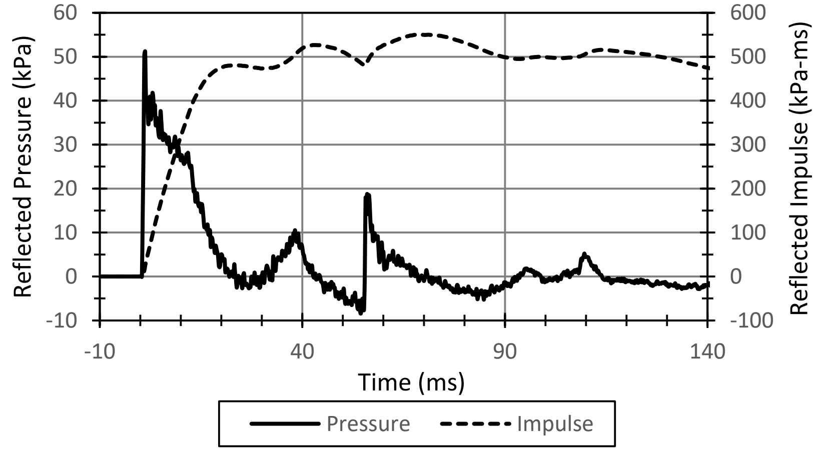

(a) Pressure and Impulse

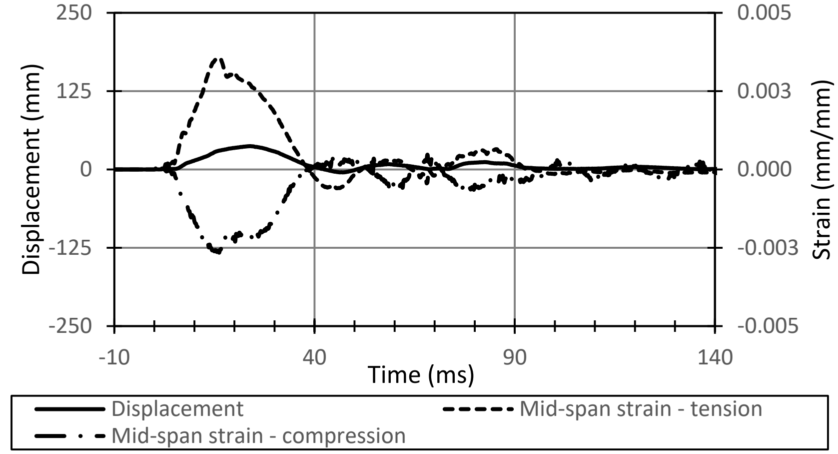

(b) Displacement and Strain

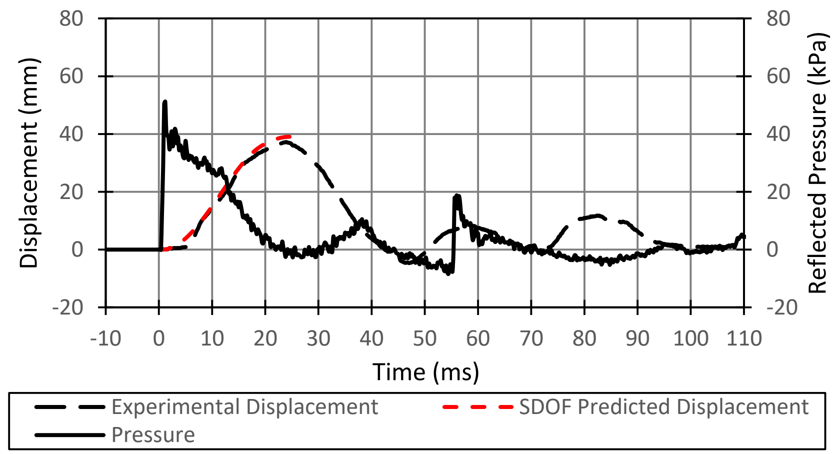

(c) SDOF Prediction

Figure B1.23: Dynamic Test Results for CLT5-7

(a) Rolling Shear on Lower Right Side Following Light Flexural Failure

Figure B1.24: Dynamic Test Damage for CLT5-7